International Journal of Geophysics

Structure and Dynamics of Ionospheric Plasma

Guest Editors: Lucilla Alfonsi and Libo Liu

Structure and Dynamics of Ionospheric Plasma

International Journal of Geophysics

Structure and Dynamics of Ionospheric Plasma

Guest Editors: Lucilla Alfonsi and Libo Liu

Editorial Board

Contents

Hindawi Publishing Corporation
International Journal of Geophysics
Volume 2011, Article ID 952104, 2 pages
doi:10.1155/2011/952104

Editorial

Structure and Dynamics of Ionospheric Plasma

Lucilla Alfonsi[1] and Libo Liu[2]

[1] *Istituto Nazionale di Geofisica e Vulcanologia, Via di Vigna Murata 605, 00143 Rome, Italy*
[2] *Institute of Geology and Geophysics, Chinese Academy of Sciences, Beijing 100029, China*

Correspondence should be addressed to Lucilla Alfonsi, lucilla.alfonsi@ingv.it

Received 29 September 2011; Accepted 29 September 2011

This special issue is dedicated to the memory of Dr. Olga Pirog, who was the actual Guest Editor. The obituary below, prepared by Nelya Polekh on behalf of all her colleagues of the Irkutsk Scientific Center (Russian Academy of Sciences), opens the issue recalling to our readers her excellence and her enthusiasm as scientist and woman.

Olga Pirog was born in 1941 in Kirensk (Irkutsk region). After finishing the Irkutsk State University, she worked in Norilsk. This determined the areas of her scientific interests: high-latitude ionosphere and the magnetosphere-ionosphere interaction.

In 1974, she successfully defended her thesis for the degree of doctor of physical and mathematical sciences. She was the author of more than 150 scientific articles published in Russian and foreign journals.

Olga Pirog was a highly qualified expert in the physics of the ionosphere and the magnetosphere-ionosphere interaction. The main directions of her research were related to the experimental study of large-scale high-latitude ionosphere structures and their dynamic regime, the main ionospheric trough, manifestations of magnetospheric substorms in the ionosphere disturbances, and study of the response of the ionosphere to geomagnetic storms. Her scientific achievements in the physics and morphology of high- and mid-latitude ionosphere and ionospheric-magnetospheric relationships are well known in Russia and abroad and were presented at National conferences and International Symposiums.

She loved traveling and tourism and was interested in literature, music, painting, and history. She loved life. The tragic death happened on December, 16, 2010, crossed her plans. We lost a nice colleague, a good partner, and the beautiful woman. We will always cherish those unforgettable memories of her.

Even if nowadays the ionospheric plasma can be probed by a variety of new technologies, such as LEO satellites, rockets, incoherent scatter radars, backscattering radars, and GNSS receivers, the understanding of its physical properties is still matter of scientific debate. Its structure can change significantly in space, giving rise to the formation of electron density irregularities of different scale sizes, from thousands of kilometers to few centimeters. Ionospheric plasma shows a high degree of variability in time confirmed by a complex dynamics observed over time scales from milliseconds to decades and more. The understanding of the configuration of the ionospheric plasma is not only a scientific challenge, but can also address the needs of our society, focusing on phenomena that can significantly impair a wide range of systems and applications that are at the core of several activities embedded in our daily life. In this direction, space-weather issues, dealing with the harmful effects of the ionosphere on technological systems, will become increasingly significant as we approach the next solar maximum, predicted for 2013.

The selection of the topics included in this issue is far from being exhaustive, but it contributes to demonstrate how many questions arise from the investigation of the coupling between ionized and neutral atmosphere and from the solar-terrestrial relationship. We would like to thank the authors for their excellent contributions and patience in assisting us. Finally, the fundamental work of all reviewers on these papers is also very warmly acknowledged.

This special issue contains five papers: two of them investigate the plasma irregularities from observations and from numerical simulation; one deals with the effects of solar wind

pressure in the high latitude ionosphere in both hemispheres; another paper reports the investigation of the connection between the ionosphere and the underlying atmosphere; finally, the last paper is an overview of the ionosphere-atmosphere coupling. The first paper is by Huang, titled "Occurrence of equatorial plasma bubbles during intense magnetic storms" and presents the measurements of the ion density and velocity in the evening equatorial ionosphere by the Defense Meteorological Satellite Program (DMSP) satellites during 22 intense magnetic storms. The results of this study provide evidence that penetration electric field associated with southward IMF during the main phase of magnetic storms increases the generation of equatorial plasma bubbles in the evening sector.

The second paper, by O. V. Mingalev et al., "*Numerical simulation of the time evolution of small-scale irregularities in the F-layer ionospheric plasma*," addresses the study of the dynamics of magnetic field-aligned small-scale irregularities in the electron concentration, existing in the F-layer ionospheric plasma, investigated with the help of a mathematical model. The results of simulation indicate that the small-scale irregularity, created initially in the F-region ionosphere, decays accomplishing periodic damped vibrations, with the process being collisionless.

In the third paper, "*Effects of abrupt variations of solar wind dynamic pressure on the high-latitude ionosphere*," I. Coco and coauthors show the results of a statistical study on the effects in the high-latitude ionosphere of abrupt variations of solar wind dynamic pressure, using Super Dual Auroral Radar Network (SuperDARN) data in both hemispheres. Their results show that, during periods of quiet ionospheric conditions, the amount of radar backscatter increases when a variation in the dynamic pressure occurs, both positive (increase of the pressure) and negative (decrease of the pressure).

The fourth paper, "*The Planetary wave activity in temperatures of the stratosphere, mesosphere, and in critical frequencies of ionospheric F2 layer*," by N. M. Polekh et al., reports the analysis of vertical-incidence ionospheric sounding data and temperature measurements at stratospheric (30 km) and mesospheric (80 km) heights to investigate the interrelation between the occurrence of fluctuations with periods of planetary waves in temperature variations at different heights and in F2 layer critical frequency variations (foF2) under low solar activity conditions for the time interval 2006-2007. Their findings reveal a similarity between periodic structures for the variations in the parameters involved.

In the last paper, "*Electrodynamical coupling of earth's atmosphere and ionosphere: an overview*," A. K. Singh et al. give a brief review of the electrical processes coupling the atmosphere and ionosphere, reporting their present understanding of how these events play key role in energy transfer from the lower atmosphere to the ionosphere.

Lucilla Alfonsi
Libo Liu

Hindawi Publishing Corporation
International Journal of Geophysics
Volume 2011, Article ID 401858, 10 pages
doi:10.1155/2011/401858

Research Article

Occurrence of Equatorial Plasma Bubbles during Intense Magnetic Storms

Chao-Song Huang

Boston College, Institute for Scientific Research, 400 St Clement's Hall, 140 Commonwealth Avenue, Chestnut Hill, MA 02467, USA

Correspondence should be addressed to Chao-Song Huang, chaosong.huang@bc.edu

Received 8 February 2011; Accepted 29 April 2011

Academic Editor: Lucilla Alfonsi

An important issue in low-latitude ionospheric space weather is how magnetic storms affect the generation of equatorial plasma bubbles. In this study, we present the measurements of the ion density and velocity in the evening equatorial ionosphere by the Defense Meteorological Satellite Program (DMSP) satellites during 22 intense magnetic storms. The DMSP measurements show that deep ion density depletions (plasma bubbles) are generated after the interplanetary magnetic field (IMF) turns southward. The time delay between the IMF southward turning and the first DMSP detection of plasma depletions decreases with the minimum value of the IMF B_z, the maximum value of the interplanetary electric field (IEF) E_y, and the magnitude of the Dst index. The results of this study provide strong evidence that penetration electric field associated with southward IMF during the main phase of magnetic storms increases the generation of equatorial plasma bubbles in the evening sector.

1. Introduction

Intense geomagnetic storms occur when the solar wind with strong, persistent southward interplanetary magnetic field (IMF) impacts on the Earth's magnetosphere. The interplanetary electric field (IEF) associated with southward IMF penetrates to the equatorial ionosphere, creating an eastward electric field on the dayside and a westward electric field on the nightside. Penetration electric fields in the ionosphere have been extensively studied with the incoherent scatter radar chain including the Sondrestrom, Millstone Hill, Arecibo, and Jicamarca radars at ~75° W geographic longitude, as well as with other space-based and ground-based measurements [1–14], and numerically simulated with global ionospheric models [15–18]. Huang et al. [6, 7, 14] and Huang [11] found that penetration electric fields in the ionosphere can last for several hours without obvious attenuation during continuous southward IMF. Huang et al. [8] reported that penetration efficiency, which is defined as the ratio of the change of the equatorial ionospheric electric field to the change of the IEF, is ~10% on the dayside.

The purpose of this paper is to study how penetration electric fields affect the generation of plasma bubbles in the evening equatorial ionosphere during intense magnetic storms. Plasma bubbles are first generated in the bottomside F region and then penetrate the F peak to the topside F region [19–32]. However, the occurrence of equatorial plasma bubbles during magnetic storms has not been fully understood. In earlier studies, some investigators suggested that magnetic storms suppressed equatorial spread F (ESF) in the evening sector. Rastogi et al. [33] reported that the enhanced magnetic activity reduced the occurrence of equatorial radio scintillations and spread F during premidnight hours. Watanabe and Oya [34] found that the occurrence probability of plasma bubbles decreased during magnetically active periods for the local time in premidnight. Singh et al. [35] found that increased magnetic activity inhibited premidnight bubble generation. Palmroth et al. [36] analyzed the correlation between the occurrence of equatorial density depletions and the Kp index and concluded that the magnetic activity decreased the number of depletions in the evening sector.

Recent studies showed that magnetic activity may increase the occurrence of equatorial plasma bubbles. Fejer et al. [37] suggested that penetration electric fields associated

with southward IMF during the early main phase of magnetic storms is eastward in the evening sector and will drive the equatorial F region to move upward, producing favorable condition for the excitation of the Rayleigh-Taylor instability. Huang et al. [38, 39] found that plasma bubbles develop in the evening sector during the early stages of high magnetic activity periods, which suggests that penetration electric fields during southward IMF are responsible for driving plasma bubbles. Basu et al. [40, 41] suggested that the eastward penetration electric field at dusk during the main phase of magnetic storms causes a rapid lift of the equatorial ionosphere and sets off plasma instabilities to form plasma bubbles or bite-outs. Huang [11] and Huang et al. [14] examined the measurements of the Defense Meteorological Satellite Program (DMSP) satellite and found that the penetration electric field at dusk is eastward, lasts for several hours during the main phase of magnetic storms, and causes large upward ion drift in the equatorial ionosphere. The numerical simulations of Keskinen et al. [26] show that a prompt eastward penetration electric field during magnetic storms can increase the vertical drift of the evening equatorial F region plasma and result in the generation of plasma bubbles. Kelley and Retterer [13] used measured electric fields as input into the ionospheric model and successfully reproduced the large-scale plasma bubbles in the equatorial ionosphere during an intense magnetic storm. The simulation results are in good agreement with the measurements of the Jicamarca incoherent scatter radar.

Recent studies have increased the understanding of the influence of geomagnetic activity on the generation of equatorial plasma bubbles. However, further investigations are necessary to determine how rapidly plasma bubbles are generated in response to penetration electric fields and how the response time of the ionosphere varies with the interplanetary electric field and with the strength of geomagnetic activity. In this paper, we present the DMSP satellite measurements of the equatorial ionospheric ion velocity and density in the evening sector and perform a statistical analysis of the occurrence of plasma bubbles during the main phase of intense magnetic storms.

2. Observations

We first present examples of penetration electric fields during magnetic storms. Figures 1(a)–1(d) show the IMF B_z component, the IEF E_y (dawn-to-dusk) component, the ion vertical velocity in the equatorial ionosphere, and the Dst index on 9 November 2004, respectively. The solar wind data were measured by the Advanced Composition Explorer (ACE) satellite located at $\sim 220\, R_E$ upstream and have been shifted to the Earth's bow shock nose with the minimum variance analysis technique developed by Weimer et al. [42]; the IMF components are plotted in the GSM coordinate. In all cases analyzed in this paper, the solar wind and IMF data have been shifted to the bow shock nose with the above technique.

The IMF was weakly southward or close to zero before 1900 UT and became strongly southward between 1900 and 2043 UT, as indicated by the yellow shading. The first storm of this sequence started at ~2000 UT on 7 November, and the Dst index reached a minimum value of −373 nT at 0600 UT on 8 November and remained below −100 nT on 8-9 November. The southward IMF between 1900 and 2043 UT on 9 November caused a significant intensification of the storm, and the Dst index reached another minimum value of −223 nT at 2100 UT. The Jicamarca incoherent scatter radar was in the afternoon sector (1400–1543 LT) during the period of southward IMF. Shown in Figure 1(c) is the ion vertical velocity measured by the Jicamarca radar. The maximum upward ion velocity at ~2000 UT reached $\sim 130\, \mathrm{m\, s^{-1}}$. The enhanced ionospheric ion drift had a shape similar to that of the IEF and was obviously caused by penetration electric field. The penetration electric field lasted for 1.7 hours during the period of storm intensification.

Because equatorial spread F and plasma bubbles occur in the postsunset sector, we need to determine how the plasma drift in the evening ionosphere responds to magnetic storms. In this study, we use the measurements of the DMSP F13 satellite to derive the ion drift velocities. The orbit of F13 crosses the equator near 1800 LT at an altitude of 848 km. Because ion drift velocities vary with latitude, we perform second-order polynomial fits to data taken between ±10° magnetic latitudes and use the polynomial-fit values at the magnetic equatorial crossing to represent the ion drift velocity at the magnetic equator. To quantify storm-time ion drift enhancements, it is necessary to establish quiet-time references. This is important because ion velocity data measured by satellites may include offsets. The quiet-time reference is derived from the data during duskside equatorial crossings during 10 quiet days, 5 days just before and after the magnetic storm. The details of the DMSP data processing are given by Huang et al. [14].

Figures 1(e)–1(h) show the storm case on 29–31 October 2003. The shaded intervals represent the periods of southward IMF. The ionospheric ion drift velocity was measured by the DMSP F13 satellite. The green line in Figure 1(g) is the quiet-time reference accumulated near the time of the October 2003 storm, and the red dots represent the ion vertical velocity on the storm days. The ion vertical velocities, including the reference, are mostly negative (downward) during the period of interest in this case. F13 data were acquired near the 1800 LT where the prereversal enhancement should be in evidence during both quiet and main-phase intervals. Downward drifts apparent in Figure 1(g) indicate a bias in value in F13 measurements of the ion vertical velocity. However, the ion velocity differences between the storm-time and reference values were caused by the penetration electric fields and reached $\sim 120\, \mathrm{m\, s^{-1}}$. In particular, the enhanced ion vertical drift lasted for ~6 hours during the second and third shaded periods when the geomagnetic activity was strengthening [14].

The DMSP measurements presented in Figures 1(e)–1(h) reveal important features of the equatorial ionospheric ion vertical drift at dusk in response to magnetic storms. The ion vertical drift is significantly enhanced in the upward direction. The enhanced upward ion drift can last for up to 6 hours during continuous southward IMF and will move the F region to high altitudes conducive for the generation of the Rayleigh-Taylor instability and plasma bubbles.

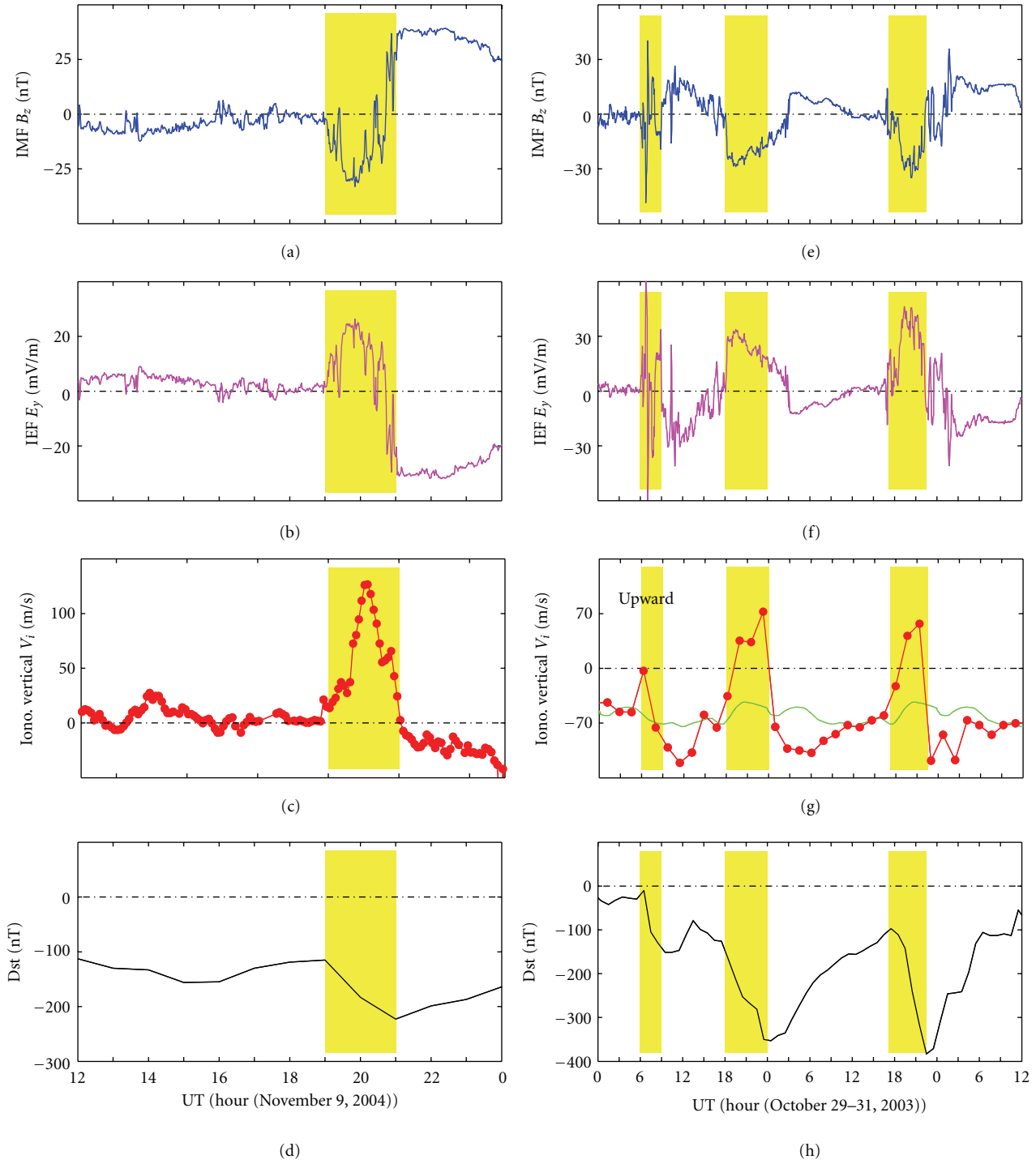

FIGURE 1: Examples of penetration electric fields during magnetic storms. Figures 1(a)–1(d) show interplanetary magnetic field (IMF) south-north (B_z) component, interplanetary electric field (IEF) dawn-dusk (E_y) component, (c) ion vertical velocity in the equatorial ionosphere measured by the Jicamarca incoherent scatter radar, and (d) Dst index on 9 November 2004, respectively. Figures 1(e)–1(h) show the case during 29–31 October 2003; the ion vertical velocity in Figure 1(g) was measured by the DMSP F13 satellite. The shaded regions denote the periods of southward IMF and enhanced vertical ion drift.

We focus on the generation of equatorial plasma bubbles following IMF southward turning during intense magnetic storms. Figure 2 depicts (a) the IMF B_z, (b) the ion density between $\pm 50^\circ$ magnetic latitudes measured by the DMSP F14 satellite at 2000 MLT, and (c) the ion density measured by the DMSP F15 satellite at 2130 MLT on 29 October 2003. The orbital period of the DMSP satellites is ~102 min, and each satellite has ~14 complete orbits every 24 hours. In Figure 2(a), UT is plotted as the vertical axis, and the yellow shadings denote the intervals of southward IMF.

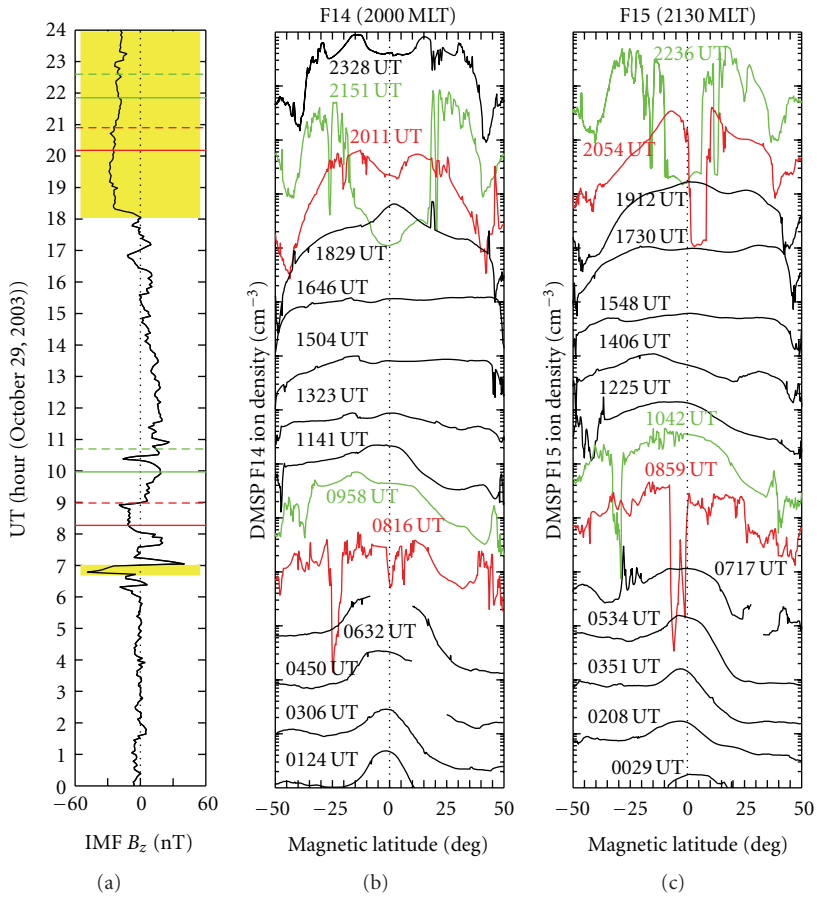

FIGURE 2: Occurrence of equatorial plasma bubbles during the periods of southward IMF on 29 October 2003. Figures 2(a)–2(c) show the IMF B_z and the ionospheric ion density measured by the DMSP F14 and F15 satellites, respectively.

In Figures 2(b) and 2(c), the ion density is plotted in logarithm scale, and UT represents the time when the satellite crossed the magnetic equator. The ion density varies, in general, between 10^3 and 10^5 cm^{-3} in the latitude range of $\pm 50^\circ$. Because the ion density distributions over 14 orbits are plotted in Figure 2(b) (and Figure 2(c)), the density values are not marked for each specific orbit.

A strong southward turning of the IMF occurred between 0637 and 0656 UT, with a minimum value of −48 nT, as denoted by the yellow shading in Figure 2(a). F14 detected significant ion density depletions at 0816 UT (the red line in Figure 2(b)) and at 0958 UT (the green line in Figure 2(b)). Similarly, F15 detected significant ion density depletions at 0859 and 1042 UT. The solid horizontal red and green lines in Figure 2(a) denote the UT when F14 detected the ion density depletions, and the dashed red and green lines denote the times for F15. The ion density showed normal variations with latitude before 0800 UT, and the ion density depletions were detected shortly after the IMF southward turning. The time delay between the IMF southward turning at 0637 UT and the first detection of plasma depletions by F14 at 0816 UT is ~100 min.

The IMF was generally northward between 0900 and 1800 UT, and the ionosphere became quiet again. The IMF became strongly southward after 1800 UT. F14 detected significant ion density depletions at 2011 and 2151 UT, and F15 detected ion density depletions at 2054 and 2236 UT. The time delay between the IMF southward turning at 1800 UT and the first detection of plasma depletions by F14 at 2011 UT is ~2.2 hours.

The data on 30 October 2003 presented in Figure 3 are the continuation of Figure 2 for the same storm case. The IMF remained southward until 0300 UT, and F15 detected ion density depletions at 0014 and 0153 UT. The IMF was mostly northward between 0300 and 1830 UT, with some fluctuations between 1600 and 1830 UT, and then became southward again after 1830 UT. F15 detected ion density depletions at 2039 UT and 2221 UT, and F14 detected ion density depletions at 2137 and 2315 UT. The time delay between the IMF southward turning at 1830 UT and the first detection of plasma depletions by F15 at 2039 UT is ~2.1 hours.

Figures 2 and 3 reveal important relationship between IMF orientation and occurrence of ionospheric plasma depletions. The ionosphere was rather quiet during the periods of northward IMF, and significant plasma depletions occurred ~2 hours after the IMF turned southward. The generation of the equatorial ionospheric plasma depletions was caused by the southward IMF.

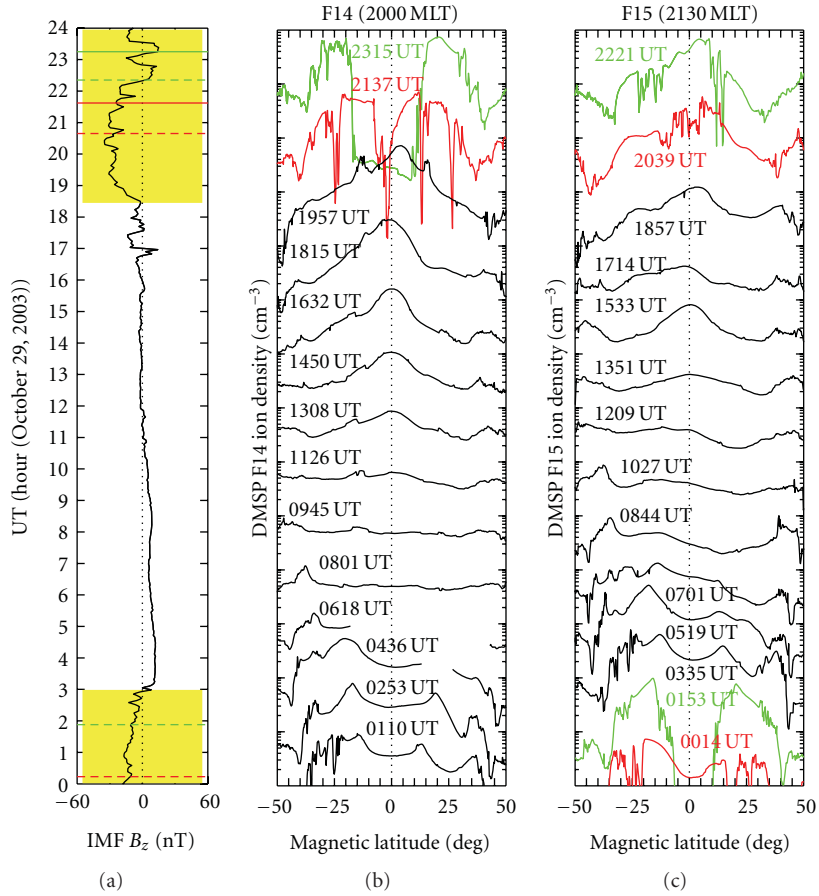

FIGURE 3: Occurrence of equatorial plasma bubbles during the periods of southward IMF on 30 October 2003. Figures 3(a)–3(c) show the IMF B_z and the ionospheric ion density measured by the DMSP F14 and F15 satellites, respectively.

The deep ion density depletions in the low-latitude ionosphere are plasma bubbles. Equatorial plasma bubbles result from the nonlinear evolution of the Rayleigh-Taylor instability. A unique feature of plasma bubbles is the existence of large upward ion drift caused by polarization electric field inside the depletion region (e.g., [43]). In order to show this feature, we plot the ion density and ion vertical velocity in Figure 4. Figures 4(a) and 4(b) present the data measured by F15 around 0859 UT on 29 October 2003, and the shaded region denotes the ion density depletions. The ion density was decreased by ~2 orders of magnitude, and the upward ion velocity reached more than 2000 m s^{-1}. The very large upward ion velocity is the plasma $\mathbf{E} \times \mathbf{B}$ drift caused by the polarization electric field and is the evidence that the plasma depletions are bubbles. The plasma particles inside bubbles are moved to high altitudes by upward $\mathbf{E} \times \mathbf{B}$ drifts and then flow down along the magnetic field lines to higher latitudes.

In Figures 4(c) and 4(d), the ion density and velocity were measured by F14 around 2137 UT on 30 October 2003. The upward ion velocity inside the depletions near the magnetic equator was enhanced, compared to the plasma drifts outside the depletion region. In contrast, the ion velocity became downward at −25° magnetic latitude. The magnetic field lines have large dip angle at −25° magnetic latitude. When the depleted magnetic flux associated with the equatorial plasma bubble reaches this latitude, the plasma flow has a significant component along the magnetic field lines. The downward ion velocity at higher latitudes was related to the field-aligned plasma flow.

The ion vertical velocity was upward inside the plasma depletions at 14° magnetic latitude in Figure 4(d). The dip angle of the magnetic field lines at 14° magnetic latitude is about 15°, and the ion vertical velocity might be dominated by the $\mathbf{E} \times \mathbf{B}$ drift and upward. At −25° magnetic latitude, the dip angle of the magnetic field lines is about 36°, and the ion vertical velocity could be dominated by the field-aligned plasma flow and become downward. In addition, the orbit of the DMSP satellite is not along the magnetic field lines. The plasma depletions at 14∘ and −25° magnetic latitudes had a longitudinal difference of ~10° and could be two separate bubbles. The ion vertical velocity inside separate bubbles may behave differently.

It should be mentioned that low-latitude ionospheric plasma depletions can become very wide during intense magnetic storms. For example, deep plasma depletions measured by F14 at 2151 UT on 29 October 2003 (Figure 2(b)) and at 2315 UT on 30 October 2003 (Figure 3(b)) cover a latitudinal range of 30–40°. Such wide depletions are not the normal plasma bubbles. The wide plasma depletions are caused by continuous lifting of the F region driven by

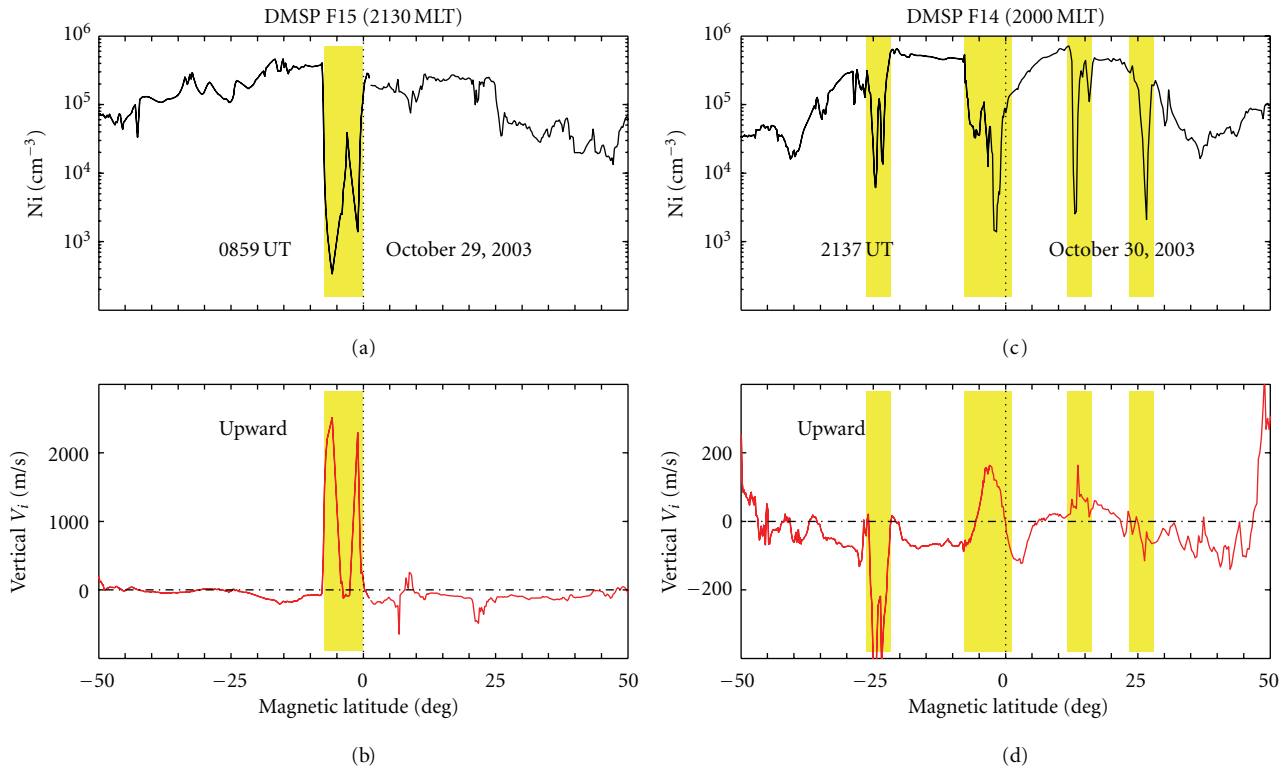

Figure 4: Latitudinal structures of ionospheric ion density and vertical ion drift associated with equatorial plasma bubbles. The shaded regions indicate ion density depletions (plasma bubbles).

strong penetration electric fields. When the entire F region has moved to altitudes higher than the DMSP orbit, the ion density at the DMSP orbit becomes very low. The wide plasma depletions result from the long-lasting penetration electric field during continuous southward IMF.

We now carry out a statistical analysis of the occurrence of equatorial plasma bubbles during intense magnetic storms and use the DMSP measurements for the identification of plasma bubbles. The orbital path of the DMSP satellites is at 840 km altitude. Any plasma bubbles that are below 840 km are not detected by the DMSP satellites. Our criterion for case selection is as follows. There are no plasma bubbles for ~10 hours before the IMF turns southward, and plasma bubbles occur shortly after the IMF southward turning. We assume that the occurrence of the plasma bubbles is the consequence of the IMF southward turning and penetration electric field.

We made a search of the Dst data over 1995–2005 and found 80 intense magnetic storms with minimum Dst value of less than −100 nT. Almost all of the intense storms were associated with strong southward IMF. We then checked the DMSP measurements during these storms. In some storm cases, ion density depletions occurred both before and after IMF southward turning, and such cases are excluded in our analyses because we cannot determine whether the ion density depletions were related to the IMF southward turning. We finally found 22 storms that satisfy the criterion. The examples given in Figures 2 and 3 are from this set.

The Dst index during the 22 storms is plotted in Figure 5. The epoch time is chosen to be the time of the maximum Dst value just before the storm main phase, which generally corresponds to the initial phase of magnetic storms. The dot on the line of each individual storm represents the earliest time at which deep ion density depletions were detected by one DMSP satellite after the IMF southward turning. For example, in the case of the IMF southward turning at 0637 UT in Figure 2, the first detection of plasma depletions was made by the F14 satellite at 0816 UT, and we do not count the subsequent detections by F15 at 0859 UT, by F14 at 0958 UT, and by F15 at 1042 UT. In other words, each magnetic storm is counted only once in Figure 5. It can be seen that the first DMSP detections of ion density depletions occurred within 2-3 hours from the storm initial phase. The plasma depletions in the statistics include all events, irrespective of whether they are plasma bubbles generated by the Rayleigh-Taylor instability or larger-scale depletions caused by eastward penetration electric fields. In most cases, plasma bubbles with strong upward ion drift were first detected.

It should be noted that the initial phase of magnetic storms with an increase of the Dst index is generally caused by a sudden enhancement of the solar wind pressure and does not necessarily correspond to IMF southward turning. The penetration electric field, which lifts the equatorial ionosphere in the evening sector, is primarily determined by southward IMF. Therefore, we use the time delay between the IMF southward turning and the first detection of equatorial ion density depletions as a measure of the effect of penetration electric fields on the generation of equatorial plasma bubbles.

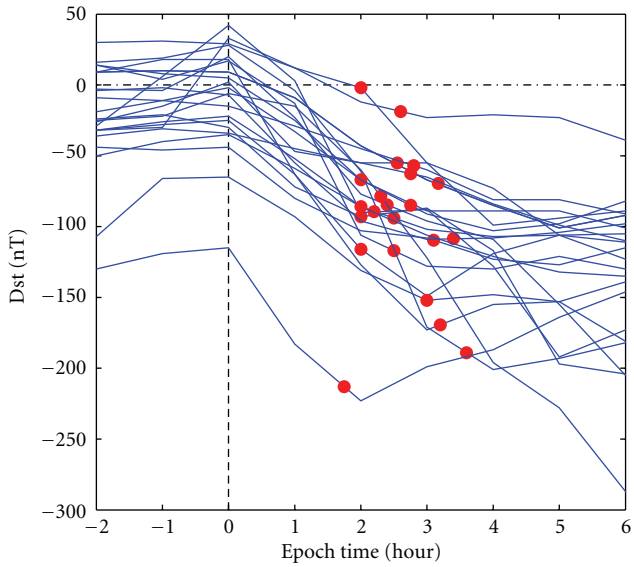

Figure 5: Epoch analysis of the Dst index during 22 intense magnetic storms. The dot in each storm case represents the time of the first detection of equatorial plasma density depletions (plasma bubbles) by a DMSP satellite in the evening sector.

Figure 6 shows how the time delay between IMF southward turning and the first detection of equatorial plasma bubbles varies with the minimum value of the IMF B_z, the maximum value of the IEF E_y, and the minimum Dst value. The time delay becomes shorter when the magnitude of southward IMF becomes larger (Figure 6(a)). The IEF E_y is determined primarily by the IMF B_z. The IEF E_y penetrates to the equatorial ionosphere in the evening sector and lifts the F region there. The larger the IEF E_y is, the faster the F region moves upward. As a result, the equatorial plasma bubbles are generated within a shorter time, so the time delay becomes shorter when the IEF E_y is larger (Figure 6(b)). The time delay also becomes shorter when the absolute value of the minimum Dst is larger (Figure 6(c)), implying that the time delay is shorter during stronger storms. The results in Figure 6 demonstrate the role of southward IMF and penetration electric field in the generation of equatorial plasma bubbles.

The average time delay between IMF southward turning and the first detection of plasma bubbles by one DMSP satellite is 142 min in the 22 storm cases. The DMSP satellites may not be able to detect all plasma bubbles. Measurements from four DMSP satellites are available in most cases of our study. The orbit of the F13 satellite is close to the dawn-dusk meridian plane around 1800 LT. The local time interval with high occurrence probability of plasma bubbles is between 1900–2200 LT (e.g., [34]), and F13 is generally outside the bubble region. A complete DMSP orbit surrounding the Earth takes ~102 min. If there are three satellites flying across the bubble region, the bubble region will be sampled, on average, every ~35 min. The longitudinal (or local time) coverage of a plasma bubble is limited, and the bubble cannot be seen by a satellite if the satellite orbit does not go exactly through the bubble. Furthermore, the orbital altitude of the DMSP satellites is ~840 km, and all plasma bubbles below 840 km are not detected by the satellites. The yellow shadings in Figure 6 cover most data points, and the data scatter in Figure 6 is caused by these characteristics of the DMSP measurements. It is certain that the satellites will miss some bubbles. In other words, there are more plasma bubbles than the DMSP measurements. Therefore, the real-time delay between the IMF southward turning and the generation of plasma bubbles should be shorter than 142 min. Although some uncertainties exist in the DMSP measurements of plasma bubbles, Figure 6 clearly indicates that the time delay decreases with the minimum value of the IMF B_z, the maximum value of the IEF E_y, and the strength of magnetic storms.

3. Discussion

The penetration electric field after IMF southward turning is eastward on the dayside and westward on the nightside. However, the reversal of the penetration electric field does not occur at the dawn-dusk meridian (0600–1800 LT). The numerical simulations [15–18] show that the low-latitude penetration electric field is eastward in the evening sector and that the reversal occurs at 2200–2300 LT. The DMSP satellite measurements presented in the right column of Figure 1 show that penetration electric field at dusk is indeed eastward. The eastward penetration electric field will move the F region to higher altitudes. When the lifted F region reaches the height where the ion-neutral collision frequency is small enough, the Rayleigh-Taylor instability will grow rapidly, resulting in the generation of equatorial plasma bubbles. The time delay in Figure 6 is the delay between the IMF southward turning and the first detection of ion density depletions. The Rayleigh-Taylor instability must have been excited in the bottomside F region at earlier times.

The IMF is in general strongly southward during the main phase of intense magnetic storms. As shown in Figure 6, the time delay between IMF southward turning and plasma bubble detection becomes shorter as the magnitude of the IMF B_z/IEF E_y increases. In particular, plasma bubbles can reach the DMSP orbital altitude of 840 km within 100 min from IMF southward turning in a number of cases. The observed variations of the time delay with the Dst index and IMF/IEF justify the effect of penetration electric fields on the generation of ESF plasma bubbles.

Equatorial plasma bubbles often cause ionospheric scintillations. Scintillations are primarily generated near the boundary of plasma bubbles where the plasma density gradient is large. When the storm-time eastward penetration electric field is extremely strong, the equatorial F region in the evening sector can be moved to very high altitudes, and significant plasma depletions are formed over a large latitudinal range. As shown in Figure 2(b), the plasma density measured by the DMSP F14 satellite at 2151 UT became extremely low between ±20° magnetic latitudes. The latitudinal variation of the plasma density inside the depletion region was gradual and smooth, and large density gradient existed only at the boundaries. In such cases, strong scintillations occur near the boundaries of the depletion region, and only weak scintillations occur in the low-density

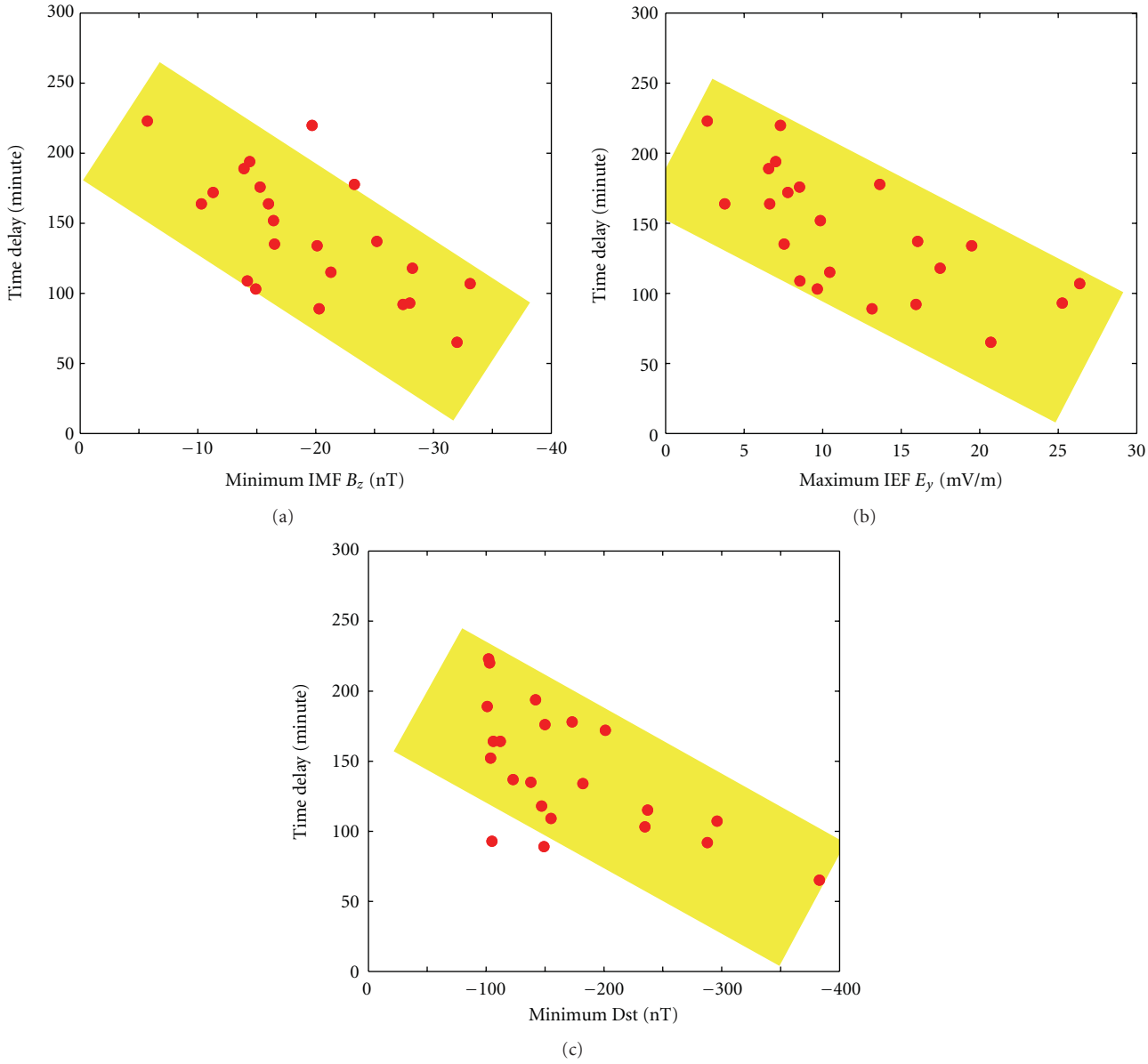

FIGURE 6: The time delay between IMF southward turning and first DMSP detection of equatorial plasma depletions as a function of (a) the minimum value of the IMF B_z, (b) the maximum value of the IEF E_y, and (c) the minimum Dst value during intense magnetic storms.

region. Abdu et al. [44] have analyzed the characteristics of ionospheric scintillations in the Brazilian sector during the magnetic storm on 30 October 2003.

Some previous studies [33–36] found that enhanced magnetic activity suppressed the occurrence of plasma bubbles in the evening sector. Neutral wind disturbances generated in the auroral zone during magnetic storms take several hours to reach the equatorial ionosphere and create westward electric field in the evening equatorial ionosphere. The westward dynamo electric field causes the equatorial F region to move downward, inhibiting the excitation of the Rayleigh-Taylor instability. The suppression of ESF and plasma bubbles in the previous studies might be related to the disturbance dynamo and occur during the storm recovery phase rather than the main phase.

The main phase of magnetic storms occurs during southward IMF, and the recovery phase generally starts when the IMF turns northward. In the storm case on 9 November 2004 (Figures 1(a)–1(d)), the IMF turned northward at 2043 UT through ~0400 UT on the next day. Overshielding electric field occurs during northward IMF [2] and will cause downward plasma drift in the evening equatorial ionosphere. The Jicamarca radar indeed measured downward ion velocity after 2043 UT, consistent with the scenario of overshielding electric field. This effect of northward IMF also contributes to the suppression of ESF and plasma bubbles during the recovery phase of magnetic storms. Abdu et al. [45] found that the evening prereversal enhancement in the vertical plasma drift and the consequent spread F generation can be totally suppressed by the overshielding electric field with

westward polarity. Our observations are consistent with the results of Abdu et al. [45].

4. Conclusions

We have presented the DMSP satellite measurements of the ion density and velocity at 840-km altitude in the evening sector during the main phase of 22 intense magnetic storms with minimum Dst value of smaller than –100 nT. It is shown that the penetration electric field at dusk is eastward and can last for several hours without effective shielding during continuous southward IMF as long as the geomagnetic activity is strengthening. The eastward penetration electric field moves the equatorial F region to higher altitudes conducive for the generation of plasma bubbles. The time delay between the IMF southward turning and the first DMSP detection of equatorial plasma depletions/bubbles is in the range of 70–220 min, with a mean value of 142 min, during the 22 magnetic storms. The time delay decreases with the minimum value of the IMF B_z, the maximum value of the IEF E_y after IMF southward turning, and the magnitude of the Dst index. In particular, the time delay becomes shorter when the value of the maximum IEF E_y is larger, indicating the effect of penetration electric fields on the generation of plasma bubbles. The IMF is in general strongly southward during the main phase of intense magnetic storms. The results of this study suggest that more plasma bubbles are expected to occur during the storm main phase and that plasma bubbles are generated more rapidly under stronger southward IMF conditions.

Acknowledgments

This work was supported by the Air Force Office of Scientific Research (AFOSR) Award FA9550-09-1-0321. The authors gratefully acknowledge the Center for Space Sciences at the University of Texas at Dallas and the US Air Force for providing the DMSP thermal plasma data. The Jicamarca Radio Observatory is operated by the Instituto Geofisico del Peru, with support from the NSF Cooperative Agreement ATM-0432565 through Cornell University. They thank the CDAWeb for providing access to the solar wind and Dst data.

References

[1] A. Nishida, "Coherence of geomagnetic DP2 fluctuations with interplanetary magnetic variations," *Journal of Geophysical Research A*, vol. 73, no. 17, pp. 5549–5559, 1968.

[2] M. C. Kelley, B. G. Fejer, and C. A. Gonzales, "An explanation for anomalous equatorial ionospheric electric field associated with a northward turning of the interplanetary magnetic field," *Geophysical Research Letters*, vol. 6, no. 4, pp. 301–304, 1979.

[3] B. G. Fejer, C. A. Gonzales, D. T. Farley, M. C. Kelley, and R. F. Woodman, "equatorial electric fields during magnetically disturbed conditions, 1. The effect of the interplanetary magnetic field ," *Journal of Geophysical Research*, vol. 84, no. 10, pp. 5797–5802, 1979.

[4] T. Kikuchi, H. Luhr, T. Kitamura, O. Saka, and K. Schlegel, "Direct penetration of the polar electric field to the equator during a DP 2 event as detected by the auroral and equatorial magnetometer chains and the EISCAT radar," *Journal of Geophysical Research A*, vol. 101, no. 8, pp. 17,161–17,173, 1996.

[5] M. C. Kelley, J. J. Makela, J. L. Chau, and M. J. Nicolls, "Penetration of the solar wind electric field into the magnetosphere/ionosphere system," *Geophysical Research Letters*, vol. 30, no. 4, Article ID 1158, 3 pages, 2003.

[6] C. S. Huang, J. C. Foster, L. P. Goncharenko, P. J. Erickson, W. Rideout, and A. J. Coster, "A strong positive phase of ionospheric storms observed by the Millstone Hill incoherent scatter radar and global GPS network," *Journal of Geophysical Research A*, vol. 110, no. 6, Article ID A06303, 13 pages, 2005.

[7] C. S. Huang, J. C. Foster, and M. C. Kelley, "Long-duration penetration of the interplanetary electric field to the low-latitude ionosphere during the main phase of magnetic storms," *Journal of Geophysical Research A*, vol. 110, no. 11, Article ID A11309, 13 pages, 2005.

[8] C. S. Huang, S. Sazykin, J. L. Chau, N. Maruyama, and M. C. Kelley, "Penetration electric fields: efficiency and characteristic time scale," *Journal of Atmospheric and Solar-Terrestrial Physics*, vol. 69, no. 10–11, pp. 1135–1146, 2007.

[9] B. G. Fejer, J. W. Jensen, T. Kikuchi, M. A. Abdu, and J. L. Chau, "Equatorial ionospheric electric fields during the November 2004 magnetic storm," *Journal of Geophysical Research A*, vol. 112, no. 10, Article ID A10304, 11 pages, 2007.

[10] H. Kil, S. J. Oh, L. J. Paxton, Y. Zhang, S. Y. Su, and K. W. Min, "Spike-like change of the vertical $\mathbf{E} \times \mathbf{B}$ drift in the equatorial region during very large geomagnetic storms," *Geophysical Research Letters*, vol. 34, no. 9, Article ID L09103, 4 pages, 2007.

[11] C. S. Huang, "Continuous penetration of the interplanetary electric field to the equatorial ionosphere over eight hours during intense geomagnetic storms," *Journal of Geophysical Research A*, vol. 113, no. 11, Article ID A11305, 10 pages, 2008.

[12] T. Kikuchi, K. K. Hashimoto, and K. Nozaki, "Penetration of magnetospheric electric fields to the equator during a geomagnetic storm," *Journal of Geophysical Research A*, vol. 113, no. 6, Article ID A06214, 10 pages, 2008.

[13] M. C. Kelley and J. Retterer, "First successful prediction of a convective equatorial ionospheric storm using solar wind parameters," *Space Weather*, vol. 6, no. 8, Article ID S08003, 4 pages, 2008.

[14] C. S. Huang, F. J. Rich, and W. J. Burke, "Storm time electric fields in the equatorial ionosphere observed near the dusk meridian," *Journal of Geophysical Research A*, vol. 115, no. 8, Article ID A08313, 14 pages, 2010.

[15] R. W. Spiro, R. A. Wold, and B. G. Fejer, "Penetration of high-latitude-electric-field effects to low latitudes during SUNDIAL 1984," *Annales Geophysicae*, vol. 6, no. 1, pp. 39–50, 1988.

[16] B. G. Fejer, R. W. Spiro, R. A. Wolf, and J. C. Foster, "Latitudinal variations of penetration electric fields during magnetically disturbed periods: 1986 SUNDIAL observations and model results," *Annales Geophysicae*, vol. 8, no. 6, pp. 441–454, 1990.

[17] J. D. Huba, G. Joyce, S. Sazykin, R. Wolf, and R. Spiro, "Simulation study of penetration electric field effects on the low- to mid-latitude ionosphere," *Geophysical Research Letters*, vol. 32, no. 23, Article ID L23101, 4 pages, 2005.

[18] N. Maruyama, A. D. Richmond, T. J. Fuller-Rowell et al., "Interaction between direct penetration and disturbance dynamo electric fields in the storm-time equatorial ionosphere," *Geophysical Research Letters*, vol. 32, no. 17, Article ID L17105, 4 pages, 2005.

[19] R. F. Woodman and C. La Hoz, "Radar observations of F-region equatorial irregularities," *Journal of Geophysical Research*, vol. 81, no. 31, pp. 5447–5466, 1976.

[20] A. J. Scannapieco and S. L. Ossakow, "Nonlinear spread-F," *Geophysical Research Letters*, vol. 3, no. 8, pp. 451–454, 1976.

[21] S. L. Ossakow and P. K. Chaturvedi, "Morphological studies of rising equatorial spread F bubbles," *Journal of Geophysical Research A*, vol. 83, no. 5, pp. 2085–2090, 1978.

[22] S. T. Zalesak, S. L. Ossakow, and P. K. Chaturvedi, "Nonlinear equatorial spread-F: the effect of neutral winds and background Pedersen conductivity," *Journal of Geophysical Research A*, vol. 87, no. 1, pp. 151–166, 1982.

[23] C. S. Huang and M. C. Kelley, "Nonlinear evolution of equatorial spread F: 1. On the role of plasma instabilities and spatial resonance associated with gravity wave seeding," *Journal of Geophysical Research A*, vol. 101, no. 1, pp. 283–292, 1996.

[24] C. S. Huang and M. C. Kelley, "Nonlinear evolution of equatorial spread F: 2. Gravity wave seeding of Rayleigh-Taylor instability," *Journal of Geophysical Research A*, vol. 101, no. 1, pp. 293–302, 1996.

[25] M. J. Keskinen, S. L. Ossakow, and B. G. Fejer, "Three-dimensional nonlinear evolution of equatorial ionospheric spread-F bubbles," *Geophysical Research Letters*, vol. 30, no. 16, Article ID 1855, 4 pages, 2003.

[26] M. J. Keskinen, S. L. Ossakow, B. G. Fejer, and J. Emmert, "Evolution of equatorial ionospheric bubbles during a large auroral electrojet index increase in the recovery phase of a magnetic storm," *Journal of Geophysical Research A*, vol. 111, no. 2, Article ID A02303, 5 pages, 2006.

[27] J. D. Huba, J. Krall, and G. Joyce, "Atomic and molecular ion dynamics during equatorial spread F," *Geophysical Research Letters*, vol. 36, no. 10, Article ID L10106, 6 pages, 2009.

[28] J. D. Huba, S. L. Ossakow, G. Joyce, J. Krall, and S. L. England, "Three-dimensional equatorial spread F modeling: zonal neutral wind effects," *Geophysical Research Letters*, vol. 36, no. 19, Article ID L19106, 5 pages, 2009.

[29] J. Krall, J. D. Huba, S. L. Ossakow, and G. Joyce, "Why do equatorial ionospheric bubbles stop rising?" *Geophysical Research Letters*, vol. 37, no. 9, Article ID L09105, 4 pages, 2010.

[30] J. Krall, J. D. Huba, G. Joyce, and T. Yokoyama, "Density enhancements associated with equatorial spread F," *Annales Geophysicae*, vol. 28, no. 2, pp. 327–337, 2010.

[31] J. M. Retterer, "Forecasting low-latitude radio scintillation with 3-D ionospheric plume models: 1. Plume model," *Journal of Geophysical Research A*, vol. 115, no. 3, Article ID A03306, 18 pages, 20110.

[32] J. M. Retterer, "Forecasting low-latitude radio scintillation with 3-D ionospheric plume models: 2. Scintillation calculation," *Journal of Geophysical Research A*, vol. 115, no. 3, Article ID A03307, 10 pages, 2010.

[33] R. G. Rastogi, J. P. Mullen, and E. MacKenzie, "Effect of geomagnetic activity on equatorial radio VHF scintillations and spread F," *Journal of Geophysical Research A*, vol. 86, no. 5, pp. 3661–3664, 1981.

[34] S. Watanabe and H. Oya, "Occurrence characteristics of low latitude ionosphere irregularities observed by impedance probe on board the Hinotori satellite," *Journal of Geomagnetism & Geoelectricity*, vol. 38, no. 1, pp. 125–149, 1986.

[35] S. Singh, D. K. Bamgboye, J. P. McClure, and F. S. Johnson, "Morphology of equatorial plasma bubbles," *Journal of Geophysical Research A*, vol. 102, no. 9, Article ID 97JA01724, pp. 20019–20029, 1997.

[36] M. Palmroth, H. Laakso, B. G. Fejer, and R. F. Pfaff Jr., "DE 2 observations of morningside and eveningside plasma density depletions in the equatorial ionosphere," *Journal of Geophysical Research A*, vol. 105, no. 8, Article ID 1999JA005090, pp. 18429–18442, 2000.

[37] B. G. Fejer, L. Scherliess, and E. R. de Paula, "Effects of the vertical plasma drift velocity on the generation and evolution of equatorial spread F," *Journal of Geophysical Research A*, vol. 104, no. 9, Article ID 1999JA900271, pp. 19859–19869, 1999.

[38] C. Y. Huang, W. J. Burke, J. S. Machuzak, L. C. Gentile, and P. J. Sultan, "DMSP observations of equatorial plasma bubbles in the topside ionosphere near solar maximum," *Journal of Geophysical Research A*, vol. 106, no. 5, pp. 8131–8142, 2001.

[39] C. Y. Huang, W. J. Burke, J. S. Machuzak, L. C. Gentile, and P. J. Sultan, "Equatorial plasma bubbles observed by DMSP satellites during a full solar cycle: toward a global climatology," *Journal of Geophysical Research A*, vol. 107, no. 12, Article ID 1434, 10 pages, 2002.

[40] S. Basu, S. Basu, K. M. Groves et al., "Response of the equatorial ionosphere in the South Atlantic region to the great magnetic storm of July 15, 2000," *Geophysical Research Letters*, vol. 28, no. 18, pp. 3577–3580, 2001.

[41] S. Basu, S. Basu, F. J. Rich et al., "Response of the equatorial ionosphere at dusk to penetration electric fields during intense magnetic storms," *Journal of Geophysical Research A*, vol. 112, no. 8, Article ID A08308, 14 pages, 2007.

[42] D. R. Weimer, D. M. Ober, N. C. Maynard et al., "Predicting interplanetary magnetic field (IMF) propagation delay times using the minimum variance technique," *Journal of Geophysical Research A*, vol. 108, no. 1, Article ID 1026, 12 pages, 2003.

[43] C. S. Huang, O. de La Beaujardiere, R. F. Pfaff et al., "Zonal drift of plasma particles inside equatorial plasma bubbles and its relation to the zonal drift of the bubble structure," *Journal of Geophysical Research A*, vol. 115, no. 7, Article ID A07316, 12 pages, 2010.

[44] M. A. Abdu, E. R. de Paula, I. S. Batista et al., "Abnormal evening vertical plasma drift and effects on ESF and EIA over Brazil-South Atlantic sector during the 30 October 2003 superstorm," *Journal of Geophysical Research A*, vol. 113, no. 7, Article ID A07313, 12 pages, 2008.

[45] M. A. Abdu, E. A. Kherani, I. S. Batista, and J. H. A. Sobral, "Equatorial evening prereversal vertical drift and spread F suppression by disturbance penetration electric fields," *Geophysical Research Letters*, vol. 36, no. 19, Article ID L19103, 5 pages, 2009.

Hindawi Publishing Corporation
International Journal of Geophysics
Volume 2011, Article ID 353640, 8 pages
doi:10.1155/2011/353640

Research Article

Numerical Simulation of the Time Evolution of Small-Scale Irregularities in the F-Layer Ionospheric Plasma

O. V. Mingalev, G. I. Mingaleva, M. N. Melnik, and V. S. Mingalev

Kola Scientific Center of the Russian Academy of Sciences, Polar Geophysical Institute, Fersman street 14, 184209 Apatity, Murmansk Region, Russia

Correspondence should be addressed to V. S. Mingalev, mingalev@pgia.ru

Received 15 February 2011; Revised 30 May 2011; Accepted 31 May 2011

Academic Editor: Lucilla Alfonsi

Dynamics of magnetic field-aligned small-scale irregularities in the electron concentration, existing in the F-layer ionospheric plasma, is investigated with the help of a mathematical model. The plasma is assumed to be a rarefied compound consisting of electrons and positive ions and being in a strong, external magnetic field. In the applied model, kinetic processes in the plasma are simulated by using the Vlasov-Poisson system of equations. The system of equations is numerically solved applying a macroparticle method. The time evolution of a plasma irregularity, having initial cross-section dimension commensurable with a Debye length, is simulated during the period sufficient for the irregularity to decay completely. The results of simulation indicate that the small-scale irregularity, created initially in the F-region ionosphere, decays accomplishing periodic damped vibrations, with the process being collisionless.

1. Introduction

Occurrence of electron density irregularities is a natural phenomenon in the Earth's ionosphere. These irregularities have a wide range of spatial scales, ranging from a few Debye lengths to thousands of kilometers. The electron density increases and depletions inside irregularities can lie in the range from a few portions to some tens of percentages. The well-known equatorial anomaly is the example of large-scale irregularities in the ionospheric F layer. Another example is the main ionospheric trough observed at subauroral latitudes [1]. The high-latitude ionosphere can contain some types of large-scale irregularities, for example, the tongue of increased values of the electron density stretched over the polar cap from the dayside to night side, polar and auroral peaks of ionization, "patches" and "blobs" of ionization, and so on [2–5]. Middle-scale irregularities with dimensions of tens of kilometers are observed in the F-layer ionosphere, too [6, 7]. It is known that small-scale irregularities, which can exist in the ionosphere, are predominately magnetic field aligned. The Earth's ionosphere can contain short-scale irregularities, having cross-section diameters of about hundreds of meters [8–11]. Also, radio aurora or small-scale turbulence of the E layer is the well-known example of short-scale irregularities [12]. Meteor plasma trails are the example of irregularities in the ionosphere, too [13].

It is known that ionospheric irregularities may be originated not only by natural processes but also as a result of active experiments in the ionospheric plasma, in particular, as a result of release of various chemically active substances into the ionosphere. Moreover, ionospheric irregularities may be formed by high-power high-frequency radio waves, pumped into the ionosphere by ground-based ionospheric heaters. These waves cause a variety of physical processes in the ionospheric plasma. Some such processes result in the formation of both large-scale electron temperature and density irregularities and small-scale, geomagnetic field-aligned irregularities in the ionosphere. Mathematical modeling of the large-scale F-layer modification by powerful high frequency waves was performed in some studies, in particular, in the papers by Meltz and LeLevier [14], Perkins and Roble [15], Mantas et al. [16], Bernhardt and Duncan [17], Hansen et al. [18], Vas'kov et al. [19], and Mingaleva et al. [20, 21]. The parameters of the small-scale irregularities, formed in

the F-layer ionosphere by powerful high frequency waves, were described in detail by Wong et al. [22]. According to their paper, diametrical sizes of these irregularities are several Debye lengths (no more that about 100), while the disturbances of the electron density in them can reach some tens of percentages. The formation of the small-scale irregularities in the F-layer ionosphere by powerful high frequency waves was considered and simulated in the study by Eliasson and Stenflo [23]. It can be noticed that such irregularities may be formed in the ionospheric plasma not only artificially but also by natural processes [22].

Just small-scale, geomagnetic field-aligned ionospheric irregularities are investigated in the present study utilizing a mathematical model developed recently in the Polar Geophysical Institute (PGI).

2. Mathematical Model

The ionospheric plasma at F-layer altitudes is supposed to be a rarefied compound consisting of electrons and positive ions in the presence of a strong, external, uniform magnetic field. The studied irregularities are assumed to be geomagnetic field-aligned, with their cross-sections being circular. The initial cross-section diameters of the irregularities are supposed to be commensurable with the Debye length. At F-layer levels, the mean free path of particles (electrons and ions) between successive collisions is much more than the cross-section diameters of the considered irregularities. Therefore, the plasma is assumed to be collisionless. Kinetic processes in such plasma are described by the Vlasov-Poisson system of equations which has been considered, for example, in the studies by Hockney and Eastwood [24], and Birdsall and Langdon [25]. This system may be written as follows:

$$\frac{\partial f_a}{\partial t} + \left(\mathbf{v}, \frac{\partial f_a}{\partial \mathbf{x}}\right) + \frac{q_a}{m_a}\left(\mathbf{E} + [\mathbf{v}\times\mathbf{B}_0], \frac{\partial f_a}{\partial \mathbf{v}}\right) = 0, \quad a = i, e, \tag{1}$$

$$\Delta\varphi(\mathbf{x}, t) = -\frac{1}{\varepsilon_0}\rho(\mathbf{x}, t), \tag{2}$$

$$\mathbf{E}(\mathbf{x}, t) = -\nabla\varphi(\mathbf{x}, t), \qquad \rho(\mathbf{x}, t) = e_0(n_i - n_e),$$
$$n_a(\mathbf{x}, t) = \int f_a(t, \mathbf{x}, \mathbf{v})d\mathbf{v}, \tag{3}$$

where $f_a(t, \mathbf{x}, \mathbf{v})$, $n_a(\mathbf{x}, t)$, m_a, and q_a are, respectively, the distribution function, concentration, mass, and charge of particles of type a, $\mathbf{x}$ is the space coordinate vector, $\mathbf{v}$ is the velocity, $\mathbf{B}_0$ is the external magnetic field, $\mathbf{E}$ is the self-consistent electric field, $\varphi(\mathbf{x}, t)$ is the electric field potential, $\rho(\mathbf{x}, t)$ is the electric charge density, ε_0 is the dielectric constant of free space, and e_0 is the proton charge. The Vlasov equation, (1), describes the evolution of the distribution functions of charged particles and the Poisson equation, (2), describes the self-consistent electric field.

As pointed out previously, the investigated irregularities are geomagnetic field-aligned. Their longitudinal sizes are much more than the cross-section diameters. Gradients of the plasma parameters in the longitudinal direction are much less than those in a plane perpendicular to a magnetic field in the vicinity of the irregularity. Therefore, plasma parameters in the vicinity of the irregularity may be considered as independent on the longitudinal coordinate. This simplification allows us to consider a two-dimensional flow of plasma in a plane perpendicular to a magnetic field line.

Not long ago, in the PGI, the two-dimensional mathematical model has been developed which is intended to simulate dynamics of the near-earth rarefied plasma [26]. In this model, the full implicit variant of the macroparticle method is applied for joint numerical solving of the Vlasov equations, (1), and the Poisson equation, (2), with the real charge-mass ratio for electrons having been used. The Poisson equation, (2), is numerically solved using a finite-difference method having the forth order of accuracy. This model has been utilized for numerical simulation of the behavior of small-scale irregularities of the electron density which can exist in the magnetospheric plasma [26]. In the present study, this model is utilized to investigate the time evolution of small-scale irregularities in the F-layer ionospheric plasma.

In this work, the simulation region lays in the plane perpendicular to the magnetic field line. The simulation region is a square and its side length is equal to 96 Debye lengths of plasma. The dimension of the simulation region is consistent with recommendations of the applied macroparticle method using a discrete Vlasov-Poisson system of equations. According to these recommendations, for the adequate representation of the real plasma, the dimension of the simulation region should be no less than 60–100 Debye length of the plasma [24, 25].

The grid width is equal to one eighth of the Debye length of the plasma. The quantity of the grid cells is 768×768. The time step for the electric field is equal to one hundredth of an equilibrium period of Langmuir oscillations of electrons. The periodical boundary conditions for the distribution func-tions and electric field are utilized in this work. In the model calculations, the number of macro-particles per species is $72 \cdot 2^{20} \approx 75.5 \cdot 10^6$; therefore, the average number of macro-particles in the Debye cell for the model plasma is equal to 2^{13}.

The temporal evolution of the small-scale irregularity, created initially in the F-layer ionospheric plasma, is numerically studied during a period sufficient for the irregularity to decay completely. The 2D2V variant of the mathematical self-consistent model of dynamics of the near-earth rarefied plasma is utilized. More specific details of the utilized mathematical model and peculiarities of the applied numerical method may be found in the study of Mingalev et al. [26].

3. Presentation and Discussion of Results

The utilized mathematical model can describe the behavior of the near-earth plasma under various conditions. The results of calculations to be presented in this paper were obtained using the input parameters of the model typical for the nocturnal ionospheric plasma at the level of 300 km. In particular, the value of the nondisturbed electron concentration (equal to the positive ion concentration) is 10^{11} m^{-3}.

The electron and ion temperatures are supposed to be equal to 1213 K and 930 K, respectively. The bulk flow velocities of electrons and positive ions are assumed to be zero. The value of the magnetic field, B_0, is $4.4 \cdot 10^{-5}$ T.

The above pointed out values yield the following quantities of some physically significant parameters. The electron thermal velocity, V_{Te}, is equal to 135.6 km/s, the equilibrium plasma frequency, ω_{pe}^0, is $1.78 \cdot 10^7$ s^{-1}. The Debye length of the plasma, λ_{De}^0, defined as $\lambda_{De}^0 = V_{Te}/\omega_{pe}^0$, is equal to $7.6 \cdot 10^{-3}$ m; the electron gyro radius, R_{ce}, is $17.5 \cdot 10^{-3}$ m. The equilibrium period of Langmuir oscillations of electrons, T_{pe}, is $3.52 \cdot 10^{-7}$ s. The period of cyclotron oscillations of electrons, T_{ce}, is equal to $8.12 \cdot 10^{-7}$ s, that is, approximately a factor of 2.3 larger than the equilibrium period of Langmuir oscillations of electrons ($T_{ce} \approx 2.3 \cdot T_{pe}$). The collision mean free path of charged particles is about 50 m. The mean free time of electron between successive collisions with other particles, T_{freepath}, is larger than the equilibrium period of Langmuir oscillations of electrons by a factor of about 1047 ($T_{\text{freepath}} \approx 1047 T_{pe}$).

Taking the input parameters of the mathematical model typical for the nocturnal ionosphere at the level of 300 km, we have calculated the time evolution of the distribution functions of charged particles as well as self-consisting electric field for two distinct on principle situations. In these situations, the initial distributions of electric charge density have been different. The first situation corresponds to homogeneous spatial distributions of the electron and positive ion concentrations at the initial moment inside the simulation region, with the plasma being electrically neutral and the electric charge density being equal to zero.

The second situation corresponds to homogeneous spatial distribution of the positive ion concentration only. The spatial distribution of the electron concentration, at the initial moment, contains a circular irregularity at the center of the simulation region. Inside the irregularity, the electric neutrality of the plasma is broken whereas, beyond it, the plasma is electrically neutral at the initial moment.

Simulation results, obtained for the first situation when the process started from the completely electrically neutral state, indicate that the spatial distributions of the electron and positive ion concentrations tend to retain a homogeneity and electrical neutrality of the plasma. However, short-scale nonregular fluctuations of the calculated parameters of the plasma arise near their initial values. In particular, the electric charge density and electric field fluctuate, with amplitudes of the fluctuations being very little. We calculate two orthogonal components of the electric field, E_x and E_y, lying in the plane perpendicular to the magnetic field. It turns out that the maximal amplitudes of the electric field component fluctuations do not exceed a value of 10^{-5} V/m at all grid cells of the simulation region.

It is of interest to consider a decrease of electron concentration, n_e, relatively to the initial value of the nondisturbed electron concentration (equal to the positive ion concentration), n_0, that is, the ratio $(n_0 - n_e)/n_0$, which will be referred to as a relative decrease of the electron concentration. The results of calculations indicate that the maximal amplitude of this quantity does not exceed a value of 10^{-5} at all grid cells of the simulation region (Figure 1). At one separate point of the simulation region, the calculated parameters of the plasma fluctuate near their initial values (Figure 1, middle curve).

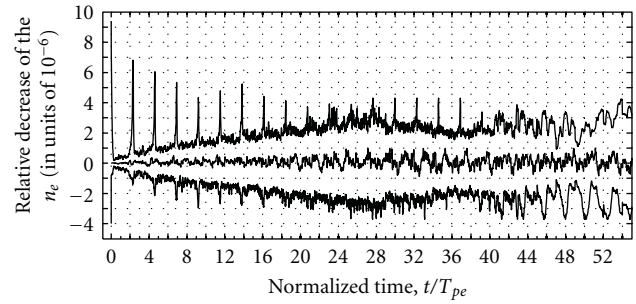

FIGURE 1: The time variations of maximal (top curve) and minimal (bottom curve) values of the relative decrease of the electron concentration, computed at all grid cells of the simulation region. Also, the time variation of the relative decrease of the electron concentration, calculated at the center of the simulation region (middle curve). The results were obtained for the first situation with the start from the completely electrically neutral state. The values are given in units of 10^{-6}. The normalized time, t/T_{pe}, that is, the time in units of the equilibrium period of Langmuir oscillations of electrons, T_{pe}, is shown on the abscissa.

One of the physically significant parameters of the plasma, filling in a volume X, is a potential energy of the plasma

$$W_{\text{pot}}(t) = \frac{1}{2} \int_X \rho \cdot \varphi \, dx, \tag{4}$$

where ρ and φ are the same quantities as in (2). Let W_{kin}^0 be the initial kinetic energy of electrons filling in the volume X. A normalized potential energy of the plasma may be defined as $W_{\text{pot}}(t)/W_{\text{kin}}^0$.

Results of simulation, obtained for the first situation with the start from the completely electrically neutral state, indicate that the normalized potential energy of the plasma fluctuates (Figure 2). It is seen that the amplitudes of these fluctuations for the first situation did not exceed a value of $13 \cdot 10^{-11}$ (Figure 2). The period of plasma parameters fluctuations of shortest duration is about $(0.1\text{-}0.2) \cdot T_{pe}$. Besides, fluctuations with other periods may take place in the simulation results, in particular, with the equilibrium period of Langmuir oscillations of electrons, T_{pe}, and period of cyclotron oscillations of electrons, T_{ce}, (Figures 1 and 2).

The presence of the short-scale nonregular fluctuations of the calculated parameters of the plasma, referred to as a discrete noise, is due to the specific character of the applied macroparticle method, with the fluctuation amplitudes being conditioned by the number of macro-particles used in the calculations. It can be noticed that, in the present calculations, we use the discrete 2D2V Maxwell distribution simulated by 2^{11} macro-particles with 16 levels of energy and 128 points for azimuth angle of velocity, which were uniformly located in space in a square having the side length of $0.5 \cdot \lambda_{De}^0$.

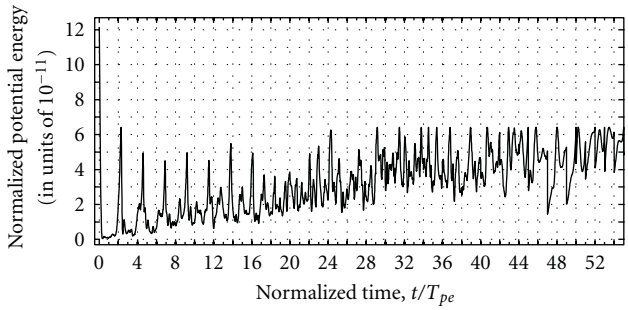

FIGURE 2: The time variation of the normalized potential energy of the plasma filling up all simulation region, $W_{\text{pot}}(t)/W^0_{\text{kin}}$. The results were obtained for the first situation with the start from the completely electrically neutral state. The values are given in units of 10^{-11}. The normalized time, t/T_{pe}, that is, the time in units of the equilibrium period of Langmuir oscillations of electrons, T_{pe}, is shown on the abscissa.

It should be emphasized that the amplitudes of the fluctuations, obtained for the first situation when process started from the completely electrically neutral state, characterize the accuracy of the applied numerical method that cannot be exceeded in following calculations. The determination of this accuracy is one of the goals of performing calculations for the first situation corresponding to homogeneous spatial distributions of electrons and positive ions inside the simulation region at the initial moment.

Let us consider the results of simulation, obtained for the second situation when, at the initial moment, the spatial distribution of the electron concentration contains a circular irregularity at the center of the simulation region, with the spatial distribution of the positive ion concentration being homogeneous in all simulation region. Calculations were made for the case in which the initially created irregularity has the cross-section diameter of $12\lambda^0_{De}$, where λ^0_{De} is the Debye length of the plasma. Inside this irregularity, a part of electrons traveled from the internal circle, having the diameter of $6\lambda^0_{De}$, into the external ring, surrounding the internal circle. Calculations were performed for the case in which the relative decrease of the electron concentration, $(n_0 - n_e)/n_0$, is equal to 0.2 in the internal circle at the initial moment. In other words, 20 percent of electrons were displaced from the center of the irregularity to its periphery. As a consequence of this displacement, an excess of positive charge appeared in the internal circle of the irregularity, while an excess of negative charge appeared in the ring surrounding it. The configuration of the initial irregularity in the plane perpendicular to the magnetic field is presented in Figure 3(a). It can be noticed that the shape, dimensions, and disturbance of the electron density of the considered irregularity correspond to the parameters of the small-scale irregularities, described in the study by Wong et al. [22].

The time evolution of the initially created irregularity was numerically simulated using the mathematical model described above. Simulation results indicate that, after initial moment, the spatial distribution of the electron concentration changes essentially while the positive ion concentration is retained practically invariable. It turns out that the initially created irregularity vanishes completely during a short period, with the plasma becoming electrically neutral in all simulation region at the moment near to the equilibrium period of Langmuir oscillations of the electrons ($t \approx T_{pe}$). Figure 3(b) illustrates this condition. Further calculations indicate that the changes in the electron concentration are continued and, after a short period, the irregularity arises again to a moment of about $(2.2\text{-}2.3)T_{pe}$. This fact is illustrated by Figure 3(c). It can be seen that the recovered irregularity almost completely coincides with the initial one presented in Figure 3(a). Later, the cycle of vanishing and recovering of the irregularity is repeated again and again (see Figures 3(d) and 3(e)). Thus, the time evolution of the initially created irregularity is accompanied by periodic vibrations. The period of these vibrations is approximately a factor of 2.3 larger than the equilibrium period of Langmuir oscillations of electrons, with the former period coinciding with the period of cyclotron oscillations of electrons, T_{ce} . In the course of time, the amplitudes of the vibrations of the electron concentration and electric field decrease smoothly, with the irregularity decaying little by little.

It is of interest to note that, in the process of evolution, additional almost symmetrical alternate rings with an excess of charge of different sign begin to appear around the initial irregularity situated in the center of the simulation region. Such rings are seen in Figure 3(e) where the spatial distribution of the relative decrease of the electron concentration, obtained after approximately 2 oscillation periods, is shown. In the course of time, these additional rings begin to fill up all simulation region, with the irregularity center remaining immovable. This condition can be seen in Figure 3(f), illustrating the spatial distribution of the relative decrease of the electron concentration, calculated after approximately 6 oscillation periods.

Simulation results, obtained for the second situation when the temporal evolution of the initially created irregularity was studied, indicate that the calculated parameters fluctuate at separate points of the simulation region. Examples of fluctuating parameters of the plasma are presented in Figure 4. It is seen from the bottom panel of Figure 4 that the amplitudes of the electric field fluctuations, obtained for the second situation when the initially created irregularity was studied, are much more than those, obtained for the first situation when the process started from the completely electrically neutral state (Figure 4(a)). In the first situation, they did not exceed a value of 10^{-5} V/m while, in the second situation, they can exceed a value of 0.2 V/m (Figure 4). In the second situation, it is easy to see that the electric field fluctuations possess of two main periods, namely, the period of Langmuir oscillation of electrons and period of cyclotron oscillations of electrons (Figure 4(b)).

Results of simulation, obtained for the second situation, indicate that the normalized potential energy of the plasma can fluctuate. From Figure 5, it is seen that the normalized potential energy of the plasma, $W_{\text{pot}}(t)/W^0_{\text{kin}}$, demonstrates periodic damped vibrations. The period of the vibrations, having maximal amplitudes, is close to the period of cyclotron oscillations of electrons, which is approximately

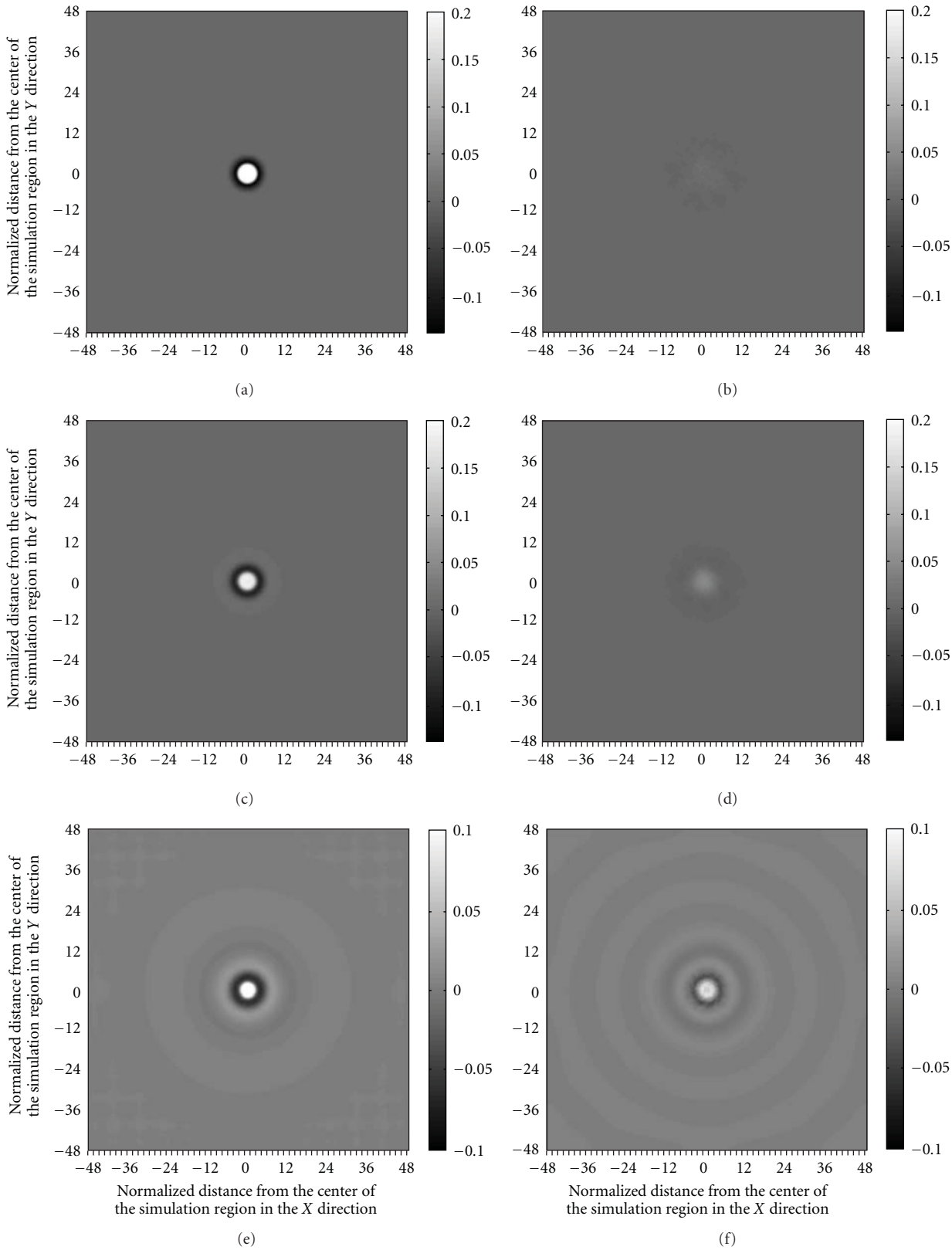

Figure 3: The calculated spatial distributions of the relative decrease of the electron concentration, $(n_0 - n_e)/n_0$ in the plane perpendicular to the magnetic field. The normalized distances, $\mathbf{X}/\lambda^0_{D_e}$ and $\mathbf{Y}/\lambda^0_{D_e}$, that is, the distances in units of the Debye length, $\lambda^0_{D_e}$, from the central point of the simulation region are shown on the horizontal ($\mathbf{X}$) and vertical ($\mathbf{Y}$) axes. The results, obtained for the second situation when the temporal evolution of the initially created irregularity was studied, are given for the following moments: (a) $t = 0$, (b) $t = T_{pe}$, (c) $t = 2.2 \cdot T_{pe}$, (d) $t = 3 \cdot T_{pe}$, (e) $t = 4.4 \cdot T_{pe}$, and (f) $t = 14.09 \cdot T_{pe}$.

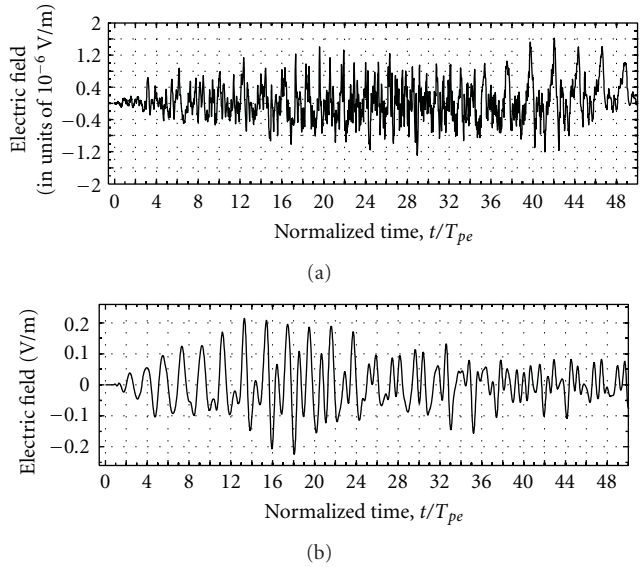

Figure 4: The time variations of one component of the electric field, namely, E_x, lying in the plane perpendicular to the magnetic field, calculated at the center of the simulation region for the first situation with the start from the completely electrically neutral state (a), also E_x, calculated at the point, displaced from the center of the simulation region in the **X** direction for a distance of sixteen Debye lengths ($16 \cdot \lambda^0_{D_e}$), for the second situation when the initially created irregularity was studied (b). The electric field components are given in units of 10^{-6} V/m in (a) and in V/m in the (b). The normalized time, t/T_{pe}, that is, the time in units of the equilibrium period of Langmuir oscillations of electrons, T_{pe}, is shown on the abscissa.

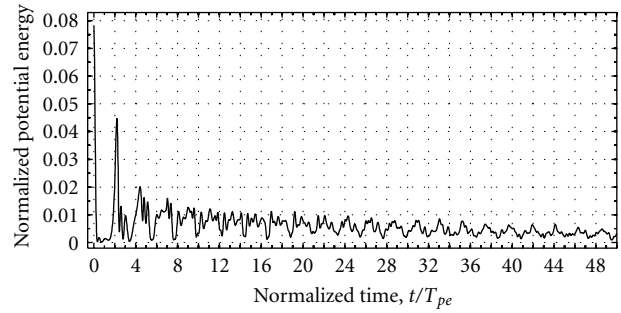

Figure 5: The time variation of the normalized potential energy of the plasma filling up all simulation region, $W_{\text{pot}}(t)/W^0_{\text{kin}}$. The results were obtained for the second situation when the initially created irregularity was studied. The normalized time, t/T_{pe}, that is, the time in units of the equilibrium period of Langmuir oscillations of electrons, T_{pe}, is shown on the abscissa.

a factor of 2.3 larger than the equilibrium period of Langmuir oscillations of electrons. The amplitude of these vibrations decreases from the initial value of about 0.08 to a quantity, approximately a factor of 10 less than the initial value, with the achieved quantity remaining almost invariable in further calculations (Figure 5). The time interval of about $35T_{pe}$ (approximately 15 vibration periods of the irregularity) is sufficient for the amplitude of the normalized potential energy of the plasma to become almost invariable. Results of simulations indicate that, during this time interval, the considered irregularity lost almost completely its initial structure, was diffused, and decayed. It should be emphasized that this time interval is much less than the mean free time of electron between successive collisions with other particles. Consequently, the process of decaying the initially created irregularity is really collisionless, with the application of the Vlasov-Poisson system of equations for the description of this process having been justified.

As was noted earlier, the applied mathematical model has been utilized for numerical simulation of the behavior of small-scale irregularities of the electron density which can exist in the magnetospheric plasma [26]. In spite of differences of plasma parameters in the magnetosphere and ionosphere, the behavior of small-scale irregularities turns out to be similar. Magnetospheric small-scale irregularities were found to decay accomplishing periodic damped vibrations. The period of the vibrations with maximal amplitudes turned out to be a factor of approximately 1.3-1.4 larger than the equilibrium period of Langmuir oscillations of electrons. The former period proves to be equal to the period of cyclotron oscillations of electrons. The time interval of approximately 20 Langmuir oscillation periods of electrons (about 15 vibration periods of the irregularity) was a characteristic time of existence of the initially created irregularity in the magnetospheric plasma at the level of about 3000 km [26]. It can be seen that, in essence, the results, presented in this paper, are similar to the results, obtained in [26].

4. Summary and Concluding Remarks

In this paper, the time evolution of the small-scale irregularities in the F-layer ionospheric plasma was numerically simulated using the two-dimensional mathematical model, developed recently in the PGI. The model is based on numerical solving the Vlasov-Poisson system of equations, with the Vlasov equations describing the distributions functions of charged particles and the Poisson equation governing the self-consistent electric field. The full implicit variant of the macro-particle method is applied for numerical solving of the system of equations, with the real charge-mass ratio for electrons having been used.

The investigated irregularities are supposed to be geomagnetic field-aligned, with their cross-section being circular. The cross-section diameters of the irregularities are much less than their longitudinal dimensions. Gradients of the plasma parameters in a plane perpendicular to a magnetic field are much more than those in the longitudinal direction in the vicinity of the irregularity. Consequently, the latter gradient may be omitted and the flow of plasma may be considered as two-dimensional in the plane perpendicular to the magnetic field.

Calculations were made of the time evolution of the distribution functions of charged particles as well as the self-consisting electric field for conditions typical for the nocturnal ionospheric plasma at the level of 300 km. Firstly,

to determine the accuracy of the mathematical model, calculations were performed for the situation corresponding to homogeneous spatial distributions of electrons and positive ions inside the simulation region at the initial moment, that is, when the process started from the completely electrically neutral state. As a consequence, the amplitudes of the so-called discrete noise of the numerical model were determined.

Secondly, the temporal evolution of the initially created irregularity was numerically simulated which has the parameters typical for small-scale irregularities in the F-layer ionospheric plasma. Simulation results indicated that, in the course of time, the irregularity decays accomplishing periodic damped vibrations.

The irregularity vanishes and recovers periodically, with its parameters fluctuating. In particular, the normalized potential energy of the plasma demonstrates periodic damped vibrations. The period of the vibrations with the maximal amplitudes is close to the period of cyclotron oscillations of electrons which is approximately a factor of 2.3 larger than the equilibrium period of Langmuir oscillations of electrons. During the process of evolution, around the initial irregularity, additional almost symmetrical alternate rings with an excess of charge of different sign began to appear. In the course of time, these additional rings filled up all simulation region.

The time interval of about 15 vibration periods of the irregularity is sufficient for the irregularity to lose almost completely its initial structure, to be diffused, and to decay. This time interval is much less than the mean free time of electron between successive collisions with other particles. Therefore, the process of destroying the initially created irregularity is substantially collisionless.

Acknowledgments

This study was partially supported by the Division of Physical Sciences of the Russian Academy of Sciences through the program "Plasma processes in the solar system" and by the RFBR Grant no. 10-01-00451.

References

[1] R. J. Moffett and S. Quegan, "The mid-latitude trough in the electron concentration of the ionospheric F-layer: a review of observations and modelling," *Journal of Atmospheric and Terrestrial Physics*, vol. 45, no. 5, pp. 315–343, 1983.

[2] J. Buchau, B. W. Reinisch, E. J. Weber, and J. G. Moore, "Structure and dynamics of the winter polar cap F region," *Radio Science*, vol. 18, no. 6, pp. 995–1010, 1983.

[3] R. W. Robinson, R. T. Tsunoda, J. F. Vickrey, and L. Guerin, "Sources of F region ionization enhancement in the nighttime auroral zone," *Journal of Geophysical Research*, vol. 90, pp. 7533–7546, 1985.

[4] R. T. Tsunoda, "High-latitude F region irregularities: a review and synthesis," *Reviews of Geophysics*, vol. 26, pp. 719–760, 1988.

[5] A. S. Besprozvannaya, G. A. Zherebtsov, O. M. Pirog, and T. I. Shchuka, "Dynamics of electron density in the auroral zone during the magnetospheric substorm on December 22, 1982," *Geomagnetism and Aeronomy*, vol. 28, no. 1, pp. 66–70, 1988.

[6] D. B. Muldrew and J. F. Vickrey, "High-latitude F region irregularities observed simultaneously with ISIS1 and Chatanika radar," *Journal of Geophysical Research*, vol. 87, no. A10, pp. 8263–8272, 1982.

[7] S. Basu, E. Mac Kenzie, S. Basu et al., "Simultaneous density and electric field fluctuation spectra associated with velocity shears in the auroral oval," *Journal of Geophysical Research*, vol. 93, no. A1, pp. 115–136, 1988.

[8] E. J. Fremouw, C. L. Rino, R. C. Livingston, and M. C. Cousins, "A persistent subauroral scintillations enhancement observed in Alaska," *Geophysical Research Letters*, vol. 4, pp. 539–542, 1977.

[9] E. Martin and J. Aarons, "F layer scintillations and the aurora," *Journal of Geophysical Research*, vol. 82, pp. 2717–2722, 1977.

[10] L. Kersley, C. D. Russell, and S. E. Pryse, "Scintillation and EISCAT investigations of gradient-drift irregularities in the high latitude ionosphere," *Journal of Atmospheric and Terrestrial Physics*, vol. 51, no. 4, pp. 241–247, 1989.

[11] S. E. Pryse, L. Kersley, and C. D. Russell, "Scintillation near the F layer trough over northern Europe," *Radio Science*, vol. 26, no. 4, pp. 1105–1114, 1991.

[12] R. A. Greenwald, "Diffuse radar aurora and the gradient drift instability," *Journal of Geophysical Research*, vol. 79, pp. 4807–4810, 1974.

[13] Y. S. Dimant, M. M. Oppenheim, and G. M. Milikh, "Meteor plasma trails: effects of external electric field," *Annales Geophysicae*, vol. 27, no. 1, pp. 279–296, 2009.

[14] G. Meltz and R. E. LeLevier, "Heating the F-region by deviative absorption of radio waves," *Journal of Geophysical Research*, vol. 75, pp. 6406–6416, 1970.

[15] F. W. Perkins and R. G. Roble, "Ionospheric heating by radio waves: predictions for Arecibo and the satellite power station," *Journal of Geophysical Research*, vol. 83, no. 4, pp. 1611–1624, 1978.

[16] G. P. Mantas, H. C. Carlson, and C. H. La Hoz, "Thermal response of F-region ionosphere in artificial modification experiments by HF radio waves," *Journal of Geophysical Research*, vol. 86, no. A2, pp. 561–574, 1981.

[17] P. A. Bernhardt and L. M. Duncan, "The feedback-diffraction theory of ionospheric heating," *Journal of Atmospheric and Terrestrial Physics*, vol. 44, no. 12, pp. 1061–1074, 1982.

[18] J. D. Hansen, G. J. Morales, and J. E. Maggs, "Daytime saturation of thermal cavitons," *Journal of Geophysical Research*, vol. 94, no. A6, pp. 6833–6840, 1989.

[19] V. V. Vas'kov, Y. S. Dimant, and N. A. Ryabova, "Magnetospheric plasma thermal perturbations induced by resonant heating of the ionospheric F-region by high-power radio wave," *Advances in Space Research*, vol. 13, no. 10, pp. 25–33, 1993.

[20] G. I. Mingaleva, V. S. Mingalev, and I. V. Mingalev, "Simulation study of the high-latitude F-layer modification by powerful HF waves with different frequencies for autumn conditions," *Annales Geophysicae*, vol. 21, no. 8, pp. 1827–1838, 2003.

[21] G. I. Mingaleva, V. S. Mingalev, and I. V. Mingalev, "Model simulation of the large-scale high-latitude F-layer modification by powerful HF waves with different modulation," *Journal of Atmospheric and Solar-Terrestrial Physics*, vol. 71, no. 5, pp. 559–568, 2009.

[22] A. Y. Wong, J. Santoru, C. Darrow, L. Wang, and J. G. Roederer, "Ionospheric cavitons and related nonlinear phenomena," *Radio Science*, vol. 18, no. 6, pp. 815–830, 1983.

[23] B. Eliasson and L. Stenflo, "Full-scale simulation study of the initial stage of ionospheric turbulence," *Journal of Geophysical Research A*, vol. 113, no. 2, Article ID A02305, 2008.

[24] R. W. Hockney and J. W. Eastwood, *Computer Simulation Using Particles*, McGraw-Hill, New York, NY, USA, 1981.

[25] C. K. Birdsall and A. B. Langdon, *Plasma Physics via Computer Simulation*, McGraw-Hill, New York, NY, USA, 1985.

[26] O. V. Mingalev, I. V. Mingalev, and V. S. Mingalev, "Two-dimensional numerical simulation of dynamics of small-scale irregularities in the near-Earth plasma," *Cosmic Research*, vol. 44, no. 5, pp. 398–408, 2006.

Hindawi Publishing Corporation
International Journal of Geophysics
Volume 2011, Article ID 207514, 8 pages
doi:10.1155/2011/207514

Research Article

Effects of Abrupt Variations of Solar Wind Dynamic Pressure on the High-Latitude Ionosphere

Igino Coco,[1] Ermanno Amata,[1] Maria Federica Marcucci,[1] Danila Ambrosino,[1] and Simon G. Shepherd[2]

[1] *Istituto di Fisica dello Spazio Interplanetario (IFSI), Istituto Nazionale di Astrofisica (INAF), Via del Fosso del Cavaliere, 100, 00133 Rome, Italy*
[2] *Thayer School of Engineering at Dartmouth, Dartmouth College, 8000 Cummings Hall, Hanover, NH 03755-8000, USA*

Correspondence should be addressed to Igino Coco, igino.coco@ifsi-roma.inaf.it

Received 16 February 2011; Accepted 8 April 2011

Academic Editor: Lucilla Alfonsi

We show the results of a statistical study on the effects in the high-latitude ionosphere of abrupt variations of solar wind dynamic pressure, using Super Dual Auroral Radar Network (SuperDARN) data in both hemispheres. We find that, during periods of quiet ionospheric conditions, the amount of radar backscatter increases when a variation in the dynamic pressure occurs, both positive (increase of the pressure) and negative (decrease of the pressure). We also investigate the behaviour of the Cross-Polar Cap Potential (CPCP) during pressure variations and show preliminary results.

1. Introduction

The variations of solar wind dynamic pressure are known to affect the energy and momentum transfer from the solar wind to the magnetosphere-ionosphere system. To this respect, two important factors are the rise time and the duration of the pressure perturbation. For short rise times strong transient perturbations are observed both in the magnetosphere and in the ionosphere until a new location of the magnetopause boundary is established (e.g., [1, 2]). On the other hand, the duration of a pressure perturbation determines whether the effects will be localized or global [3]. If the duration is long enough to engulf most of the magnetosphere in the solar wind region of enhanced/reduced pressure, the pressure variation causes typical global increases of the geomagnetic field strength measured at the geostationary orbit, and on the ground at equatorial and middle latitudes, which are usually called Sudden Commencements (SC) or Sudden Impulses (SI), depending on whether they are followed by a geomagnetic storm (SC), or not (SI); in such cases, often one refers to the pressure variation itself as an SI, and this is the notation we will follow from now on.

The energy transfer from the solar wind to the magnetosphere and the ionosphere during SIs can be huge, especially when the Interplanetary Magnetic Field (IMF) has a negative B_z component. This has been shown for example by Boudouridis et al. [4], who calculated the geoeffectiveness of a number of pressure variations as the ratio between the variation of the Cross-Polar Cap Potential (CPCP), that is, the maximum electrostatic potential difference in the polar cap, as measured by DMSP ionospheric satellites, and the potential driven by the solar wind across the magnetosphere, obtained as the product of the solar wind electric field and the variation of the magnetospheric size due to the pressure pulse. The CPCP is often considered as a good proxy for the energy transfer between the solar wind and the magnetosphere-ionosphere system [5]. They found that the geoeffectiveness, or the solar wind-magnetosphere-ionosphere coupling efficiency can increase by about 80% during a pressure variation with negative IMF B_z. Moreover, some case studies have shown that even when IMF B_z is positive, the occurrence of an abrupt pressure variation can favor reconnection processes in the polar cusps and stimulate energy injection in the polar cap [6, 7]. The present work is aimed at describing, from a statistical point of

view, the effects of SIs on the high-latitude ionosphere by means of Super Dual Auroral Radar Network (SuperDARN) measurements [8, 9]. Here we recall that the SuperDARN radars are based on coherent backscatter: the emitted radio signals are backscattered by density irregularities in the ionosphere, which follow the motion of the ambient plasma, so that the autocorrelation functions of the lag times of the backscattered power allow reconstruction of the Doppler velocities of the plasma structures in the ionosphere with respect to the ground. The SuperDARN radars monitor the high-latitude ionosphere in both Hemispheres simultaneously and continuously, detecting the backscattered signals along 16 directions (beams) and 75 range gates along each beam, for a total field of view of about 52° for each radar.

Auroral oval expansions to lower latitudes have been often observed after pressure variations (e.g., Zhou and Tsurutani [10]): this means the particle precipitation increases and modifies the ionospheric density. Precipitation affects the plasma gradients in the ionosphere at every spatial scale from hundreds of kilometers to meters, thus affecting the radar backscatter as well (e.g., Villain et al. [11]). The effects of geomagnetic disturbances induced by interplanetary drivers on the radar echoes have been recently investigated (e.g., Ballatore et al. [12]; Wild and Grocott [13]). A good correlation between the echo activity and the IMF B_z component and the solar wind electric field (or the reconnection rate) has been shown; furthermore, the global level of scatter seems to maximize prior to the substorm onsets and, in the nightside ionosphere, backscatter poleward of ~70° magnetic latitude is reduced, with radar echoes shifting to lower latitudes.

A previous work by Coco et al. [14] (Co2005 in the following) reported clear effects on the Northern Hemisphere (NH) SuperDARN echoes following the SIs taking into account 178 events from November 1997 until September 2000; in more detail, the authors found an increase of the echoes closely related to solar wind dynamic pressure enhancements (positive SIs), during periods with low ionospheric activity (as monitored by the AE index level). The database of the SIs has now been extended until the end of year 2004, including Southern Hemisphere (SH) radar data. In Section 2 we will briefly recall the analysis technique already used by Co2005, with some new features, and in Section 2.1 we will describe the results for the new extended database in the Northern and Southern hemispheres. A first attempt to evaluate the CPCP in a statistical way for our new set of events has been outlined in Section 3, as regards both the analysis technique and the description of preliminary results. Discussion and conclusions are presented in Section 4.

2. Data Base and Analysis Method

We selected about 300 events of pressure variations from ACE data (October 2000–December 2004) with the following characteristics:

(1) solar wind dynamic pressure roughly constant over at least 30 minutes before and after the SI ($Q \leq 0.5$ where $Q = 2\sigma_p/|p|$, $|p|$ is the average of the dynamic pressure over the 30-minute periods and σ_p is the standard deviation),

(2) $|\Delta p| > 3$ nPa, where Δp is the jump (positive or negative) in pressure,

(3) $\Delta t \leq 10$ min, where Δt is the rise (fall) time of the pressure jump.

The selection criteria aim to isolate clear pressure variations whose duration is long enough to cause a global effect on the magnetosphere-ionosphere system: a pressure discontinuity which travels on average with a speed of $300 \div 400$ km/s, covers between 80 and $120\,R_E$ in 30 minutes (point 1), thus involving the whole magnetospheric cavity in the interaction; the other criteria (points 2 and 3) are arbitrarily chosen after careful inspection of a preliminary larger data base of pressure variations and represent typical limits for shocks.

We then divided the events in two classes, Increases (Is) and Decreases (Ds) of solar wind dynamic pressure, and we took and inspected all available data of IMF and solar wind parameters in a 2-hour period centred at the event. In the previous study, for each event Co2005 calculated a delay to account for propagation from WIND position to the centre of the Earth, simply as

$$\Delta\tau(\text{ev}) = \frac{X_{\text{WIND}}}{V_{\text{SW}}(X)}, \tag{1}$$

where $X_{\text{WIN/ACE}}$ is the position of the spacecraft along the GSM X direction, and $V_{\text{SW}}(X)$ is the component of the solar wind velocity along the same direction. On this basis they defined an expected event time on the ground as $T_g = T_{\text{WIND}} + \Delta\tau$. One has to bear in mind, however, that the delay calculated as in (1) is not very accurate, due to possible propagation effects of the pressure discontinuities from L1 to Earth. For that reason a better evaluation of the delay time has been performed, looking at the response of 5 ground-based magnetometers close to the geomagnetic equator. 1-minute resolution data from these stations have been visually inspected and, when a clear SI effect (sudden increase/decrease of the H component) was detected, the time when the effect began was taken as T_g. Otherwise, T_g has been calculated as in (1), using ACE data instead of WIND.

The effects of a SI as observed at ground may result from the superposition of effects depending on various conditions in the ionosphere, in the magnetosphere, and in the solar wind; therefore, it is reasonable to group the events into subsets, to study the echo response for each of them. The most relevant parameter to group the events is the Auroral Electrojet index (AE), introduced by Davis and Sugiura [15] to monitor the occurrence of auroral phenomena and more generally magnetospheric substorms. For each event we built a data base comprising of (1) one hour of AE index (with 1-minute resolution) data centered on T_g, and (2) one hour of SuperDARN data (with 2-minutes resolution), also centred on T_g, from all the available radars in the NH and SH.

Let $M = \langle \text{AE} \rangle + \sigma$, and $Q = (2\sigma)/\langle \text{AE} \rangle$, where $\langle \text{AE} \rangle$ is the time average of AE and σ its standard deviation

calculated over a $[-30, 10]$ min interval about T_g. In this regard, a natural choice would have been the $[-30, 0]$ min interval; however, we extended it by 10 min to allow for the remaining uncertainties in the T_g determination. We define the following:

(i) *Quiet* event: an event which satisfies one of the following conditions:

(1) $M < 200$ nT,

(2) $200 \leq M \leq 300$ nT, and $Q \leq 0.5$.

(ii) *Disturbed* event: an event which satisfies one of the following conditions:

(1) $M > 400$ nT,

(2) $300 \leq M \leq 400$ nT, and $Q \geq 0.5$.

(iii) *Intermediate* event: an event which satisfies one of the following conditions:

(1) $200 \leq M \leq 300$ nT, and $Q > 0.5$,

(2) $300 \leq M \leq 400$ nT, and $Q < 0.5$.

The *Intermediate* class has the purpose of clearly separating the *Quiet* and *Disturbed* events. Consequently, *Intermediate* events, 42 in number (24 Is and 18 Ds), are excluded from the following analysis.

In Co2005 the details of the analysis are described. For each event of the data base a Rate of Scattering (RS) is calculated as a function of time, as the percent ratio of the number of detected echoes during a 2-minute time bin, and the total number of echoes over the one-hour interval of the event. We excluded the echoes coming from ground scatter and we retained only the ionospheric echoes for which the signal-to-noise ratio was greater than 6 dB, and the events for which the total number of echoes was greater than 5000. Then, a Mean Rate of Scattering (MRS) as a function of time is built for each subset of events, simply as the average over the number of events in the set, of the RS of the single events (equation $3 \div 5$ in Section 3 of Co2005). Through the standard deviation $\sigma(t_i)$ of the MRS, where t_i is a 2-minute time bin, a statistical error $\epsilon(t_i) = \sigma(t_i)/\sqrt{N}$, where N is the number of events of the set, is associated to the MRS of each bin.

2.1. Results for the Echoes Statistics. In Table 1 information about the statistics are summarized. SuperDARN coverage is less abundant in the SH with respect to the NH, and this is evident in the total number of events and echoes, practically halved in the SH for all the subsets. Moreover, one can note the number of Ds is almost half the number of Is; this stems from the nature itself of the pressure decrease phenomena: very often pressure perturbations are driven by shock fronts in the solar wind which compress the plasma ahead of them, leaving broad regions of denser plasma behind, whose contours are not so neat and sharp both in space and time. The consequence of this is that steep and strong pressure decreases are less common than increases. The definition of the RS and MRS are therefore appropriate in order to make the statistical results show up, regardless of the different numbers of echoes and events in the different subsets. Of course a risk exists that events with very few echoes influence too much the statistics: for that reason, a threshold of 5000 echoes has been set in order to accept or discard an event, which seems reasonable considering the average number of echoes per event is about 40000 for NH and 20000 for SH.

Table 1: An overview of the echoes statistics for the different subsets of the events under study. Is and Ds stand for *Increases* and *Decreases* of solar wind dynamic pressure, NH and SH stand for Northern and Southern Hemisphere.

Set of events	Number of events	Number of echoes
Quiet Is NH	73	2827600
Quiet Is SH	50	907922
Quiet Ds NH	35	1550229
Quiet Ds SH	29	621471
Disturbed Is NH	73	2490800
Disturbed Is SH	54	1091885
Disturbed Ds NH	42	1823510
Disturbed Ds SH	35	652196

Figure 1 shows the MRS as a function of the scan time, t_i, for *Quiet* events. $T = 0$ corresponds to T_g. Figures 1(a) and 1(c) refer to the NH, while Figures 1(b) and 1(d) refer to the SH; Figures 1(a) and 1(b) refer to the Is, Figures 1(c) and 1(d) to the Ds. The MRS trends show a clear rise of the echoes in both Hemispheres, and for both Is and Ds starting close to T_g, more evident for the SH.

Figure 2 shows the same quantity for *Disturbed* events, with the same arrangement as for Figure 1. The set of *Disturbed* events is far less homogeneous than the *Quiet* events set: this stems from its definition and results from a careful inspection of the single events, as well. Therefore, the MRS trends are more difficult to interpret and understand. In the NH a rising trend of the MRS is observed for both Is and Ds, starting 4-5 minutes after T_g. In the SH no clear trends can be inferred from data.

3. The Cross-Polar Cap Potential

Maps of the high-latitude CPCP have been calculated for each event using the technique of Ruohoniemi and Baker [16]: the polar cap potential contours are obtained through a spherical harmonic expansion, whose coefficients are determined through a least square fit of the measured Super-DARN line-of-sight velocities; where data coverage is poor ar absent, data from the empirical model of Ruohoniemi and Greenwald [17] (RG96) have been put in the maps. The RG96 model consists in a superposed epoch analysis of many years of SuperDARN convection velocity measurements and gives average pictures of the ionospheric convection as a function of orientation and strength of the IMF. The use of the model data in the fit is extensively explained in Shepherd and Ruohoniemi [18]: the number of model vectors added to

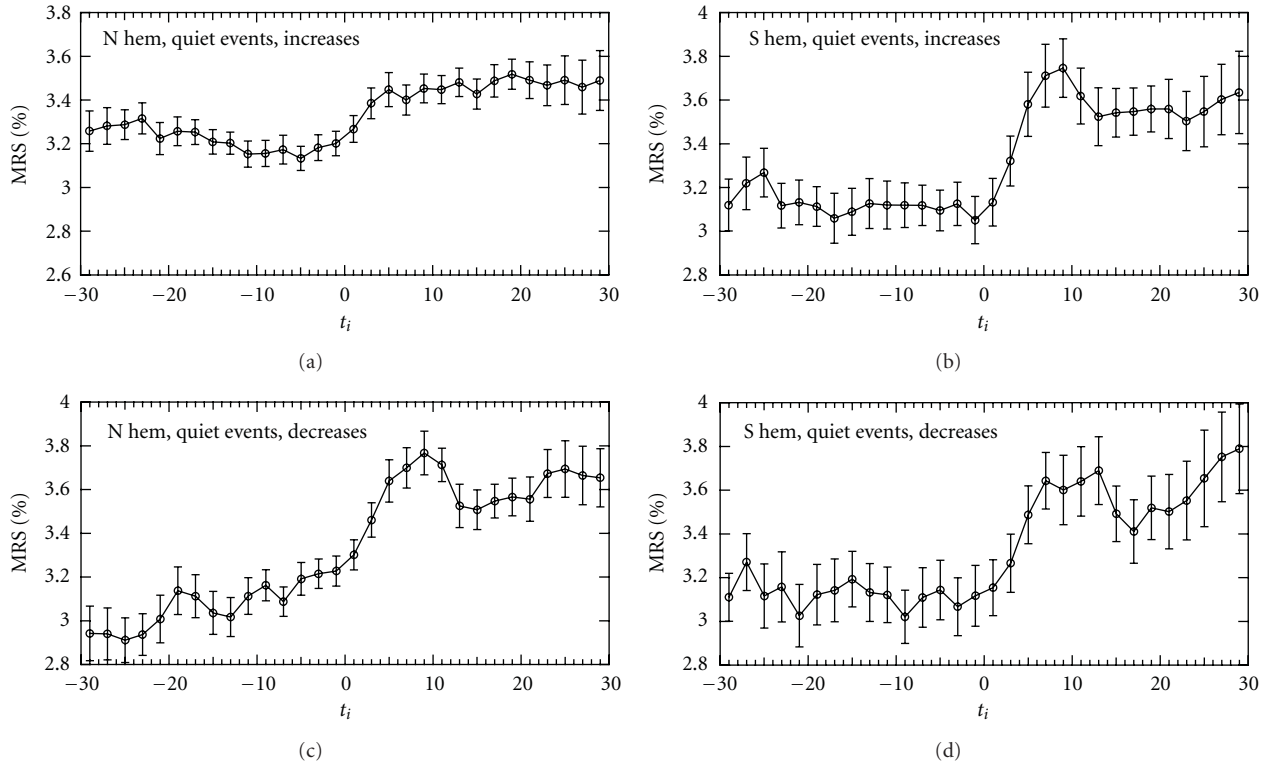

Figure 1: MRS as a function of the scan time, t_i, for *Quiet* events: (a) NH Is; (b) SH Is; (c) NH Ds; (d) SH Ds.

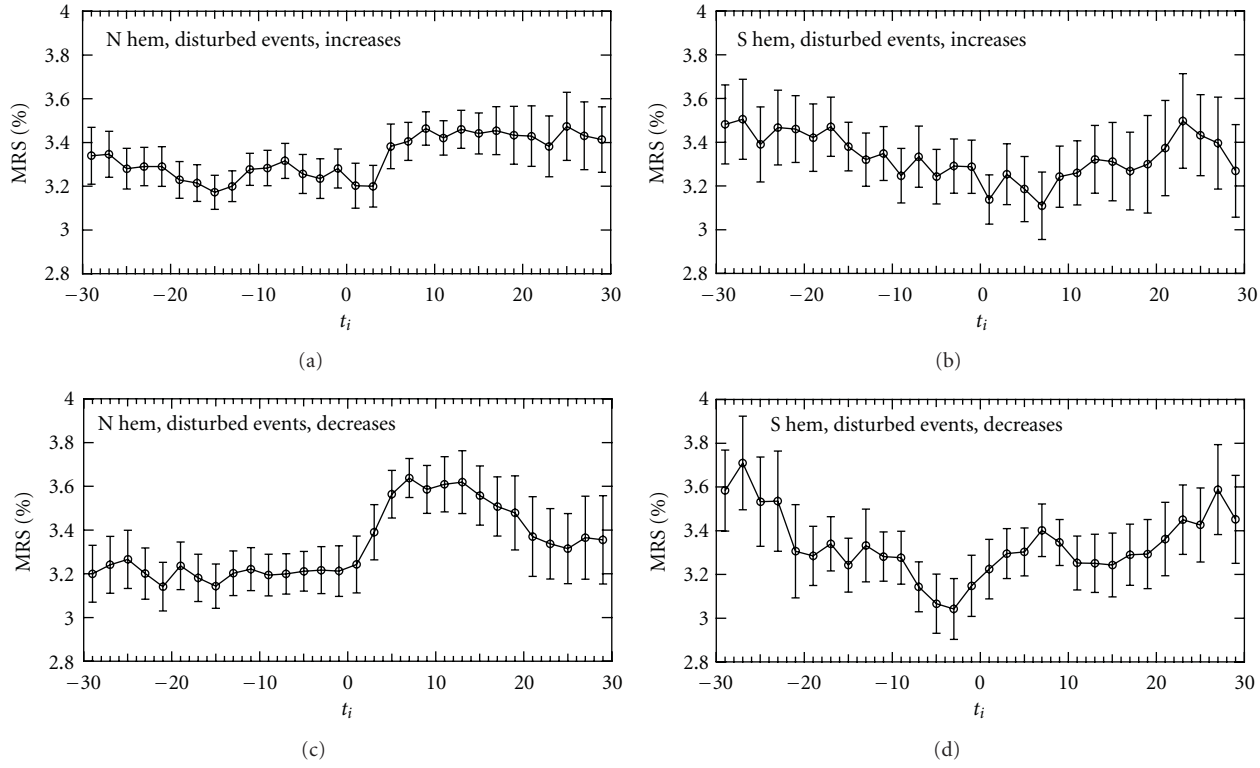

Figure 2: MRS as a function of the scan time, t_i, for *Disturbed* events: (a) NH Is; (b) SH Is; (c) NH Ds; (d) SH Ds.

Table 2: An overview of the echoes statistics for the different subsets of the events used for the PCP analysis. Is and Ds stand for *Increases* and *Decreases* of solar wind dynamic pressure, NH and SH stand for Northern and Southern Hemisphere.

Set of PCP events	Number of events	Number of echoes
Quiet Is NH	31	1077530
Quiet Is SH	21	238995
Quiet Ds NH	14	610360
Quiet Ds SH	13	362373
Disturbed Is NH	21	683244
Disturbed Is SH	21	421303
Disturbed Ds NH	13	608818
Disturbed Ds SH	15	339407

the measured vectors is the minimum required to constrain the spherical harmonic expansion at every order and in all the points of the space grid. The spatial distribution of the measured velocities is a feature even more important than the mere number of data points: the symmetries of the ionospheric convection are such that few points located in strategic regions (e.g., throats or points of flux reversal of the convection cells) often allow a better reconstruction of the whole potential pattern than a denser distribution of points concentrated in the core of a single convection cell only.

In order to test the weight of the model data with respect to the measured data, for each event of our data base, 25 convection maps were generated: one using "true" IMF data from ACE (delayed by T_g) and the others obtained imposing fixed values of IMF, in order to fall in all the different cases of the RG96 convection model. For each scan i of each event j average values $\mu_k^j(i)$ and standard deviations $\sigma_k^j(i)$ were calculated over the set of the 25 CPCP (ΔV_k) calculated from the maps. Let $N_j(i)$ be the number of ΔV_k so that $\Delta V_k > \mu_k^j(i) + \sigma_k^j(i)$ or $\Delta V_k < \mu_k^j(i) - \sigma_k^j(i)$. If $N_j(i) \leq 8$ for at least the 70% of the scans, i, the event j has been taken as good. This just means that the velocity distribution is good enough so that the calculated CPCP is reliable: data dominate over the model.

Given the new set of events, h, survived from the above criterion, for each scan, i, up to 5 CPCP over 25 are removed (the 3 lowest and the 2 highest values), and new averages μ'_{hi} and errors $\epsilon_{hi} = \sigma'_{hi}/\sqrt{20}$ have been calculated. For a given set of N events, one can finally calculate the average CPCP for each scan, $V_{\mathrm{av}}(i)$ as: $V_{\mathrm{av}}(i) = [\sum_{j=1,N} \mu'_j(i)]/N$. The associated errors are obtained using the standard propagation formula [19].

3.1. Results of the CPCP Statistics. Table 2 summarizes the characteristics of the data base after the severe selection imposed by the criteria described above. The number of events and echoes has been dramatically reduced for all the subsets, so that one cannot completely exclude that one or few particular cases influence the statistics. Moreover the distribution of echoes and events is no more homogeneous all over the years (not shown in the table), and seasonal effects can occur as well. However, in the subsets where a clear trend can be recognized, careful inspections of the single events confirmed the overall trends.

Figure 3 shows the average CPCP $V_{\mathrm{av}}(i)$ as a function of the scan time, t_i for *Quiet* events: Figure 3(a) is for NH Is, Figure 3(b) is for SH Is, Figure 3(c) is for NH Ds, and Figure 3(d) is for SH Ds. The clearest behaviours show up for the NH Is, where an average increase of 2.5 kV of CPCP is observed very well correlated with the SIs occurrence, and for the SH Ds, where the CPCP starts to increase shortly after T_g, but more gradually.

Figure 4 shows the same quantity for *Disturbed* events with the same arrangements as for Figure 3. No clear trends can be inferred from the data: the CPCP is highly variable and there are not particular changes in the curves that could be associated to the SIs occurred at T_g.

4. Discussion and Conclusions

The results for *Quiet Is* seem to confirm the previous results by Co2005, also for the SH. We propose the following interpretation: when the pressure pulse hits the magnetopause, a fast compressional MHD wave is launched, and couples to a shear Alfvén wave at a resonance position which depends on the local Alfvén speed (e.g., Samson et al. [20]); this results in a field line resonance which induces soft particle precipitation in the F region and a consequent increase of the ionospheric irregularities and of MRS. On the other hand, the precipitation of trapped electrons due to loss cone instability induced by the SIs in the magnetosphere can also account for the MRS increase.

An interesting new result which shows up from the extended data base is the average increase of the echoes in both Hemispheres for the *Quiet Ds* set. This seems to confirm the hypothesis by Araki [2] that a sudden decrease of the solar wind dynamic pressure should give rise to the same kind of current systems in the magnetosphere and the ionosphere as for a sudden increase: ground-based high-latitude magnetometers usually show the signatures of pairs of vortex-like current structures in the ionosphere, induced by Alfvén waves aligned with the geomagnetic field, and symmetric across noon. The direction of the currents (clockwise or counterclockwise) depends on local time and on the nature of the pressure pulse. Very few studies exist for decreases of the solar wind pressure: Araki and Nagano [21] showed that the Araki model is consistent for both increases and decreases of the pressure, while Takeuchi et al. [22, 23] found that Ds provoke more or less the same currents system as Is, and there are no appreciable differences in the distribution and current circulation of the vortices pairs. Nevertheless, an energy transfer from the pressure discontinuity to the ionosphere occurs all the same, capable of exciting field-aligned waves and current vortices: as a consequence, an average increase of the ionospheric irregularities is observed.

As for the *Disturbed* events sets, the new results show no evidence of the decrease of the radar echoes reported by Co2005: during high active periods, the ionosphere often

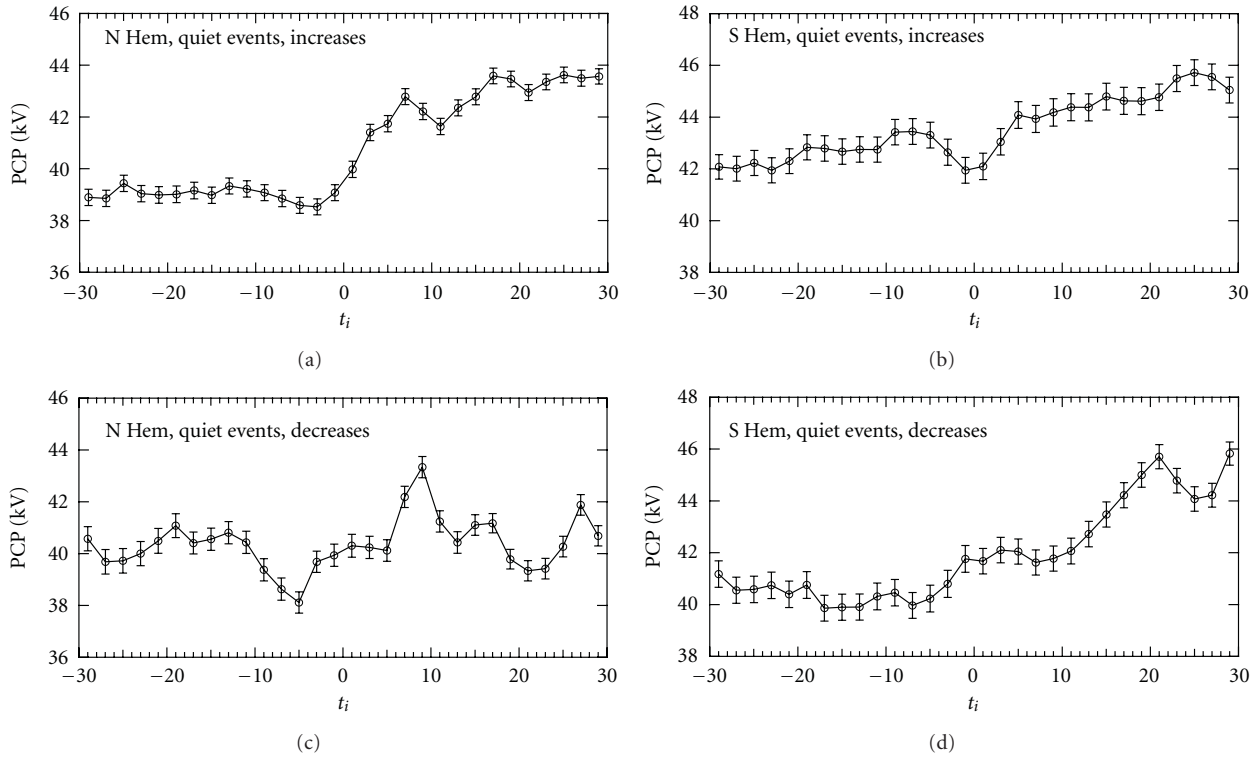

FIGURE 3: $V_{\text{av}}(i)$ (PCP) as a function of the scan time, t_i, for *Quiet* events: (a) NH Is; (b) SH Is; (c) NH Ds; (d) SH Ds.

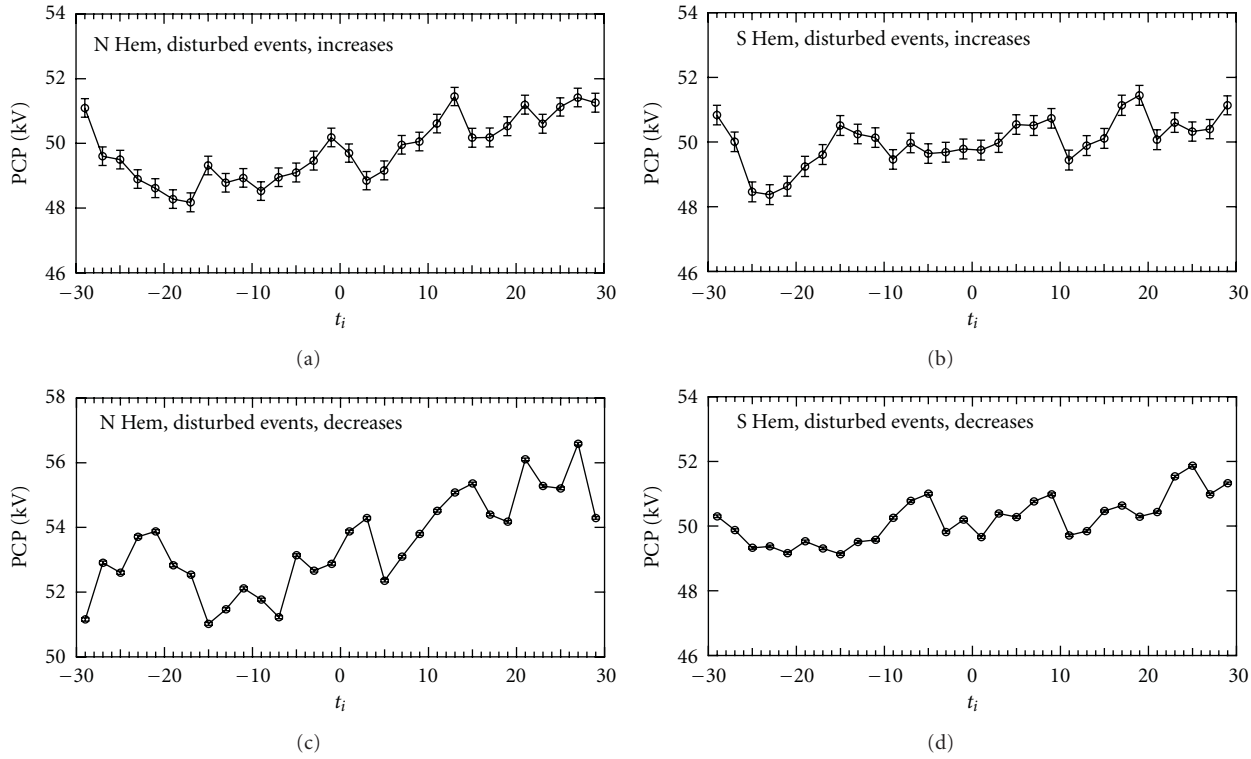

FIGURE 4: $V_{\text{av}}(i)$ (PCP) as a function of the scan time, t_i, for *Disturbed* events: (a) NH Is; (b) SH Is; (c) NH Ds; (d) SH Ds.

suffers the effects of geomagnetic storms and substorms, so that the occurrence of an SI can be masked by other phenomena already at play. Where some particular behaviour can be isolated, there is rather an increase of the echoes (NH Is and Ds). It has also to be noted that a selection of the events according to the IMF (B_z or the clock angle) has not yet been done for the new database; Co2005, for example, found that all the behaviours of the echoes were stronger when IMF B_z was negative, as one would expect, because of the greater amount of energy transferred from solar wind to the magnetosphere and the ionosphere with such IMF orientation. Furthermore, a future study will possibly join the data bases of Co2005 and that of the present work together, in order to encompass at least one complete solar cycle and allow to test the echo response as a function of solar activity and seasonal variations.

Unfortunately the statistics dramatically diminish when one attempts to take into account the CPCP, because a reliable evaluation of this quantity requires very good data coverage. Nevertheless, encouraging preliminary results have been obtained which confirm the increase of CPCP caused by a pressure pulse for *Quiet* events. Again the effect of an increased energy transfer from the solar wind to the magnetosphere and the ionosphere during SIs, is possibly masked during disturbed periods.

Acknowledgments

The authors would like to thank N. Ness and D. McComas for the use of ACE Magnetic Field Instrument and Solar Wind Experiment data, respectively; the CDAWeb team; the World Data Center for Geomagnetism, Kyoto, Japan, for providing AE index and equatorial magnetograms; the principal investigators of the SuperDARN radars in the Northern and Southern Hemispheres. This work is supported by the Italian National Program for the Antarctic Research (PNRA) under projects 2004/7.1 and 2004/7.2; I. Coco thanks the Scientific Committee for Antarctic Research (SCAR) for the financial support through the SCAR Fellowship Program 2007-2008. This work was partially supported by ASI under Contract no. I/015/07/0 "Studi di Esplorazione del Sistema Solare".

References

[1] D. G. Sibeck, "A model for the transient magnetospheric response to sudden solar wind dynamic pressure variations," *Journal of Geophysical Research*, vol. 95, pp. 3755–3771, 1990.

[2] T. Araki, "A physical model of the geomagnetic sudden commencement, in "solar wind sources of magnetospheric ultra–low–frequency waves"," *Geophysical Monograph Series*, vol. 81, no. 270, pp. 183–200, 1994.

[3] A. Boudouridis, E. Zesta, L. R. Lyons, P. C. Anderson, and D. Lummerzheim, "Effect of solar wind pressure pulses on the size and strength of the auroral oval," *Journal of Geophysical Research*, vol. 108, no. A4, 2003.

[4] A. Boudouridis, E. Zesta, L. R. Lyons, P. C. Anderson, and D. Lummerzheim, "Enhanced solar wind geoeffectiveness after a sudden increase in dynamic pressure during southward IMF orientation," *Journal of Geophysical Research*, vol. 110, no. 5, 2005.

[5] G. Chisham, M. P. Freeman, G. A. Abel et al., "Remote sensing of the spatial and temporal structure of magnetopause and magnetotail reconnection from the ionosphere," *Reviews of Geophysics*, vol. 46, no. 1, 2008.

[6] G. Provan, M. Lester, S. W. H. Cowley et al., "Modulation of dayside reconnection during northward interplanetary magnetic field," *Journal of Geophysical Research*, vol. 110, no. A10, 2005.

[7] I. Coco, E. Amata, M. F. Marcucci, D. Ambrosino, J. P. Villain, and C. Hanuise, "The effects of an interplanetary shock on the high-latitude ionospheric convection during an IMF B_y -dominated period," *Annales Geophysicae*, vol. 26, no. 9, pp. 2937–2951, 2008.

[8] R. A. Greenwald, K. B. Baker, J. R. Dudeney et al., "DARN/SuperDARN—a global view of the dynamics of high-latitude convection," *Space Science Reviews*, vol. 71, no. 1–4, pp. 761–796, 1995.

[9] G. Chisham, M. Lester, S. E. Milan et al., "A decade of the Super Dual Auroral Radar Network (SuperDARN): scientific achievements, new techniques and future directions," *Surveys in Geophysics*, vol. 28, no. 1, pp. 33–109, 2007.

[10] X. Zhou and B. T. Tsurutani, "Rapid intensification and propagation of the dayside aurora: large scale interplanetary pressure pulses (fast shocks)," *Geophysical Research Letters*, vol. 26, no. 8, pp. 1097–1100, 1999.

[11] J. P. Villain, C. Beghin, and C. Hanuise, "ARCAD3–SAFARI coordinated study of auroral and polar F–region ionospheric irregularities," *Annales Geophysicae*, vol. 4, pp. 61–68, 1986.

[12] P. Ballatore, J. P. Villain, N. Vilmer, and M. Pick, "The influence of the interplanetary medium on SuperDARN radar scattering occurrence," *Annales Geophysicae*, vol. 18, pp. 1576–1583, 2001.

[13] J. A. Wild and A. Grocott, "The influence of magnetospheric substorms on SuperDARN radar backscatter," *Journal of Geophysical Research*, vol. 113, no. 4, 2008.

[14] I. Coco, E. Amata, M. F. Marcucci et al., "Effects on SuperDARN HF radar echoes of sudden impulses of solar wind dynamic pressure," *Annales Geophysicae*, vol. 23, no. 5, pp. 1771–1783, 2005.

[15] T. N. Davis and M. Sugiura, "Auroral electrojet activity index AE and its universal time variations," *Journal of Geophysical Research*, vol. 71, p. 785, 1966.

[16] J. M. Ruohoniemi and K. B. Baker, "Large-scale imaging of high-latitude convection with Super Dual Auroral Radar Network HF radar observations," *Journal of Geophysical Research*, vol. 103, no. 9, pp. 20797–20811, 1998.

[17] J. M. Ruohoniemi and R. A. Greenwald, "Statistical patterns of high–latitude convection obtained from Goose Bay HF radar observations," *Journal of Geophysical Research*, vol. 101, pp. 21 743–21 763, 1996.

[18] S. G. Shepherd and J. M. Ruohoniemi, "Electrostatic potential patterns in the high-latitude ionosphere constrained by SuperDARN measurements," *Journal of Geophysical Research*, vol. 105, no. 10, pp. 23005–23014, 2000.

[19] J. H. Taylor, *An Introduction to Error Analysis, The Study of Uncertainties in Physical Measurements*, chapter 3, University Science Books, 1982.

[20] J. C. Samson, R. Rankin, and V. T. Tikhonchuk, "Optical signatures of auroral arcs produced by field line resonances: comparison with satellite observations and modeling," *Annales Geophysicae*, vol. 21, no. 4, pp. 933–945, 2003.

[21] T. Araki and H. Nagano, "Geomagnetic response to sudden expansions of the magne tosphere," *Journal of Geophysical Researc*, vol. 93, p. 3983, 1988.

[22] T. Takeuchi, T. Araki, H. Luehr et al., "Geomagnetic negative sudden impulse due to a magnetic cloud observed on May 13, 1995," *Journal of Geophysical Research*, vol. 105, no. 8, pp. 18835–18846, 2000.

[23] T. Takeuchi, T. Araki, A. Viljanen, and J. Watermann, "Geomagnetic negative sudden impulses: interplanetary causes and polarization distribution," *Journal of Geophysical Research*, vol. 107, no. 7, p. 1096, 2002.

Hindawi Publishing Corporation
International Journal of Geophysics
Volume 2011, Article ID 341935, 7 pages
doi:10.1155/2011/341935

Research Article

The Planetary Wave Activity in Temperatures of the Stratosphere, Mesosphere and in Critical Frequencies of Ionospheric F2 Layer

N. M. Polekh, G. V. Vergasova, E. S. Kazimirovsky, N. P. Perevalova, V. I. Kurkin, and M. A. Chernigovskaya

Institute of Solar-Terrestrial Physics, SB RAS, P.O. Box 291, Irkutsk, Russia

Correspondence should be addressed to N. M. Polekh, polekh@iszf.irk.ru

Received 28 February 2011; Revised 29 April 2011; Accepted 19 May 2011

Academic Editor: Libo Liu

A large body of experimental evidence lends credit to the existence of a close relationship between ionospheric parameters and the underlying atmosphere. Vertical-incidence ionospheric sounding data and temperature measurements at stratospheric (30 km) and mesospheric (80 km) heights have been used in investigating the interrelation between the occurrence of fluctuations with periods of planetary waves in temperature variations at different heights and in *F2* layer critical frequency variations (foF2) under low solar activity conditions for the time interval 2006-2007. The distinctive characteristics of the manifestation of common periodicities of the wave structures under consideration are discussed. The statistically significant periods of stratospheric and mesospheric temperature fluctuations vary from 11 to 49 days, whereas foF2 periodograms show higher-frequency fluctuations with periods of 5, 8, 9, and 10 days. The study revealed a similarity between periodic structures for the variations in the parameters involved.

1. Introduction

Research into ionospheric variability and its causes has attracted considerable scientific and practical interest. The chief causes of the variability and the basis for its forecast are variations in the intensity of EUV radiation, solar wind, and corpuscular fluxes and magnetosphere-ionosphere coupling. It is the extraterrestrial control of the ionosphere, which is known as coming from above. In recent decades, the idea about the close relationship between ionospheric processes and processes (primarily with the dynamics) in the lower atmosphere was established and experimentally confirmed. This implies that a part of ionospheric variability is caused by atmospheric processes. It is called "effect from below" [1–3]. This effect occurs through the generation, propagation, and dissipation of internal atmospheric (planetary, tidal and acoustic gravity) waves. These waves, together with electric fields, can influence aeronomic processes in the thermosphere, electrodynamic drifts, and, as a result, ionospheric electron density distribution causing changes in ionospheric parameters which govern the operating conditions of radio and telecommunication HF systems [4, 5]. Although it is well known that planetary waves are incapable of propagating directly up to the heights of the ionospheric F2 region [6], several observations of planetary wave-type oscillations (PWTOs) with periods (2–30 days) in parameters of F2-region ionosphere were reported [7–12]. It was assumed that magnetic activity and variations in winds in the lower and middle thermosphere (MLT) play a key role in generation of PWTO in the ionosphere [11, 12]. It has not yet been fully ascertained whether the PWs penetrate from the lower atmosphere using tides which readily penetrate to ionospheric heights, with their amplitude modulated by planetary waves as a carrier or, alternatively, these oscillations are generated directly within the *F2* layer. Pancheva et al. [11, 13] suggested that tides modulated by the planetary waves, and particularly the semidiurnal tides which propagate freely upwards in the thermosphere, are capable to transfer the PW effect to ionospheric levels. Planetary wave signatures, with periods of approximately 16, 10, and 5 days, have been observed at altitudes ranging from 30 km to 220 km over Halley (76°S, 26°W), Antarctica [14]. The authors suggested there is duct of the quasi 16-day planetary wave from stratospheric midlatitudes to mesospheric high latitudes and a strong link between planetary waves in the mesosphere and F2-region. Mukhtarov et al. [15] investigated correlations: (i) between

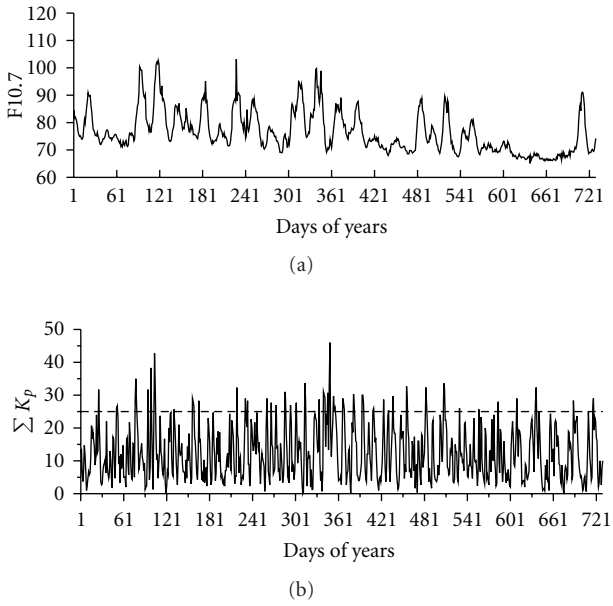

Figure 1: Variations of the F10.7 (a) and daily summary index of magnetic activity Kp (b) during 2006-2007. The quiet level is shown by a dotted line.

quasiperiodic variations of the sunspot numbers, solar wind, Bz and Kp-index with periods of PW and the analogous variability in the geomagnetic field, foF2, and total electron content (TEC) and (ii) between the PWs mainly present in the temperatures (20–120 km) with analogous variability in the geomagnetic field, foF2, and TEC. They found that 18-day wave observed in the F-region plasma (foF2, TEC) could be allocated to simultaneous 18-day planetary wave observed in the MLT region with large (~70 km) vertical wavelength. The observed oscillations with periods ~9, ~14, and ~24–27 days were approved to be of solar origin.

The objective of this paper is to investigate wave structure of temperature variations at stratospheric and mesospheric heights and in variations of critical frequencies of ionospheric F2 layer (foF2) over East Siberia during the solar minimum period of 2006-2007. This period includes few solar terrestrial disturbance events which furnishes an excellent opportunity to study the influences of the processes "from below" on ionospheric electron density variations.

2. Technique and Results

Figure 1 shows change of the flux of a solar radio emission on a wave of 10.7 cm (F10.7) which is the index (proxy) of solar activity. It is evident, that F10.7 does not exceed 110 (in units 10^{-22} W/(Hz·м^2). Figure 1(a) plots the variations of the daily summary index of magnetic activity, Kp. The dotted line shows a quiet undisturbed level. It is possible to identify several intervals characterized by higher magnetic activity (March-April 2006 and December 2006) when moderate and stronger magnetic storms were observed. Except for these intervals, the levels of magnetic activity corresponded to quiet or weakly disturbed magnetic conditions.

For the analysis we used variations of the atmospheric temperature at heights of 30 and 80 km that corresponds to level of pressure 10 hPa and 0.01 hPa, respectively. These data were obtained by means of the scanning Microwave Limb Sounder (MLS) installed aboard the EOS Aura spacecraft [16]. The Aura EOS satellite is a part of the "A-Train" mission. These satellites, intended for observation of the Earth and situated on the orbits with close parameters, make it possible to carry out unique comprehensive investigations. They fly one after another above the same regions of the Earth with an interval of 15 min and form the database for creation of a common image of the global climate changes. The satellites have a polar orbit (a period of rotation is about 100 min with a height of 705 km). The spatial coverage is almost global (from −82° to 82° by the latitude). Vertical profiles are measured with an interval of ~25 s every 1.5° (~165 km) along the orbital trajectory. About 15 flies of the satellite are carried out during a day. The MLS scans the Earth limb in the flight direction, recording the microwave emission in five spectral bands (at frequencies of 118, 190, 240, 640 GHz and 2.5 THz). The data of MLS measurements are used for retrieval of profiles of the chemical composition, relative humidity, and temperature of atmospheric areas from the troposphere and stratosphere up to the upper mesosphere as functions of height of isobaric surfaces represented in hPa. The data of MLS measurements are used for retrieval of temperature profiles from the troposphere and stratosphere up to the upper mesosphere as functions of height of isobaric surfaces represented in hPa (http://disc.sci.gsfc.nasa.gov/Aura/MLS/). The effective range is from 316 to 0.001 hPa (about 9–92 km); the accuracy in temperature measurements is 0.5–2 K; the vertical resolution is about 3 km. The computer code is devised, which enables obtaining the two vertical profiles of temperature over given point using input parameters: coordinates of point (latitude and longitude), distance to the satellite orbit, and local time (day or night) depending on ascending or descending satellite orbit. Analysis of the temporal and altitude temperature variations in stratosphere, and mesosphere for the Irkutsk region (52°N, 104°E) over the period from August 2004 to March 2008 has been made by Chernigovskaya [17], and considerable differences of the temperature regimes in the middle atmosphere for the summer and winter seasons periods were revealed. The distribution of temperature during 2006-2007 at heights of 30 and 80 km over Irkutsk region is shown in Figures 2(a) and 2(b).

To study wave structure in F region we used hourly values of the critical frequencies (foF2), obtained at Irkutsk station (52.5°N, 104°E) during 2006-2007. To order to eliminate the main diurnal variation in this parameter we used deviations of observed foF2 from sliding 27-day median (ΔfoF2). As an example variations of ΔfoF2 during 2006-2007 relating to midnight are shown in Figure 2(c).

The high-resolution spectral analysis method of the "correloperiodogram" was selected to determine the prevailing periodicities in foF2 and stratospheric and mesospheric temperatures. This algorithm devised by Kopecky and Kuklin [18] was widely used in the studies of periodic processes in atmospheric and ionospheric parameters [19–21]. The

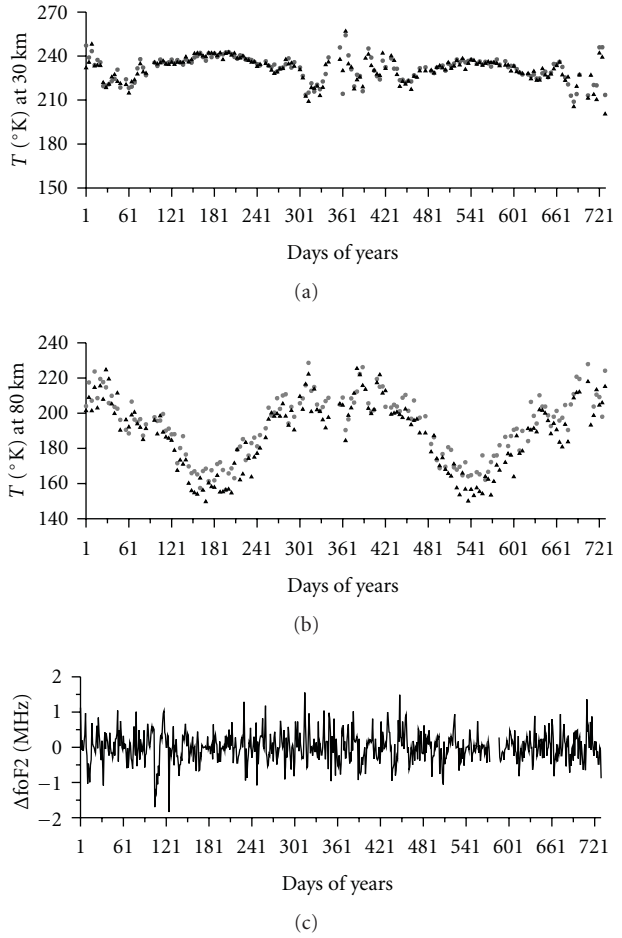

Figure 2: The distribution of temperature during 2006-2007 at heights of 30 km (a) and 80 km (b) over Irkutsk: grey circles—day temperature, triangles—night temperature and deviations of foF2 from median, concerning local midnight (c).

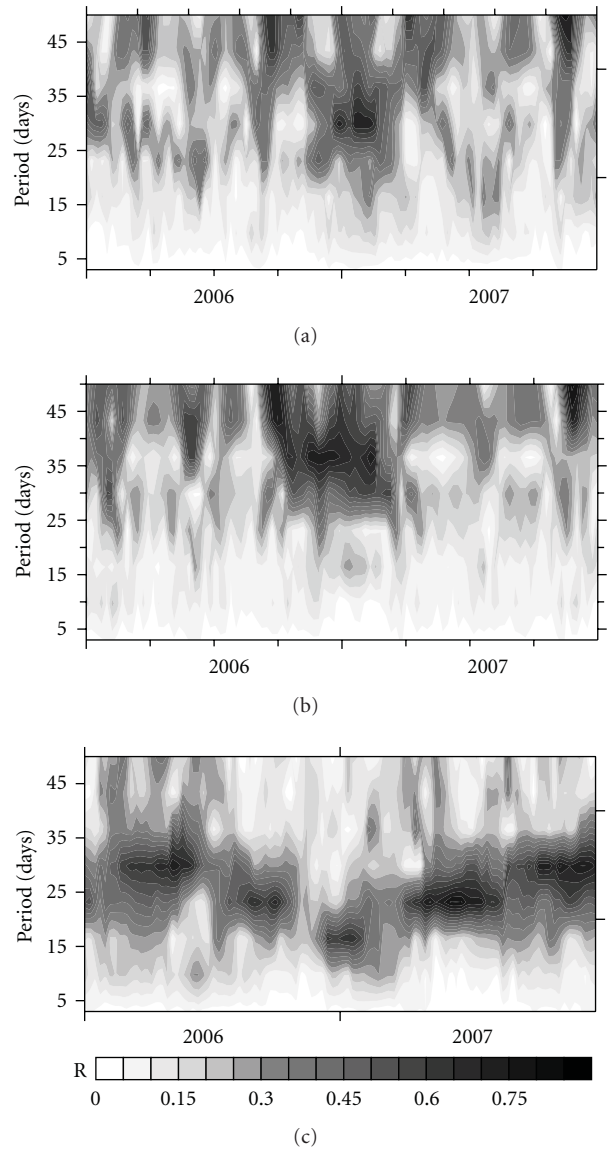

Figure 3: Periodogram spectra of stratospheric temperature (a), mesospheric temperature (b), ΔfoF2 (c) in the period range of 5–50 days. Statistical significance level corresponds to $R \geq 0.3$.

validity of the resulting periodicities was verified from the 0.95 computer confidence level by using the Fisher test method.

By applying the correloperiodogram method to a 2-year-long series of temperature variation observations, it was received that significant fluctuations with periods >15 days were present in stratospheric temperature variations, and there were no fluctuations with the periods <15 days. No statistically significant periods of fluctuations were revealed in mesospheric temperature variations for the interval concerned. It does not mean that the fluctuations with periods of planetary waves may not exist in mesosphere. As shown in [14, 22], waves with periods of 5–20 days must exist in the mesosphere, but their amplitudes must be small compared to the long-period waves, and therefore their amplitudes are not significant. As far as the foF2 variations are concerned, periodic structure is clearly pronounced: fluctuations with statistically significant periods of 2, 3, 5, 9, 14, 16-17, 18-19, 22-23, 24-25, 28-29, and of more than 30 days were revealed.

Subsequently, in examining the seasonal features of the occurrence of fluctuations with periods of planetary waves we used a so-called "dynamic correloperiodogram method" [19, 20]. We generated time series of the same length corresponding to the midday and midnight hours. Using the "time window" involving 90 values (three months) with a subsequent step of sliding equal to 5 days, we calculated the periodograms. Thus 637 periodograms were obtained for each parameter. Figure 3 provides the results from such a dynamic periodogram analysis that was applied to time series of stratospheric and mesospheric temperatures and to deviations of critical frequencies corresponding to the midnight hours. The statistically significant periods of 11 to 49 days were detected. The comparison to results in Figure 3 points out a difference between the characteristics of PWTO in the ionosphere, the mesosphere, and the stratosphere. As can be seen, in the stratosphere and the mesosphere the

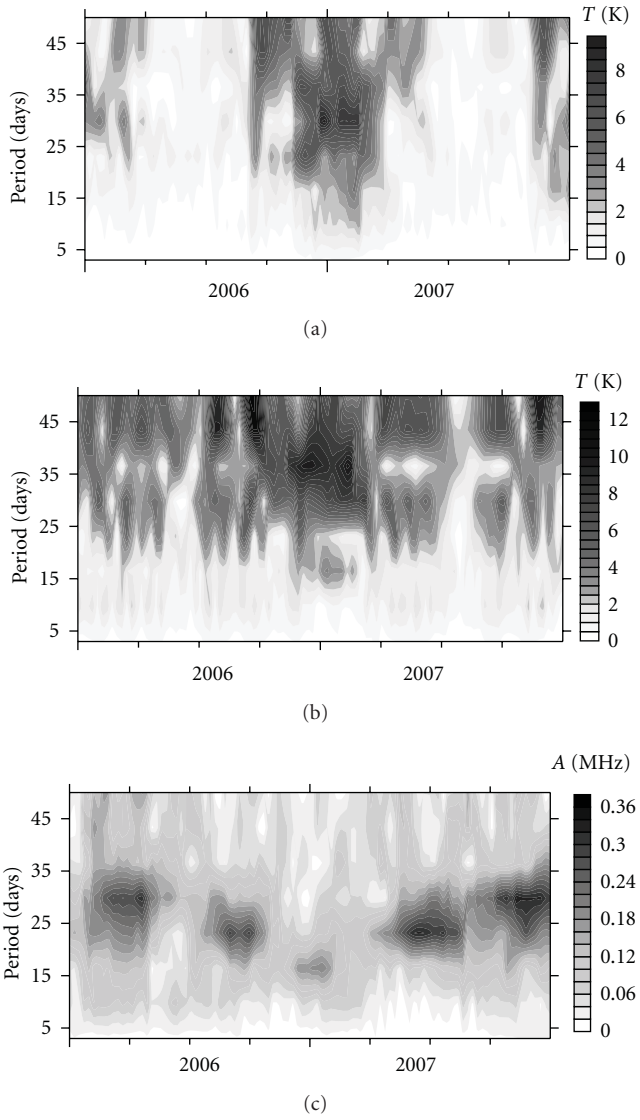

Figure 4: Amplitude spectra, calculated in period range of 5–50 days for stratospheric temperature (a), mesospheric temperature (b), and ΔfoF2 (c).

strongest wave activity occurs in the wintertime and has periods above 25 days and more, while the strongest wave in foF2 variations has periods of 8–27 days.

Figure 4 shows the oscillation amplitude with periods of planetary waves in stratospheric and mesospheric temperature and foF2 variations. Maximum values of PWTO amplitudes in stratospheric temperature variations are observed in the winter. With the increasing oscillation period, the amplitude increases to reach 7-8 K in fluctuations with periods of 25–30 days. Maximum fluctuation amplitudes in mesospheric temperature variations are observed in oscillations with periods of 40–44 days in the spring and autumn and in oscillations with periods of 25–35 days in the winter. The largest PWTO amplitudes in foF2 variations were recorded during equinoxes.

For all years considered it was determined the number of days during which the oscillations were detected. Figure 5

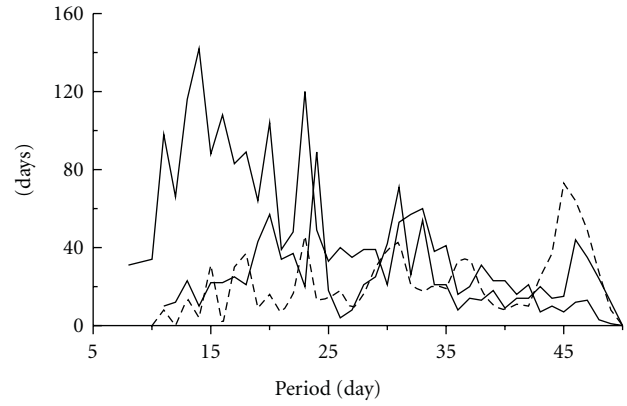

Figure 5: The occurrence of the wave oscillation with various periods in the temperature and ΔfoF2 during 2006-2007: thick line—ΔfoF2; thin line—the stratospheric temperature, dotted line—the mesospheric temperature.

demonstrates the occurrence of wave oscillations of each period. Four groups of fluctuations can be identified, namely, 16-day fluctuations (periods ranging from 13 to 19 days), 24-day fluctuations (periods ranging from 20 to 28 days), 33-day fluctuations (periods ranging from 29 to 35 days), and 43-day fluctuations (periods ranging from 40 to 47 days). It can be identified the separate group of 10-day oscillations (covering a range of periods from 8 to 12 days) in foF2 variations. Fluctuations of the first and the second groups occur more often in stratospheric temperature and, especially, foF2 variations than do the others. But they are rather uncommon in mesospheric temperature variations. Fluctuations of the fourth group with periods >40 days are dominant in mesospheric temperature variations.

In order to study the occurrence of wave oscillation of different groups, the probability of finding an oscillation of these groups for a given month has been calculated as the number of the oscillations found for corresponding month, during two years considered, averaged by the total number of these oscillations of the corresponding months of available data. Figure 6 illustrates seasonal dependency of probability of wave occurrence in parameters under consideration. The 16-day oscillations have maximum occurrence during the first half of year in stratospheric temperature variation, and in variations of mesospheric temperature during autumn: winter, while during other months their activity is small or almost disappears (e.g., in variations of mesospheric temperature). This result is a good agreement with those obtained previously [21]. There is no marked strong seasonal dependence in foF2 variations the PWTO of 16-day period. There is a trend towards increased wave activity during summer [22]. The planetary wave type oscillation of 24-day period is predominant during summer in variations of mesospheric temperature. In variations of stratospheric temperature and foF2 this wave appears during almost the entire year.

As for the oscillations with a period of 33 days, they appear almost the entire year: in the mesospheric temperature, these waves often appear during the winter and spring, in foF2 variations they occur during equinox, and in

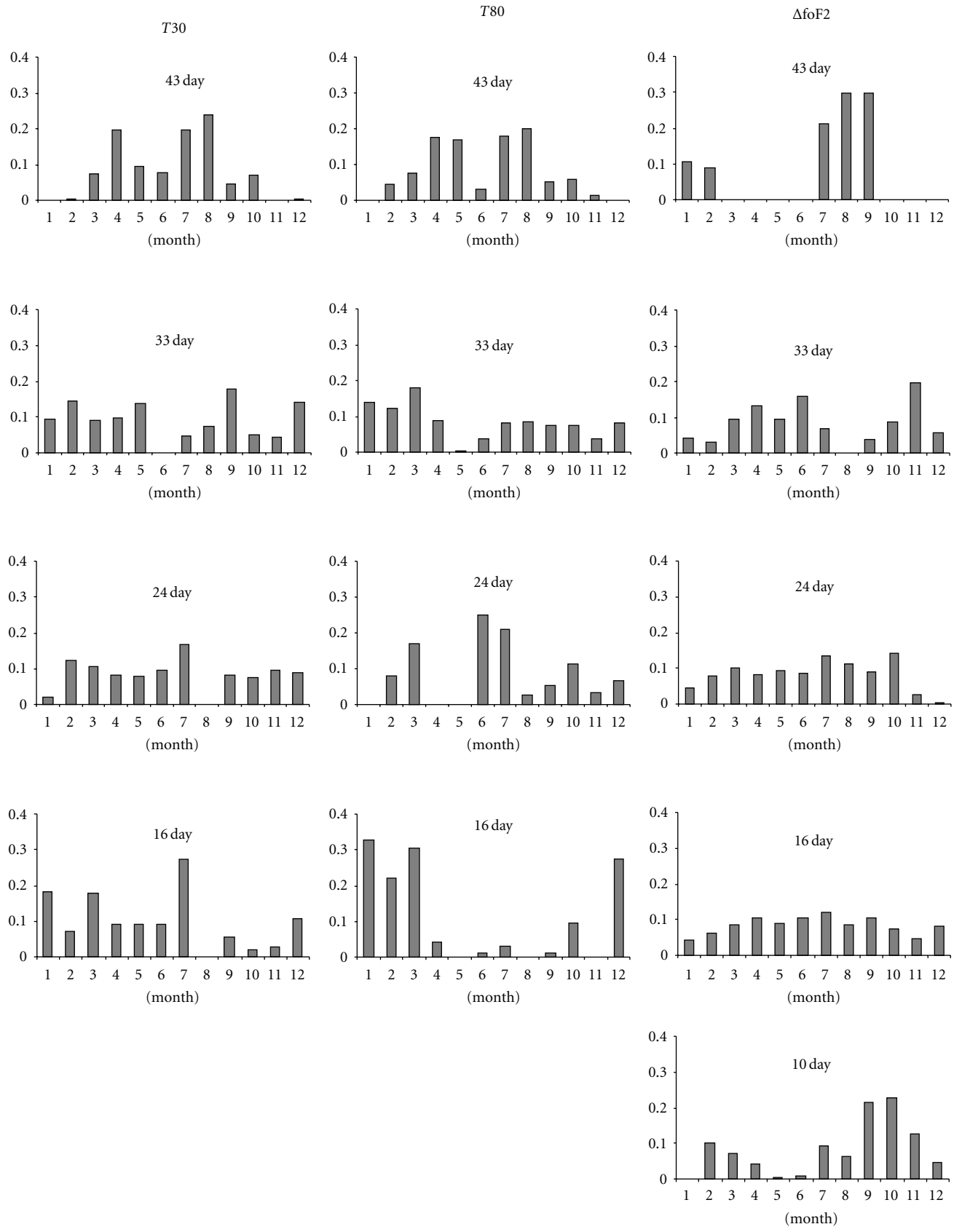

Figure 6: The seasonal dependence of the probability of wave occurrence: T30—in the stratospheric temperature, T80—in mesospheric temperature, ΔfoF2—in critical frequency deviations.

Table 1: Correlation coefficients between occurring oscillations with periods of planetary waves in variation of the temperature parameters and the ionospheric parameter for some periods.

16-day period	24-day period	33-day period	43-day period
$K_{1,2} = 0.39$	$K_{1,2} = 0.59$	$K_{1,2} = 0.17$	$K_{1,2} = 0.918$
$K_{1,3} = 0.266$	$K_{1,3} = 0.166$	$K_{1,3} = -0.54$	$K_{1,3} = 0.39$
$K_{2,3} = -0.475$	$K_{2,3} = 0.398$	$K_{2,3} = -0.41$	$K_{2,3} = 0.34$

The first parameter: the stratospheric temperature at 30 km; the second parameter: the mesospheric temperature at 80 km; the third parameter: the deviations of foF2.

variations of stratospheric temperature their wave activity is maximal during autumn equinox.

The seasonal dependence of occurrence of oscillations with periods more than 40 day shows semiannual structure the most pronounced in variations foF2.

It should be remarked that there is the seasonal dependence of occurrence of oscillations with period of 10 days in foF2 variation. These oscillations seem to be present mainly during both equinoxes, specially during autumn equinox.

For each of the selected groups of oscillations, we calculated the correlation coefficients between the number of days of fluctuations occurrence during the year by months in the variations of stratospheric temperatures with analogous variations in mesospheric temperature and in foF2 with regard to the >0.90 confidence level by the Fisher criterion (Table 1).

It was seen that for 24-day and 43-day periods of PWTO a statistically significant correlation between the occurring oscillations in the stratospheric and mesospheric temperature variations was found. In addition, we obtained a weak correlation between fluctuations with a period of 18-19 days in the stratosphere with the 17-18 days fluctuations of the electron density ($r = 0.598$). It indicates a few similarities of wave structures revealed in stratosphere, mesosphere, and ionosphere. The major similarity is the existence of the wave activity in the stratosphere, the mesosphere, and the ionosphere during winter. As shown in [8], 50% of PWTO intensity in the F2 layer ionosphere occurs due to solar variability. Prominent variations of the solar origin occur with about 27-28 days which is approximately the solar rotation period and its subharmonics. It is possible that in the winter this wave activity in F2 layer ionosphere may be enhanced by the forcing upward propagating 18-day wave with large vertical wavelength [15, 22]. But the solar influence may not only produce a positive correlation between solar parameters and ionospheric characteristics. Changes in the wind system due to solar-induced changes in temperature and pressure lead to changes in mass transport that can cause negative correlation. Because of this, the question of atmosphere-ionosphere coupling by PW remains open. The complexity of the possible relationships between the middle and lower atmospheric parameters and the ionospheric characteristics dictates a need for further investigation under national and international programs using multidisciplinary approach, based on continuous coordinated observations in order to test the hypothesis that the planetary waves in the stratosphere and mesosphere have influence on the ionosphere.

3. Summary

The activity of the planetary wave-type oscillations in the stratosphere, mesosphere, and ionosphere has been studied using temperature variations at 30 km, 80 km heights and *F2*-layer critical frequency variations (foF2) at Irkutsk (52°N, 104°E) under low solar activity conditions for the time interval 2006-2007. The spectral analysis of the wave structure in the stratospheric and mesospheric temperature variations and in the foF2 variations has revealed the existence of fluctuations with periods of planetary waves, having different amplitude characteristics. These oscillations have periods typical for planetary waves and their wave activity is the strongest during winter. There is a considerable difference: in the ionosphere the dominant periods are shorter than the typical periods of planetary waves in the stratosphere and the mesosphere.

In the stratosphere the maximum fluctuation amplitudes are observed in oscillations with periods of 20–30 days during winter. In the mesosphere maximum amplitudes are detected in oscillations with periods of 30–35 days during winter and autumn the and in oscillations with periods of 25–45 days in the winter. The largest PWTO amplitudes in foF2 variations were recorded during equinoxes.

A statistically significant correlation between the occurring oscillations with the 40 days in the stratospheric and the mesospheric temperature variations and between the occurring oscillations with the period of 18 days in the stratospheric temperature variations and in the variations of foF2 was founded.

The obtained results are in agreement with those obtained previously by other researches and provide additional information on oscillations with periods of planetary waves in the stratosphere, the mesosphere, and the ionosphere over Eastern Siberia.

Acknowledgments

This work was supported by the Ministry of Education and Science of the Russian Federation (Project no. 14.740.11.0078) and the Russian Foundation for Basic Research (Grant no. 11-05-00892-a).

References

[1] E. S. Kazimirovsky, "Coupling from below as a source of ionospheric variability: a review," *Annals of Geophysics*, vol. 45, no. 1, pp. 1–29, 2002.

[2] E. Kazimirovsky, M. Herraiz, and B. A. de la Morena, "Effects on the ionosphere due to phenomena occurring below it: a review," *Surveys in Geophysics*, vol. 24, no. 2, pp. 139–184, 2003.

[3] J. Laštovička, "Forcing of the ionosphere by waves from below," *Journal of Atmospheric and Solar-Terrestrial Physics*, vol. 68, no. 3–5, pp. 479–497, 2006.

[4] J. Laštovička, V. Fišer, and D. Pancheva, "Long-term trends in planetary wave activity (2–15 days) at 80–100 km inferred from radio wave absorption," *Journal of Atmospheric and Terrestrial Physics*, vol. 56, no. 8, pp. 893–899, 1994.

[5] H. Rishbeth, "F-region links with the lower atmosphere?" *Journal of Atmospheric and Solar-Terrestrial Physics*, vol. 68, no. 3–5, pp. 469–478, 2006.

[6] A. I. Pogoreltsev, A. A. Vlasov, K. Fröhlich, and C. Jacob, "Planetary waves in coupling the lower and upper atmosphere," *Journal of Atmospheric and Solar-Terrestrial Physics*, vol. 69, no. 17-18, pp. 2083–2101, 2007.

[7] E. M. Apostolov, D. Altadill, and R. Hanbaba, "Spectral energy contributions of quasi-periodic oscillations (2–35 days) to the variability of the foF2," *Annales Geophysicae*, vol. 16, no. 2, pp. 168–175, 1998.

[8] J. Laštovička, P. Križan, P. Šauli, and D. Novotná, "Persistence of the planetary wave type oscillations in *fo*F2 over Europe," *Annales Geophysicae*, vol. 21, no. 7, pp. 1543–1552, 2003.

[9] C. Borries and P. Hoffmann, "Characteristics of F2-layer planetary wave-type oscillations in northern middle and high latitudes during 2002 to 2008," *Journal of Geophysical Research*, vol. 115, no. 11, Article ID A00G10, 2010.

[10] M. A. Abdu, T. K. Ramkumar, I. S. Batista et al., "Planetary wave signatures in the equatorial atmosphere-ionosphere system, and mesosphere- E- and F-region coupling," *Journal of Atmospheric and Solar-Terrestrial Physics*, vol. 68, no. 3–5, pp. 509–522, 2006.

[11] D. Pancheva, N. Mitchell, R. R. Clark, J. Drobjeva, and J. Lastovicka, "Variability in the maximum height of the ionospheric F2-layer over Millstone Hill (September 1998–March 2000); influence from below and above," *Annales Geophysicae*, vol. 20, no. 11, pp. 1807–1819, 2002.

[12] J. Xiong, W. Wan, B. Ning, L. Liu, and Y. Gao, "Planetary wave-type oscillations in the ionosphere and their relationship to mesospheric/lower thermospheric and geomagnetic disturbances at Wuhan (30.6°N, 114.5°E)," *Journal of Atmospheric and Solar-Terrestrial Physics*, vol. 68, no. 3–5, pp. 498–508, 2006.

[13] D. V. Pancheva, P. J. Mukhtarov, M. G. Shepherd et al., "Two-day wave coupling of the low-latitude atmosphere-ionosphere system," *Journal of Geophysical Research*, vol. 111, no. 7, Article ID A07313, 2006.

[14] A. R. Lawrence and M. J. Jarvis, "Initial comparisons of planetary waves in the stratosphere, mesosphere and ionosphere over Antarctica," *Geophysical Research Letters*, vol. 28, no. 2, pp. 203–206, 2001.

[15] P. Mukhtarov, D. Andonov, C. Borries, D. Pancheva, and N. Jakowski, "Forcing of the ionosphere from above and below during the Arctic winter of 2005/2006," *Journal of Atmospheric and Solar-Terrestrial Physics*, vol. 72, no. 2-3, pp. 193–205, 2010.

[16] M. J. Schwartz, A. Lambert, G. L. Manney et al., "Validation of the Aura Microwave Limb Sounder temperature and geopotential height measurements," *Journal of Geophysical Research*, vol. 113, Article ID D15S11, 2008.

[17] M. A. Chernigovskaya, "Morphological features of the atmosphere temperature regime in the south region of East Siberia," in *Proceedings of the 15th International Symposium on Atmospheric and Ocean Optics/Atmospheric Physics*, vol. 7296 of *Proceedings of SPIE*, 2008.

[18] M. Kopecky and G. V. Kuklin, "About the 11-year variations of the mean life duration of a group sun spots," *Issledovaniia Geomagnetizmu Aeronomii i Fizike Solntsa*, vol. 2, pp. 167–175, 1971 (Russian).

[19] C. Haldoupis, D. Pancheva, and N. J. Mitchell, "A study of tidal and planetary wave periodicities present in midlatitude sporadic E layers," *Journal of Geophysical Research*, vol. 109, no. 2, Article ID A02302, 2004.

[20] V. D. Kokourov, G. V. Vergasova, and E. S. Kazimirovsky, "Oscillations with planetary wave periods in variations in the ionospheric parameters over Irkutsk ," *Geomagnetism and Aeronomy*, vol. 49, no. 7, pp. 172–179, 2009.

[21] G. V. Vergasova, E. S. Kazimirovsky, and N. M. Polekh, "Relation of long-period variations in the critical frequencies of the F2 layer to geomagnetic activity," *Geomagnetism and Aeronomy*, vol. 49, no. 1, pp. 63–69, 2009.

[22] M. J. Lopez-Gonzalez, E. Rogriguez, Garcia-Comas et al., "Climatology of planetary wave oscillations with periods of 2–20 days derived from O_2 atmospheric and OH(6-2) airglow observations at mid-latitude with SATI," *Annales Geophysics*, vol. 27, pp. 3645–3662, 2009.

Hindawi Publishing Corporation
International Journal of Geophysics
Volume 2011, Article ID 971302, 13 pages
doi:10.1155/2011/971302

Review Article

Electrodynamical Coupling of Earth's Atmosphere and Ionosphere: An Overview

A. K. Singh,[1] Devendraa Siingh,[2] R. P. Singh,[3] and Sandhya Mishra[1]

[1] *Department of Physics, University of Lucknow, Lucknow 226007, India*
[2] *Indian Institute of Tropical Meteorology, Pune 411-008, India*
[3] *Physics Department, Banaras Hindu University, Varanasi 221005, India*

Correspondence should be addressed to A. K. Singh, aksphys@gmail.com

Received 24 March 2011; Revised 31 July 2011; Accepted 9 September 2011

Academic Editor: Lucilla Alfonsi

Electrical processes occurring in the atmosphere couple the atmosphere and ionosphere, because both DC and AC effects operate at the speed of light. The electrostatic and electromagnetic field changes in global electric circuit arise from thunderstorm, lightning discharges, and optical emissions in the mesosphere. The precipitation of magnetospheric electrons affects higher latitudes. The radioactive elements emitted during the earthquakes affect electron density and conductivity in the lower atmosphere. In the present paper, we have briefly reviewed our present understanding of how these events play a key role in energy transfer from the lower atmosphere to the ionosphere, which ultimately results in the Earth's atmosphere-ionosphere coupling.

1. Introduction

The atmosphere of the Earth is a layer of gases surrounding the Earth that is retained by Earth's gravity. The atmosphere protects life on the Earth by absorbing the ultraviolet solar radiation, warming the surface through heat retention (greenhouse effect), and reducing temperature extremes between day and night. Based on temperature distribution, atmosphere is divided into the troposphere, stratosphere, mesosphere, and thermosphere. The temperature in the thermosphere remains almost constant (Figure 1) [1]. The stratosphere and mesosphere regions are also grouped as the middle atmosphere. The region above the middle atmosphere is called the upper atmosphere where solar radiation and other sources ionize the neutral constituents forming plasma of ions and electrons. The region extending from the mesosphere to the thermosphere is called ionosphere where plasma dynamics is controlled by the collisions between the ionized particles and neutrals as well as between the ionized particles themselves. The region above the ionosphere is known as the magnetosphere. In this region, charged particles dynamics is controlled by the Earth's magnetic field because the density collision frequency is very low. There is no sharp boundary between the upper ionosphere and the lower magnetosphere region.

The ionosphere system is mainly controlled by various external sources of forcing and number of mechanisms operative in the system to convert, transport, and redistribute the input energy. Solar extreme ultraviolet (EUV) radiation and particle energy from the sun in the form of precipitating solar wind plasma energetic particle influence from the above, while tides, planetary waves, gravity waves, electromagnetic waves in wide frequency range, turbulence, convection, and so forth from the below. Even processes taking place below/on/above the surface of the Earth also affect the ionosphere and its processes. In fact, lower atmosphere/middle atmosphere/upper atmosphere (ionosphere)/magnetosphere acts as a multi-coupled system. The coupling occurs mainly through the dynamical, chemical, and electrical processes.

The ionosphere reacts to various phenomena such as lightening discharges, functioning of high-power transmitters, high-power explosion, earthquakes, volcano eruptions, and typhoons through a chain of interconnected processes in the lithosphere-atmosphere-ionosphere interaction system. Thunderstorms play a major role in transferring energy from the atmosphere to the ionosphere [3] and in establishing

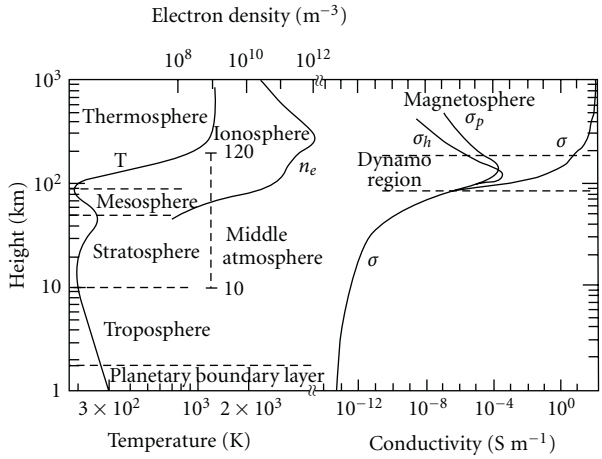

Figure 1: Variation of temperature, electron density and electrical conductivity of various atmospheric layers, after [1].

electrical coupling between atmosphere and ionosphere through the global electric circuit (GEC). The Earth's surface has a net negative charge, and there is an equal and opposite positive charge distributed throughout the atmosphere above the surface. The electrical structures of the lower atmosphere, GEC, and conductivity profile shown in Figure 1 are deeply influenced by cosmic ray flux [4], high-power transmitted waves [5–7], and earthquakes [8]. Lightening-generated whistler mode waves scatter radiation belt trapped electrons which precipitate into the lower ionosphere and result into the additional ionization and formation of ionospheric inhomogeneities [9, 10]. The powerful high-frequency transmitted waves produce ionospheric heating which, in turn, causes generation of ultra-low-frequency (ULF) and extremely low-frequency (ELF) waves [11], the formation of very low-frequency (VLF) ducts and other types of inhomogeneities [12, 13], the acceleration of ions, and the excitation of atmospheric emissions in different spectral bands [14]. The effects of these processes on the GEC (including the ionosphere) are not yet fully understood.

The convective activity in thunderstorms produces gravity waves which propagate to the lower ionosphere and deposit energy and momentum through the process of breaking and absorption and may help in the initiation of sprites and other transient luminous events (TLEs) [15–17]. The converse problem is the generation of acoustic gravity waves by sprites and other TLEs. The thermal energy deposited in the neutral atmosphere within a sprite volume ($\sim 10^4$ km^3) during short (<1 ms) duration may produce an impulsive pressure pulse that propagates laterally outward as an acoustic/gravity wave [18]. The energy deposited by a large sprite could be as large as $\sim$1 GJ [19]. The acoustic gravity wave causes spatial and temporal modulation of plasma density and electric conductivity in the ionospheric E layer. The associated wave instability causes generation of related field-aligned currents and plasma density irregularities in the upper ionosphere [20]. The satellite observations anomalous DC electric field, ULF magnetic pulsations, small scale plasma inhomogeneities, and correlated ELF emissions [21] may be considered as experimental evidence for these processes. However, the full knowledge of the interconnection between gravity waves and TLEs remains unresolved.

The purpose of this paper is to review briefly the present understanding of the link between most of the processes operative in the lower atmosphere and their electrodynamic coupling with the ionosphere. After this introduction, Section 2 deals with a more detailed description of physics of the atmosphere-ionosphere coupling. Various coupling processes including AC and DC phenomena are discussed in Section 3. Brief summary is given in Section 4 with some discussions.

2. Physics of Earth's Atmosphere-Ionosphere (AI) Coupling

Thunderstorms and lightning discharges are the main sources of electromagnetic and electrostatic energy in the Earth's atmosphere. Electrostatics involves the buildup of charge on the surface of objects due to contact with other surfaces. Although charge exchange happens whenever any two charged surfaces contact and separate, the effects of charge exchange are usually only noticed when at least one of the surfaces has high resistance to electrical flow. In thunderstorms, a rapid vertical rearrangement of deep air layers takes place. Large processes promote, shape vertical and horizontal air motions, and processes within storms control the development of rain and strong local winds. Vigorous vertical air currents and thunderstorms are a consequence of excessive warmth and moisture at low altitudes.

Thunderstorm consists of a cluster of clouds. Electrical charges generate and separate during the developmental stage of thunderstorm and are neutralized during lightning discharges. Numerous processes operating within the environment of a mature convective cloud with varying effectiveness and time dependencies affect cloud electrification [22, 23]. The charging of thunderstorms can be discussed as inductive charging or noninductive charging. An inductive process requires preexisting electric fields to induce charges on a particle so that when it rebounds from another particle, charge is separated and the field is enhanced. In the atmosphere, the fair-weather electric field resulting from positive charges in the atmosphere and negative charges on the ground could be considered as the preexisting field. However, there are experimental results from airborne instruments which require some other processes of charging [22]. Noninductive processes are independent of the presence of an external electric field. In an ordinary thundercloud, the smaller ice crystals are charged positively and move upward, whereas larger graupel particles charged negatively descend relative to the smaller particles under the action of gravity. This is the normal situation, depending on the prevailing conditions of temperature, liquid water content, and mixing in the thunderstorm. Situation in thunderstorm is quite variant, and charging process may not remain as discussed above [24]. To better understand these phenomena, further investigations

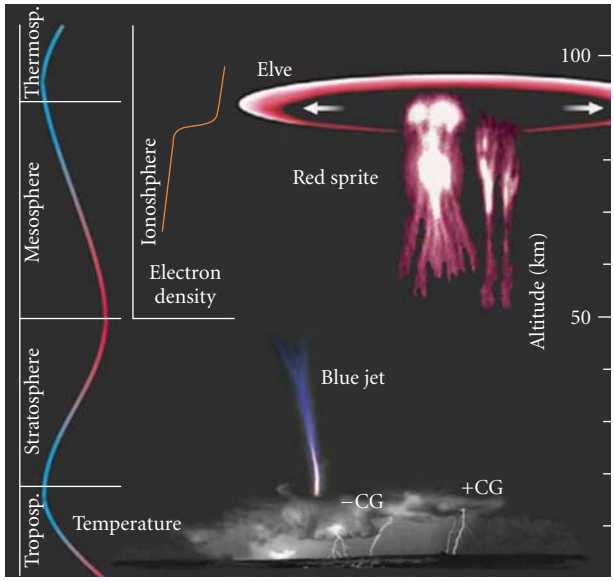

FIGURE 2: Depiction of various optical events in the atmosphere and the altitude at which they occur, credit [2].

involving both precise measurements of time development of electric field inside the cloud and simulations are required.

The charge buildup during the active period of a thunderstorm ultimately results into lightning discharge either through the processes of dielectric breakdown or runaway breakdown [29–32]. The electric field computation favours runaway breakdown mechanism [33]. However, discharge processes are not fully understood, and further observations and works are required. Lightning discharge creates charge imbalance in the cloud/thunderstorm, and as a result upward propagating quasi-electrostatic field initiates from the upper charge-layer of thunderstorm. This quasi-electrostatic field connects troposphere with the stratosphere and the lower ionosphere for a very short duration. There are about 40 to 100 lightning discharges occurring every second. Apart from the upward propagating quasi-electrostatic fields, lightning discharge current generates intense electromagnetic pulses of ~20 GW peak powers [34] which may cause significant ionospheric disturbances because of the heating and acceleration of electrons, production of ionization, optical emissions, and so forth.

The upward propagating quasi-electrostatic causes transient luminous events (sprites, blue jets/gigantic jets, elves, etc.) in the stratosphere and the mesosphere which influence the lower ionosphere with additional ionization and formation of ionospheric inhomogeneities and has motivated scientists all over the world to reexamine our understanding of the electrical processes and properties of the atmosphere. Figure 2 shows the variety of transient luminous events and the typical altitude at which they occur. Sprites may occur in cluster of short-lived (~50 ms) two, three, or more carrot-shaped emissions of ~1 km thickness over a horizontal distance of 50–100 km, with the separation between sprite elements of ~10 km [2, 35]. The upper portion of the sprites is red, with wispy, faint blue tendrils extending to 40 km or at time as low as the cloud top and bright region is in the altitude range 65–85 km [35]. They typically last for 5–50 ms and may take the form of one or more vertical columns of a few hundred meter radius for the smaller column sprites or large jellyfish-shaped structures of tens of kilometers of radius and extending from the ionosphere D-region almost down to the thunderstorm cloud tops [2, 35]. The knowledge gained from laboratory experiment of gas discharges at subatmospheric pressure has been used to understand sprite spectroscopy and associated phenomena [25]. Figure 3 shows broad identical spectral characteristics of light of positive column of the laboratory tube and sprites [25]. The difference in spectral characteristics may be due to difference in applied electric field, gas pressure, and gas composition in the mesosphere and gas tube discharges. Physical processes associated with sprites and other optical events are also associated with thunderstorm activity in the troposphere and are thought to result in the gradual build-up of conductivity changes in the lower ionosphere [36]. Liszka [37] suggested the generation of infrasound waves by sprites, whose signatures were detected by a network sensors in Sweden [38]. The shape of the chirp signature in the spectrograms of infrasound can be explained by the horizontal size of the sprite [39]. Neubert et al. [40] have concluded that sprite detection by infrared is an attractive alternative to optical detection, because it is not limited by clear viewing condition or by the absence of daylight.

Elves are concentric rings of optical emissions propagating horizontally outwards at the bottom edge of ionosphere between 75–95 km altitudes caused by the electromagnetic pulse radiated by the cloud to ground lightning discharge current of either polarity. Elves produce average electron density enhancements of 210–460 electrons cm^{-3} over large (165–220 km diameter) circular regions having an assumed 10 km altitude extent [41, 42] and hence produce perturbation in electrical conductivity of the mesosphere which can be evaluated by measuring changes in the amplitude of VLF waves [43, 44] from transmitters and propagating in the Earth-ionosphere waveguide. Mika [45] has discussed experimental data in which the incident VLF transmitter signal seems to be scattered from horizontally extended diffuse regions of electron density enhancements, most likely associated with halos or diffuse regions of the upper part of carrot sprites, rather than small-scale streamers observed at lower altitudes. The electromagnetic pulse (EMP) generating elves also create ionization [46, 47], which depends on its intensity. The individual contributions of different components of constituent gas to the optical emissions of sprite/elves are not known. An attempt should be made to investigate lightning chemistry and energetics in the region of sprites/elves. This may require future studies using a large number of narrow band filters in optical observations and kinetic modeling in theoretical analyses.

The transient luminous events provide a link between tropospheric processes in the thunderstorms and mesospheric processes in the upper atmosphere, and their studies also promise to improve our understanding of the elusive mesosphere, perhaps the least understood layer of Earth's atmosphere. Hiraki et al. [48] suggested that sprites may

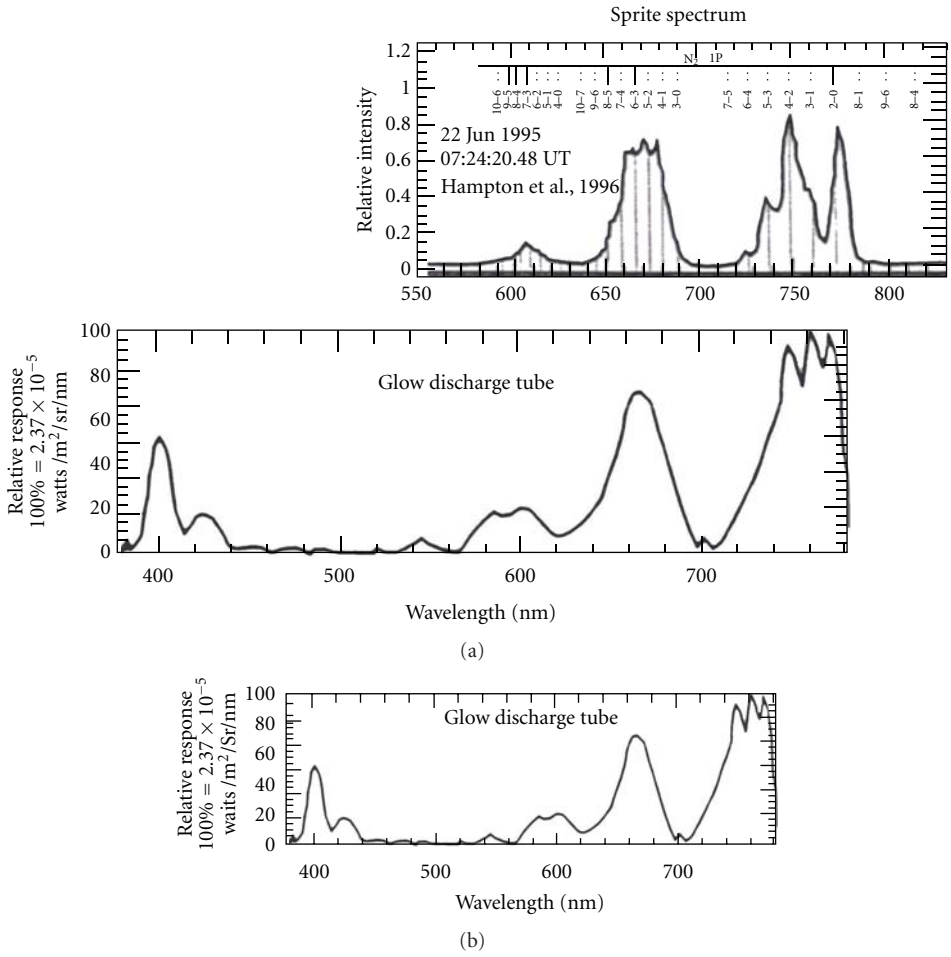

Figure 3: Comparison of optical spectra for (a) sprite in the mesosphere and for (b) the positive column of large glow discharge tube, after [25].

change the concentration of NOx and HOx in the mesosphere and lower atmosphere. These chemical changes have impact on the global cooling or heating in the middle atmosphere [49–51]. Nitrogen oxides are critical components of the troposphere which directly affect the abundance of ozone and hydroxyl radicals [52]. Ozone absorbs solar ultraviolet radiation and controls the dynamic balance of the atmosphere. NOx creates ozone in the troposphere and destroys it in the stratosphere and mesosphere and thus affects the climate. This area of investigation remains unexplored.

Lightning generated whistler mode waves propagate along geomagnetic field lines without appreciable attenuation and thus connects troposphere with the ionosphere and the magnetosphere. Whistler mode waves while propagating through the equatorial region of the magnetosphere interact with the Earth's radiation belt trapped electrons and cause their precipitation in the form of plasma inhomogeneities in the high-latitude lower ionosphere. Such a type of coupling has been confirmed in ground-based observations [53], balloon measurements [54], rocket experiments [55, 56], and satellite observations [57, 58].

Thunderstorms and lightning discharges form the major current source in GEC, essential features of which are shown in Figure 4 [26]. Solar wind interactions with the Earth's magnetic generate additional current [59], and potential gradient modulation may arise from coupling of geomagnetically-induced changes in the magnetospheric dynamo through the global circuit. Precipitations from electrified clouds are also current driver [60]. The total current flowing in the atmospheric GEC is ~1-2 kA [27]. A realistic model of equivalent circuit with capacitors, resistors, and switches is shown in Figure 5 [28]. A switch is closed for a short time if a certain type of discharge occurs. For example, switch S_2 (S_3) closes for ~1 ms when positive (negative) cloud to ground discharge occurs for a particular storm. The switch S_1 closes for a few ms when a sprite occurs above a particular thunderstorm and fair-weather time constant, $r\,C \sim 2$ min ($r \sim 200$ ohms, $C \sim 0.7$ F). Generators act over <1% of Earth's surface, and remaining ~99% of the Earth's surface region acts as a load on the circuit. The total current (I) flowing in the circuit is ~1 kA [28]. The GEC is based on the concept that the quantity of electric charge has to be conserved in the Earth's atmosphere-ionosphere-magnetosphere

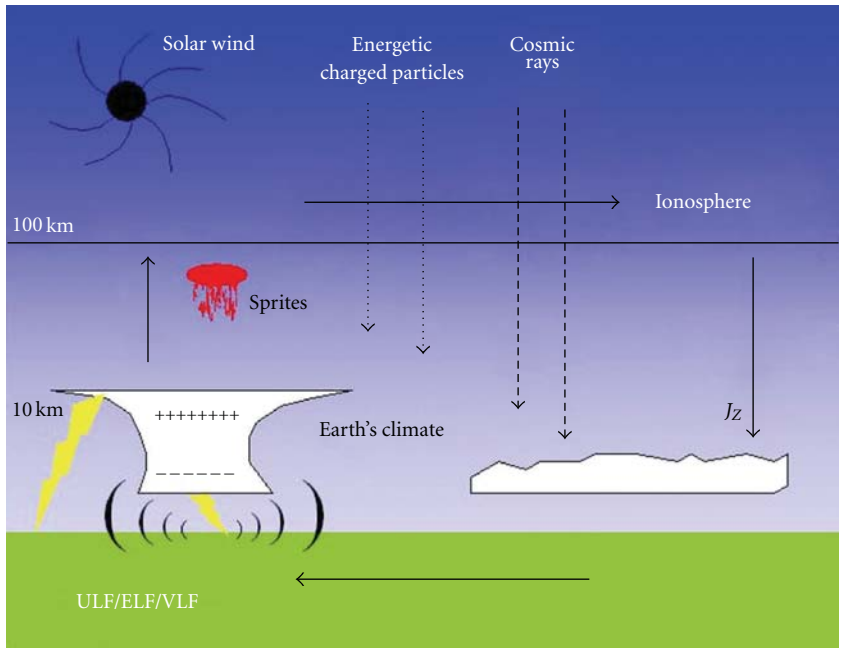

Figure 4: Essential features of the global atmospheric electric circuit [26, 27].

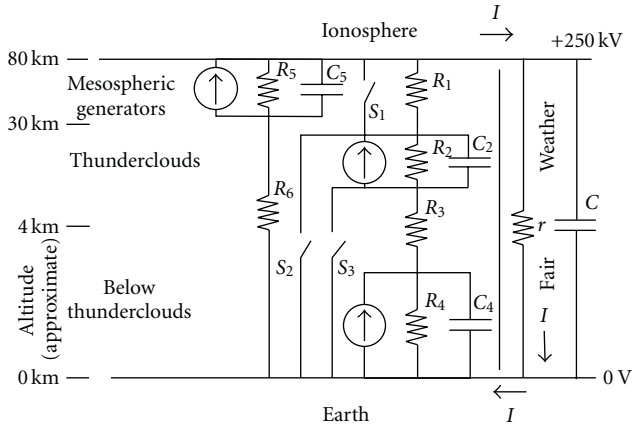

Figure 5: Diagram showing a schematic equivalent circuit for global electric circuits, credit [28].

system, that electric currents redistribute charge and that the electric currents are continuous.

The power supplied by thunderstorms is insufficient to maintain a field of magnitude observed in fair-weather regions. Rycroft et al. [61] included the generator associated with electrified clouds in the GEC model; this was found to be of the same magnitude as that due to thunderstorms. The optical phenomena occurring in the upward branch of the GEC above the thunderstorms are likely to influence only the upper atmosphere conductivity. Since they occur much less frequently (only one sprite out of 200 lightning) because of their association with intense lightning discharges [50, 62], their contribution to the ionospheric potential is very small [61]. The gigantic jets transport large quantities of negative charge discharging the atmospheric capacitor [63–66] whose effects on the ionosphere and GEC have not yet been modeled. The role of sprite/TLE events on the flow, charging/discharging of GEC, modification of electric fields near the Earth's surface remains unanswered. Since optical emissions could change electrical properties of the atmosphere and influence processes related with weather and climate, intense research activity in this area is required.

The earthquakes affect the electrodynamics of the atmosphere through the generation of electric and magnetic fields with crustal deformation, fault-failure-related piezomagnetism, stress/conductivity, electrokinetic effects, charge generation processes, thermal remagnetization, and demagnetization effects, and so forth [67]. These processes in the Earth's lithosphere relate with disturbances in the atmosphere and ionosphere. Sorokin et al. [8] discussed the processes forming the electrodynamic model of the effect of seismic and meteorological phenomena on the ionosphere. Radioactive substances and charged aerosols injected into the atmosphere modify the altitude profile of conductivity, generation of external currents, perturbation of electric field, and current in the ionospheric layer. As a result, Joule heating of the ionosphere and instability of acoustic gravity waves take place, which manifests in the formation of horizontal inhomogeneities of ionospheric conductivity. Finally, excitation of plasma density fluctuations and ULF/ELF emissions in the ionosphere, generation of field aligned currents and plasma layers, upward plasma transport, and modification of F_2-layer, and change in the ion composition of the upper ionosphere take place [68, 69]. These changes may also affect the GEC and the Earth's climate which remains a challenging problem to be solved. Figure 6 shows a schematic diagram which can be used to

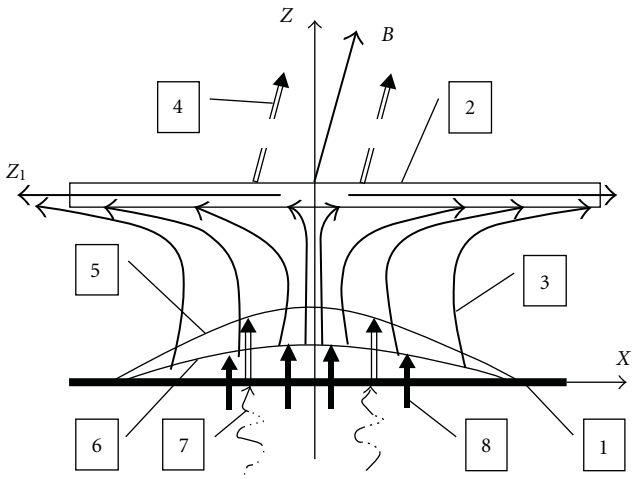

Figure 6: Schematic model used for the calculation of electric field due to the injection of charged aerosols in the atmosphere-ionosphere circuit. 1—Earth's surface, 2—ionosphere, 3—conducting current in the atmosphere and the ionosphere, 4—field-aligned current, 5—zone of upward convection of charged aerosols and external electric current formation, 6—zone of perturbation of atmospheric conductivity induced by radioactive elements emanation, 7—charged aerosols moving upward with soil gases, 8—radioactive elements emanation, credit [3].

compute external currents and enhancement of electrical conductivity in the lower atmosphere that causes an increase in the electric field in the ionosphere due to the injection of charged aerosols and radioactive elements from the solid Earth during earthquakes [3].

There are some other complex processes showing multiple scales of variability. Turbulent mixing and eddy diffusion are few other ways of transport from below. They control the relative abundances of atmospheric species in the mesosphere whose distribution tends to be independent of altitude. As part of a physical mechanism, the influence of internal atmospheric waves may be considered. The upward propagation of internal atmospheric waves (planetary waves, tides, and gravity waves) from the troposphere and stratosphere is an essential source of energy and momentum for the thermosphere and ionosphere. Weaker mesospheric gravity waves will lead to stronger winds in the upper atmosphere, which in turn will affect the ability of planetary waves to propagate, producing an additional feedback route [70]. Of course, the study of internal waves is the province of meteorology, a discipline that has enjoyed a long and independent development of its own and has its own complicated problems, sufficiently different from ionospheric physics that the two are regarded as separate but neighbouring disciplines. However, the internal waves launched by weather fronts or any other sources in the troposphere and stratosphere sometimes appear to be capable of penetrating into the ionosphere, where they dissipate most of their energy. The leakage of wave energy from the troposphere and stratosphere at least up to 100–115 km was introduced as coupling from below [71] and is considered as a mechanism of the meteorological influence on the ionosphere.

3. Various Coupling Processes

Thunderstorms directly couple the atmosphere and the ionosphere. Potential difference between the ionosphere and the Earth is maintained by thunderstorms' pumping action of lightning discharges and electrified clouds. In the Earth-ionosphere cavity, the electric field and the conduction current in the lower atmosphere are primarily controlled by ions. Ions have the characteristic parameters such as mobility, lifetime, and generation rate that vary with altitude. In recent years, some progress has been made towards understanding thunderstorm and lightning [22, 72, 73]. The essential factors in marinating the lightning discharge is the gas breakdown caused by the stored electrostatic charge in the leader head. This extends the channel into new regions. General models of the cloud charge distribution are based on electric field measurements inside a thundercloud and on the ground below the thunderstorm [75]. Earlier, an oversimplified tripolar charge structure consisting of a negative charge in the middle of the cloud, a positive charge above it, and a smaller positive charge below were widely used. Later on, a screening negative charge on the upper cloud boundary was considered [76] which are depicted in Figure 7. In the convective updraft zone of a matured thunderstorm, usually four charge layers are found and outside updraft convection region at least six charge layers are seen. Forward and rearward anvils typically contain positive charges screened with negatively charged layers. However, this model does not represent super cell storms which usually have dominant positive charge at mid-levels in place of the typical main negative charge region [77], that is, super cell storms have "inverted polarity" charge structure, and they produce mainly positive cloud-to-ground lightning. The proposed model (Figure 7) is based on balloon soundings of convective region of storms that occurred in a limited portion of the lower mid-latitudes. Its validity for storms in other mid-latitude regions, the tropics, and high latitudes are yet to be tested because of scarce *in situ* data.

The global electric circuit (GEC) links the electric field and current flowing in the lower atmosphere, ionosphere, and magnetosphere forming a giant spherical condenser [50, 59, 78], which is charged by thunderstorms and other generators to a potential of several hundred thousand volts [79] and drives a vertical current through the fair weather atmosphere's columnar resistance ($\sim 1.3 \times 10^{17}$ ohm m^{-2}). Recently, Stolzenburg et al. [30] examined electric field data of 32 balloon soundings through MCS (mesoscale convective system) stratiform regions and inferred that for 15 cases the stratiform cloud was charging the GEC, while in the other 17 cases the cloud was discharging the circuit. Thus, the overall effect of MCS on GEC could be very large or very small. Davydenko et al. [80] modeled the quasi-electrostatic electric fields and currents inside and near an isolated MCS producing positive discharges and also sprites and showed that the large ($\sim$25 A) cloud-to-ground, quasi-DC current discharges the GEC. Their full impact on the GEC and that of the positive cloud-to-ground flashes which they initiate remains to be quantified. The vertical current causes weak electrification of stratified clouds [81] and produces a vertical

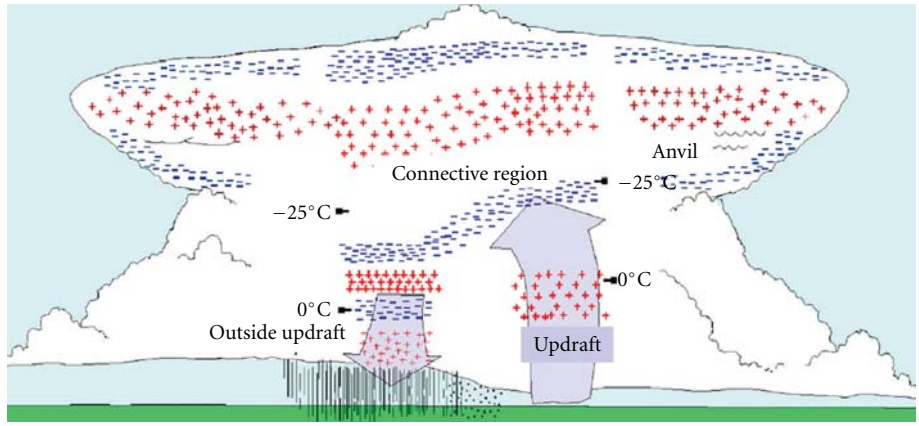

Figure 7: Conceptual model of the charge structure within an idealized isolated, mature thunderstorm based on 49 balloon sounding through different clouds, credit [22, 76].

potential gradient in the atmosphere near the Earth's surface. The circuit is closed by a horizontal current flowing through the highly conducting Earth and the ionosphere, and by vertical currents from the ground into the thunderstorm and from the top of the thunderstorm to the ionosphere.

3.1. AC Phenomena. Thunderstorm is the main source of both AC and DC coupling of the lower atmosphere and the ionosphere through lightning discharges. Return stroke of lightning discharge produces a pulse of radio energy containing waves from a few Hz up to several MHz. These signals propagate in the Earth-ionosphere wave guide over long distances (several thousand kms).The lowest frequencies of the discharge spectrum are ELF (3–3000 Hz) waves which excite the Earth-ionosphere cavity at 8, 14, 20, 26,...Hz, commonly known as Schumann resonances [82]. Resonances are being continuously excited because lightening is always occurring all over the world. Recent interest in Schumann resonance studies arose because the charge movement change (CMC) of the parent lightening discharge can be evaluated by measuring the contribution of each mode in the resonance pattern which has been used in TLEs studies [83–85]. Thus, coupling between the atmosphere near the surface of the Earth and the ionosphere can be studied on the time scale ranging from a fraction of second to less than 1 μs.

Some of the wave energy from lightning generated wave spectra propagates into the ionosphere and magnetosphere system, where it interacts with ambient plasma particles and affects the global ionospheric/magnetospheric energy budget. Waves in the very-low-frequency (VLF, 3–30 kHz) range propagate in the ducted mode along the geomagnetic field lines [86] and cause magnetospheric electron precipitation into the lower ionosphere, leading to D-region conductivity modification [87, 88]. Unducted VLF wave propagation can also take place [89]. Precipitating charged particles may participate in dissociation and ionization processes. There are VLF signatures of ionospheric disturbances associated with sprites [29, 43, 90, 91].

Hydromagnetic waves in the ultra-low-frequency (ULF, <3 Hz) propagate through the magnetosphere in one of several different modes at speeds considerably less than the speed of light. These waves interact with the ions in the ionosphere and magnetosphere. ULF waves sometimes are called magnetospheric analogues of seismic waves, which enable remote sensing of volumes from point measurements [92]. Waves in the frequency range ~0.1–5 Hz also excite the ionospheric Alfven resonator (IAR) [93, 94] which is centered on the maximum of the ionospheric F_2-region where the refractive index for Alfven waves has a maximum value. The variation of spectral resonance structure of the IAR over a solar cycle has also been studied [95]. The boundaries of IAR are at ~1000 km altitude in the topside ionosphere and in the E-region ionosphere.

The ULF-VLF electric fields were detected up to topside ionosphere over powerful Pacific Ocean typhoons [96]. However, details of the mechanisms are not yet known. Ionospheric heating due to lightning electromagnetic pulses was considered and modeled [97, 98]. Large amplitude radio waves from ground-based transmitters at VLF [99] and high frequency (HF, 3–30 MHz) [100] have been used to study ionospheric heating and modification. The associated phenomena include perturbations of electron density and temperature (increase of ionization at E-region, E-sporadic occurrence, increase of temperature, and electron density in F-region), excitation of electrostatic wave turbulence, and enhanced optical emissions.

The heating of the lower thermosphere by lightening-generated electromagnetic pulses may result into electrical breakdown and production of sprites and other optical emissions [101, 102]. The more exotic relativistic runaway (avalanche) breakdown mechanism, which can produce bremsstrahlung and gamma-rays radiations, has also been proposed and discussed [31, 103, 104]. Rowland [47] had reviewed both mechanisms. The two processes are coupled in the sprite streamer: the thermal discharge produces a beam of relativistic seed electrons that allow ignition of runaway relativistic discharge [105]. The thundercloud electric field at the lower thermosphere altitude is very transient, ~1–10 ms, consequently the observed sprite and halo phenomena are also of transient nature. The conventional breakdown

mechanism explains most observations of sprites and their associated phenomena. Gerken and Inan [106] indicated that relatively faint and diffuse sprites confined to lower altitude could be associated with very high-peak currents and short-duration lightning discharges. Adachi et al. [107] reported that the number of columns in a sprite event was proportional to the peak current intensity of positive cloud-to-ground discharges, which was not corroborated by the results of van der Velde et al. [108]. This suggests a complex relationship between sprite morphology and in-cloud lightning processes, which are not yet fully understood.

Streamers associated with sprites are needle-shaped filaments of ionization and are driven by enhanced electric fields due to charge separation in their head, and the sign of the charge in head determines polarity of streamers. Liu and Pasko [109] have modeled preionization ahead of the streamer by ionizing ultraviolet photon originating in the streamer head. Thus, they consider photo ionization to be important in determining the propagation and branching of sprite streamer. The presence of inhomogeneities in the background density could also be helpful in the formation of streamers [110]. They have also explained the polarity asymmetry in triggering sprite streamer. Blue jets sometimes appear at the top of an energetic thundercloud and propagating upwards with a vertical velocity of ~100 km s^{-1} to a maximum altitude of ~40 km or so. These are believed to be a positive streamer formed in the upward quasi-electrostatic field above the cloud [63, 101]. Many streamers originate from the surface of the leader head (both positive and negative).

Pasko and George [111] have modeled the branching streamers as fractal tree growing in three dimensions. Pasko et al. [112] reported an unusual blue jet above a relatively small thunderstorm cell in Puerto Rico, and propagating up to ~70 km altitude. Its characteristics above 42 km resembled those of sprites but having longer duration. This shows that an electrical contact was made between the top of the thunderstorm and the lower ionosphere. Gigantic jets extend from the cloud top to the ionosphere at 90 km altitude and can last up to ~0.8 sec [64, 113–115]. The observed gigantic jets were of negative polarity, produced by a normally electrified storm and therefore resembled to negative cloud-to-ionosphere discharges. Out of five gigantic jets, four events were found to be associated with ELF radio waves, while no cloud-to-ground lightning was observed to trigger these waves. This indicates that ELF waves were generated by negative cloud-to-ionosphere discharges. Each event reduces the ionospheric potential by removing 30 coulombs from the ionosphere [64], and their effect needs to be included in the GEC model.

3.2. DC Phenomena. In the atmospheric GEC, thunderstorms are thought to act as a giant battery distributed over the globe causing electric potentials up to ±100 MeV [74, 116], which are discharged in short (~1 ms) time scales by cloud-to-ground or intracloud lightning. Even upward discharges like gigantic jets also discharge the GEC. Such large potentials could produce energetic photons, X-rays [117], and even gamma rays [118], which are absorbed in the short distance in the lower atmosphere but could travel appreciable distance before being absorbed in the middle and upper atmosphere.

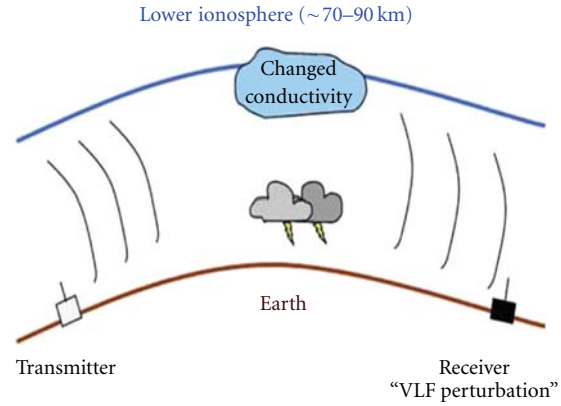

Figure 8: Diagram showing how the bottom side ionosphere and the mesosphere above a thunderstorm are probed by ground based transmitter, credit [40].

The inherent current sources [119, 120] in the mesosphere may generate large DC electric fields in the 50–70 km region [121], which has been observed via rocket measurements [122, 123] and remotely via a series of MF radar measurements [124–127]. The large DC electric fields increase the electron temperature and effective collision frequency in D-region. The enhanced electron temperature over neutral temperature violates the local thermodynamic equilibrium. During the tropospheric disturbances, tropospheric conductivity increases and the electrical coupling between the troposphere and the mesosphere results in grounding the mesospheric current source and in a significant decrease in the intensity of large mesospheric electric fields. The electron temperature and effective collision frequency decrease, which results into the D-region cooling [128, 129].

The upward electric currents associated with the charge separation process for a single active thunderstorm are ~1 A. Assuming ~1000 thunderstorms operate at a time over the entire globe, there is an upward current of ~1000 A. Theses currents charge the highly conducting ionosphere (~80 km altitude) to a potential of ~250 kV with respect to the Earth. The total charge on the plates of the Earth-ionosphere capacitor is ~2×10^5 C [59]. The electric currents (~2 pAm^{-2}) flowing from the ionosphere to the Earth's surface remote from thunderstorms depend on the electrical conductivity of the medium. The conductivity may change due to the incident flux of cosmic rays, precipitation of energetic charged particles from the magnetosphere, changes in aerosol distribution, changes in the pressure, and the temperature distribution in the troposphere. The upward quasi-electrostatic fields also change the atmospheric/lower ionospheric conductivity. Figure 8 shows the measuring principles of the change in the electrical conductivity above thunderstorms in the mesosphere and the lower ionosphere by measuring changes in the amplitudes of signals radiating from narrow band radio transmitters passing over thunderstorms region [40]. Global warming affects

distribution of aerosol, temperature, and concentration of gases in the troposphere and stratosphere and hence modifies the dynamics of the lower and the middle atmosphere [130]. These changes result into changes in thunderstorm and lightening properties. It would be interesting to study the changes produced in the GEC by the global warming phenomena.

In the study of electrical coupling of the atmosphere and the ionosphere, the latter is considered to be equipotential surface, which is not exactly true. During very active auroral conditions, the potential difference across the narrow (1° or 2° wide) auroral electrojet region may become ~100 kV. Even ionospheric dynamos may create potential differences of ~15–20 kV between low and midlatitudes. These potential differences contradict the concept of the ionosphere as an equipotential surface. Ogawa et al. [131] have studied the variation of horizontal electric field in the middle atmosphere. The issue of equipotential further complicates because spatial and temporal variations of these potentials have a variety of scale lengths and various time scales. Intense atmospheric disturbances caused by earthquakes, volcanoes, tropical storms, typhoons, and so forth also affect electrical properties of the lower ionosphere. Some definite progresses in experimental and theoretical studies of man-made and natural effects on the ionosphere have been recently made [3]. However, there is significant gap in the understanding of an origin and interconnection of many processes involved in the atmosphere-ionosphere coupling.

4. Summary

The electrodynamic coupling between the Earth's atmosphere and the ionosphere is very complex and described by the global electric circuit. Currently, many aspects are not well understood. Recent measurements show that coupling influences both the electron density and electrical conductivity. Thunderstorms are the main generators situated in the troposphere. Measurements and theoretical studies have led to some understanding of charging mechanisms and charge structures of thunderstorms, however various aspects remain unanswered. Thunderstorms are large, complex, and short-lived phenomena; the charge generation and separation mechanism and charge structure are not known, and it is difficult to model them. The electrical processes are intimately related to the cloud dynamics or motions and to the microphysics of the clouds which are incompletely known or understood. Their detailed comprehension is essential as it controls climate and its variability. For proper understanding, it is essential to make simultaneous measurements of electric parameters from different parts of thunderstorms at small time intervals.

The role of transient luminous events on the local ionospheric potentials, modification of the electric field near the Earth's surface, and charging/discharging of GEC are yet to be quantified. Even there is dispute about the breakdown mechanism involved in the mesospheric discharges generating sprites, blue jets, elves, and so forth. Lightning-generated whistler mode waves cause precipitation of Van Allen belt electrons which modify D-region conductivity. The relative importance of different types of whistler mode waves is not known.

The generation of transient mesospheric electric field needs detailed study as it provides a basis for developing coupled troposphere-mesosphere-ionosphere electrodynamic models under disturbed conditions. In fact, numerous phenomena that occur in the upper atmosphere of the Earth are caused by the sources located in the lower atmosphere and on the ground such as thunderstorms, typhoons, dust storms, earthquakes, volcanic eruptions, and radioactive emissions from the nuclear power plants. All these phenomena affect the electrical conductivity from the Earth's surface to the lower ionosphere. Variation of conductivity and external current in the lower atmosphere lead to the perturbation of electric current flowing in the GEC and to the associated DC electric field perturbations both on the Earth's surface and in the ionosphere and hence affect the electrodynamic coupling of the Earth's atmosphere and the ionosphere.

Acknowledgments

A. K. Singh is thankful to DST for financial support. A. K. Singh, D. Siingh are also thankful to Indian Space Research Organization (ISRO) for partial financial support under CAWSES program. R. P. Singh acknowledges the facilities provided by the Head, Department of Physics, BHU, Varanasi, India.

References

[1] D. K. Singh, R. P. Singh, and A. K. Kamra, "The electrical environment of the earth's atmosphere: a review," *Space Science Reviews*, vol. 113, no. 3-4, pp. 375–408, 2004.

[2] T. Neubert, "Atmospheric science: on sprites and their exotic kin," *Science*, vol. 300, no. 5620, pp. 747–749, 2003.

[3] V. M. Sorokin and V. M. Chmyrev, "Atmosphere-Ionosphere Electrodynamic coupling," in *The Atmosphere and Ionosphere*, Physics of Earth and Space Environment, pp. 97–104, Springer, New York, NY, USA, 2010.

[4] E. S. Kazimirovsky, "Coupling from below as a source of ionospheric variability: a review," *Annals of Geophysics*, vol. 45, no. 1, pp. 1–30, 2002.

[5] T. B. Jones, K. Davies, and B. Wieder, "Observations of D-Region modifications at low and very low frequencies," *Nature*, vol. 238, no. 5358, pp. 33–34, 1972.

[6] R. J. Gamble, C. J. Rodger, M. A. Clilverd et al., "Radiation belt electron precipitation by man-made VLF transmissions," *Journal of Geophysical Research A*, vol. 113, no. 10, Article ID A10211, 2008.

[7] V. O. Rapoport, V. L. Frolov, G. P. Komrakov et al., "Some results of measuring the characteristics of electromagnetic and plasma disturbances stimulated in the outer ionosphere by high-power high-frequency radio emission from the "Sura" facility," *Radiophysics and Quantum Electronics*, vol. 50, no. 8, pp. 645–656, 2007.

[8] V. M. Sorokin, V. M. Chmyrev, and A. K. Yaschenko, "Electrodynamic model of the lower atmosphere and the ionosphere coupling," *Journal of Atmospheric and Solar-Terrestrial Physics*, vol. 63, pp. 1681–1691, 2001.

[9] H. C. Chang and U. S. Inan, "Lightning-induce energetic electron precipitation from the magnetosphere," *Journal of Geophysical Research*, vol. 90, pp. 4531–4539, 1985.

[10] U. S. Inan, D. C. Shafer, W. Y. Yip, and R. E. Orville, "Subionospheric VLF signatures of nighttime D-region perturbations in the vicinity of lightning discharges," *Journal of Geophysical Research*, vol. 93, pp. 11455–11467, 1988.

[11] R. C. Moore, U. S. Inan, T. F. Bell, and E. J. Kennedy, "ELF waves generated by modulated HF heating of the auroral electrojet and observed at a ground distance of 4400 km," *Journal of Geophysical Research A*, vol. 112, no. 5, Article ID A05309, 2007.

[12] V. L. Frolov, V. O. Rapoport, G. P. Komrakov et al., "Density ducts formed by heating the Earth's ionosphere with high-power HF radio waves," *JETP Letters*, vol. 88, no. 12, pp. 790–794, 2008.

[13] G. M. Milikh, K. Papadopoulos, H. Shroff et al., "Formation of artificial ionospheric ducts," *Geophysical Research Letters*, vol. 35, no. 17, Article ID L17104, 2008.

[14] N. V. Dzhordzhio, M. M. Mogilevskii, V. M. Chmyrev et al., "Acceleration of ions in the plasma environment of the Earth by the radiation from a low-frequency transmitter on the ground," *JETP Letters*, vol. 46, pp. 405–409, 1987.

[15] H. L. Rowland, R. F. Ferseler, and P. F. Bernhardt, "Breakdown of the neutral atmosphere in the D region due to lightning driven electromagnetic pulses," *Journal of Geophysical Research*, vol. 101, pp. 7935–7945, 1996.

[16] V. P. Pasko, U. S. Inan, T. F. Bell, and Y. N. Taranenko, "Sprites produced by quasi-electrostatic heating and ionization in the lower ionosphere," *Journal of Geophysical Research A*, vol. 102, no. 3, Article ID 96JA03528, pp. 4529–4561, 1997.

[17] S. Fadnavis, D. Siingh, and R. P. Singh, "Mesospheric inversion layer and sprites," *Journal of Geophysical Research D*, vol. 114, no. 23, Article ID D23307, 2009.

[18] D. D. Sentman, E. M. Wescott, R. H. Picard et al., "Simultaneous observations of mesospheric gravity waves and sprites generated by a midwestern thunderstorm," *Journal of Atmospheric and Solar-Terrestrial Physics*, vol. 65, no. 5, pp. 537–550, 2003.

[19] M. J. Heavner, *Optical spectroscopic observations of sprites, blue jets, and elves: Inferred microphysical processes and their macrophysical implications*, Ph.D. dissertation, University of Alaska Fairbanks, 2000.

[20] V. M. Sorokin, V. M. Chmyrev, and N. V. Isaev, "A generation model of small-scale geomagnetic field-aligned plasma inhomogeneities in the ionosphere," *Journal of Atmospheric and Solar-Terrestrial Physics*, vol. 60, no. 13, pp. 1331–1342, 1998.

[21] V. M. Chmyrev, V. M. Sorokin, and O. A. Pokhotelov, "Theory of small scale plasma density inhomogeneities and ULF/ELF magnetic field oscillations excited in the ionosphere prior to earthquakes," in *Atmospheric and Ionospheric Electromagnetic Phenomena Associated with Earthquakes*, M. Hayakawa, Ed., pp. 759–776, Terrapublication, Tokyo, Japan, 1999.

[22] M. Stolzenburg and T. C. Marshall, "Charge structure and dynamics in thunderstorms," *Space Science Reviews*, vol. 137, no. 1-4, pp. 355–372, 2008.

[23] Y. Yair, "Charge generation and separation processes," *Space Science Reviews*, vol. 137, no. 1-4, pp. 119–131, 2008.

[24] C. Saunders, "Charge separation mechanisms in clouds," *Space Science Reviews*, vol. 137, no. 1-4, pp. 335–353, 2008.

[25] E. Williams, M. Valente, E. Gerken, and R. Golka, "Calibrated radiance measurements with an air-field glow discharge tube: application to sprites in the mesosphere," in *Sprites, Elves and Intense Lightning Discharges*, M. Fullekrug et al., Ed., vol. 225 of *NATO Science Series*, pp. 237–251, Springer, New York, NY, USA, 2006.

[26] M. J. Rycroft and M. Füllekrug, "The initiation and evolution of SPECIAL," *Journal of Atmospheric and Solar-Terrestrial Physics*, vol. 66, no. 13-14, pp. 1103–1113, 2004.

[27] K. L. Aplin, R. G. Harrison, and M. J. Rycroft, "Investigating earth's atmospheric electricity: a role model for planetary studies," *Space Science Reviews*, vol. 137, no. 1-4, pp. 11–27, 2008.

[28] M. J. Rycroft, "Electrical processes coupling the atmosphere and ionosphere: an overview," *Journal of Atmospheric and Solar-Terrestrial Physics*, vol. 68, no. 3-5, pp. 445–456, 2006.

[29] T. C. Marshall, M. Stolzenburg, C. R. Maggio et al., "Observed electric fields associated with lightning initiation," *Geophysical Research Letters*, vol. 32, no. 3, pp. 1–5, 2005.

[30] M. Stolzenburg, T. C. Marshall, W. D. Rust, E. Bruning, D. R. MacGorman, and T. Hamlin, "Electric field values observed near lightning flash initiations," *Geophysical Research Letters*, vol. 34, no. 4, Article ID L04804, 2007.

[31] A. V. Gurevich and K. P. Zybin, "Runaway breakdown and electric discharges in thunderstorms," *Physics-Uspekhi*, vol. 44, no. 11, pp. 1119–1140, 2001.

[32] A. V. Gurevich and K. P. Zybin, "Runaway breakdown and the mysteries of lightning," *Physics Today*, vol. 58, no. 5, pp. 37–43, 2005.

[33] A. V. Gurevich, G. G. Mitko, V. P. Antonova et al., "An intracloud discharge caused by extensive atmospheric shower," *Physics Letters Section A*, vol. 373, no. 39, pp. 3550–3553, 2009.

[34] M. A. Uman, *The Lightning Discharge*, Academic, Orlando, Fla, USA, 1987.

[35] D. D. Sentman and E. M. Wescott, "Observations of upper atmospheric optical flashes recorded from an aircraft," *Geophysical Research Letters*, vol. 20, no. 24, pp. 2857–2860, 1993.

[36] C. Haldoupis, R. J. Steiner, A. Mika et al., ""Early/slow" events: a new category of VLF perturbations observed in relation with sprites," *Journal of Geophysical Research A*, vol. 111, no. 11, Article ID A11321, 2006.

[37] L. Liszka, "On the possible infrasound generation by sprites," *Journal of Low Frequency Noise Vibration and Active Control*, vol. 23, no. 2, pp. 85–93, 2004.

[38] L. Liszka and Y. Hobara, "Sprite-attributed infrasonic chirps-their detection, occurrence and properties between 1994 and 2004," *Journal of Atmospheric and Solar-Terrestrial Physics*, vol. 68, no. 11, pp. 1179–1188, 2006.

[39] T. Farges, E. Blanc, A. Le Pichon, T. Neubert, and T. H. Allin, "Identification of infrasound produced by sprites during the Sprite2003 campaign," *Geophysical Research Letters*, vol. 32, no. 1, pp. 1–4, 2005.

[40] T. Neubert, M. Rycroft, T. Farges et al., "Recent results from studies of electric discharges in the mesosphere," *Surveys in Geophysics*, vol. 29, no. 2, pp. 71–137, 2008.

[41] S. B. Mende, H. U. Frey, R. R. Hsu et al., "D region ionization by lightning-induced electromagnetic pulses," *Journal of Geophysical Research A*, vol. 110, no. 11, Article ID A11312, 2005.

[42] Z. Cheng, S. A. Cummer, H. T. Su, and R. R. Hsu, "Broadband very low frequency measurement of D region ionospheric perturbations caused by lightning electromagnetic pulses," *Journal of Geophysical Research A*, vol. 112, no. 6, Article ID A06318, 2007.

[43] C. Haldoupis, N. Amvrosiadi, B. R. T. Cotts, O. A. van der Velde, O. Chanrion, and T. Neubert, "More evidence for

a one-to-one correlation between Sprites and Early VLF perturbations," *Journal of Geophysical Research*, vol. 115, p. A07304, 2010.

[44] C. Haldoupis, A. Mika, and S. Shalimov, "Modeling the relaxation of early VLF perturbations associated with transient luminous events," *Journal of Geophysical Research A*, vol. 114, no. 10, Article ID A00E04, 2009.

[45] A. Mika, *Very low frequency EM wave studies of transient luminous events in the lower ionosphere*, Ph.D. thesis, University of Crete, 2007.

[46] Y. N. Taranenko, U. S. Inan, and T. F. Bell, "Interaction with the lower ionosphere of electromagnetic pulses from lightning: heating, attachment, and ionization," *Geophysical Research Letter*, vol. 20, pp. 1539–1542, 1993.

[47] H. L. Rowland, "Theories and simulations of elves, sprites and blue jets," *Journal of Atmospheric and Solar-Terrestrial Physics*, vol. 60, no. 7–9, pp. 831–844, 1998.

[48] Y. Hiraki, T. Lizhu, H. Fukunishi, K. Nambu, and H. Fujiwa, "Development of a new numerical model for investigation the energetic of sprites," *Eos Transactions of American Geophysical Union*, vol. 83, no. 47, 2002.

[49] J. M. Galloway, F. J. Dentener, D. G. Capone et al., "Nitrogen cycles: past, present and future," *Biogeochemistry*, vol. 70, pp. 153–226, 2004.

[50] D. Siingh, R. P. Singh, A. K. Kamra et al., "Review of electromagnetic coupling between the Earth's atmosphere and the space environment," *Journal of Atmospheric and Solar-Terrestrial Physics*, vol. 67, no. 6, pp. 637–658, 2005.

[51] U. Schumann and H. Huntrieser, "The global lightning-induced nitrogen oxides source," *Atmospheric Chemistry and Physics*, vol. 7, no. 14, pp. 3823–3907, 2007.

[52] P. J. Crutzen, "Photochemical reactions initiated by and influencing ozone in unpolluted tropospheric air," *Tellus*, vol. 26, pp. 47–57, 1974.

[53] W. C. Burgess and U. S. Inan, "The role of ducted whistlers in the precipitation loss and equilibrium flux of radiation belt electrons," *Journal of Geophysical Research*, vol. 98, pp. 15643–15650, 1993.

[54] T. J. Rosenberg, R. A. Helliwell, and J. P. Katsufrakis, "Electron precipitation associated with discrete very low frequency emissions," *Journal of Geophysical Research*, vol. 76, p. 8445, 1971.

[55] M. J. Rycroft, "Enhanced energetic electron intensities at 100 km altitude and a whistler propagating through the plasmasphere," *Planetary and Space Science*, vol. 21, no. 2, pp. 239–251, 1973.

[56] R. J. Goldberg, S. A. Curtis, and J. R. Barcus, "Detailed spectral structure of magnetospheric electron bursts precipitated by lightning," *Journal of Geophysical Research*, vol. 92, pp. 2505–2512, 1987.

[57] H. D. Voss, W. L. Imhof, M. Walt et al., "Lightning-induced electron precipitation," *Nature*, vol. 312, no. 5996, pp. 740–742, 1984.

[58] H. D. Voss, "Satellite observations of lightning-induced electron precipitation," *Journal of Geophysical Research A*, vol. 103, no. 6, Article ID 97JA02878, pp. 11725–11744, 1998.

[59] M. J. Rycroft, S. Israelsson, and C. Price, "The global atmospheric electric circuit, solar activity and climate change," *Journal of Atmospheric and Solar-Terrestrial Physics*, vol. 62, no. 17-18, pp. 1563–1576, 2000.

[60] E. R. Williams and S. J. Heckman, "The local diurnal variation of cloud electrification and the global diurnal variation of negative charge on the Earth," *Journal of Geophysical Research*, vol. 98, no. 3, pp. 5221–5234, 1993.

[61] M. J. Rycroft, A. Odzimek, N. F. Arnold, M. Füllekrug, A. Kułak, and T. Neubert, "New model simulations of the global atmospheric electric circuit driven by thunderstorms and electrified shower clouds: the roles of lightning and sprites," *Journal of Atmospheric and Solar-Terrestrial Physics*, vol. 69, no. 17-18, pp. 2485–2509, 2007.

[62] C. L. Ziegler and D. R. Macgorman, "Observed lightning morphology relative to modeled space charge and electric field distributions in a tornadic storm," *Journal of the Atmospheric Sciences*, vol. 51, no. 6, pp. 833–851, 1994.

[63] V. P. Pasko, "Electric jets," *Nature*, vol. 423, no. 6943, pp. 927–929, 2003.

[64] H. T. Su, R. R. Hsu, A. B. Chen et al., "Gigantic jets between a thundercloud and the ionosphere," *Nature*, vol. 423, no. 6943, pp. 974–976, 2003.

[65] Y. P. Raizer, G. M. Milikh, and M. N. Shneider, "On the mechanism of blue jet formation and propagation," *Geophysical Research Letters*, vol. 33, no. 23, Article ID L23801, 2006.

[66] Y. P. Raizer, G. M. Milikh, and M. N. Shneider, "Leader-streamers nature of blue jets," *Journal of Atmospheric and Solar-Terrestrial Physics*, vol. 69, no. 8, pp. 925–938, 2007.

[67] M. Johnston, "Electromagnetic fields generated by earthquakes," in *International Handbook of Earthquake and Engineering Seismology*, W. Lee, H. Kanamori, P. Jennings, and C. Kisslinger, Eds., part A, pp. 621–634, Academic Press, 2002.

[68] M. Parrot, "Statistical study of ELF/VLF emissions recorded by a low-altitude satellite during seismic events," *Journal of Geophysical Research*, vol. 99, pp. 23339–23347, 1994.

[69] V. A. Liperovsky, O. A. Pokhotelov, C. V. Meister, and E. V. Liperovskaya, "Physical models of coupling in the lithosphere-atmosphere-ionosphere system before earthquakes," *Geomagnetism and Aeronomy*, vol. 48, no. 6, pp. 795–806, 2008.

[70] N. F. Arnold and T. R. Robinson, "Solar cycle changes to planetary wave propagation and their influence on the middle atmosphere circulation," *Annales Geophysicae*, vol. 16, no. 1, pp. 69–76, 1998.

[71] S. A. Bowhill, "Interaction between the stratosphere and ionosphere," *Annals of the International Year of the Quiet Sun*, vol. 5, pp. 83–95, 1969.

[72] P. R. Krehbiel, J. A. Riousset, V. P. Pasko et al., "Upward electrical discharges from thunderstorms," *Nature Geoscience*, vol. 1, no. 4, pp. 233–237, 2008.

[73] T. C. Marshall, M. Stolzenburg, P. R. Krehbiel, N. R. Lund, and C. R. Maggio, "Electrical evolution during the decay stage of New Mexico thunderstorms," *Journal of Geophysical Research D*, vol. 114, no. 2, Article ID D02209, 2009.

[74] V. A. Rakov and M. A. Uman, *Lightning: Physics and Effects*, Cambridge University Press, Cambridge, UK, 2003.

[75] M. Stolzenburg, "Observations of high ground flash densities of positive lightning in summertime thunderstorms," *Monthly Weather Review*, vol. 122, no. 8, pp. 1740–1750, 1994.

[76] M. Stolzenburg, W. D. Rust, B. F. Smull, and T. C. Marshall, "Electrical structure in thunderstorm convective regions 1. Mesoscale convective systems," *Journal of Geophysical Research D*, vol. 103, no. 12, pp. 14059–14078, 1998.

[77] W. D. Rust, D. R. MacGorman, E. C. Bruning et al., "Inverted-polarity electrical structures in thunderstorms in the Severe Thunderstorm Electrification and Precipitation Study (STEPS)," *Atmospheric Research*, vol. 76, no. 1-4, pp. 247–271, 2005.

[78] D. Siingh, V. Gopalakrishnan, R. P. Singh et al., "The atmospheric global electric circuit: an overview," *Atmospheric Research*, vol. 84, no. 2, pp. 91–110, 2007.

[79] R. G. Roble and L. Tzur, "The global atmospheric-electrical circuit," in *The Earth's Electrical Environment*, pp. 206–231, National Academy Press, Washington, DC, USA, 1986.

[80] S. S. Davydenko, E. A. Mareev, T. C. Marshall, and M. Stolzenburg, "On the calculation of electric fields and currents of mesoscale convective systems," *Journal of Geophysical Research D*, vol. 109, no. 11, pp. D11103–10, 2004.

[81] R. G. Harrison and K. S. Carslaw, "Ion-aerosol-cloud processes in the lower atmosphere," *Reviews of Geophysics*, vol. 41, no. 3, pp. 2–1, 2003.

[82] W. O. Schumann, "U‘ ber die strahlunglosen eigenschwingungen einer leitenden Kugel, die von einer Luftschicht und einer Ionospharenh ulle umgeben ist," *Zeitschrift Naturforschung*, vol. 7, pp. 6627–6628, 1952.

[83] E. Huang, E. Williams, R. Boldi et al., "Criteria for sprites and elves based on Schumann resonance observations," *Journal of Geophysical Research D*, vol. 104, no. 14, pp. 16943–16964, 1999.

[84] E. Greenberg, C. Price, Y. Yair, M. Ganot, J. Bór, and G. Sátori, "ELF transients associated with sprites and elves in eastern Mediterranean winter thunderstorms," *Journal of Atmospheric and Solar-Terrestrial Physics*, vol. 69, no. 13, pp. 1569–1586, 2007.

[85] E. Greenberg, C. Price, Y. Yair, C. Haldoupis, O. Chanrion, and T. Neubert, "ELF/VLF signatures of sprite-producing lightning discharges observed during the 2005 EuroSprite campaign," *Journal of Atmospheric and Solar-Terrestrial Physics*, vol. 71, no. 12, pp. 1254–1266, 2009.

[86] R. A. Helliwell, "40 years of whistlers," in *Modern Radio Science*, pp. 189–212, Oxford University Press, New York, NY, USA, 1993.

[87] C. J. Rodger, "Subionospheric VLF perturbations associated with lightning discharges," *Journal of Atmospheric and Solar-Terrestrial Physics*, vol. 65, no. 5, pp. 591–606, 2003.

[88] U. S. Inan, S. A. Cummer, and R. A. Marshall, "A survey of ELF and VLF research on lightning-ionosphere interactions and causative discharges," *Journal of Geophysical Research A*, vol. 115, no. 6, Article ID A00E36, 2010.

[89] M. Hayakawa, "Association of whistlers with lightning discharges on the Earth and on Jupiter," *Journal of Atmospheric and Terrestrial Physics*, vol. 57, no. 5, pp. 525–535, 1995.

[90] M. J. Rycroft, "Interactions between whistler-mode waves and energetic electrons in the coupled system formed by the magnetosphere, ionosphere and atmosphere," *Journal of Atmospheric and Terrestrial Physics*, vol. 53, no. 9, pp. 849–858, 1991.

[91] A. Mika, C. Haldoupis, R. A. Marshall, T. Neubert, and U. S. Inan, "Subionospheric VLF signatures and their association with sprites observed during EuroSprite-2003," *Journal of Atmospheric and Solar-Terrestrial Physics*, vol. 67, no. 16, pp. 1580–1597, 2005.

[92] A. K. Singh, "Ultra low frequency waves," in *Solar Terrestrial Environment: Space Weather*, R. P. Singh, R. Singh, and A. K. Singh, Eds., pp. 429–440, Allied, New Delhi, India, 2003.

[93] P. P. Belyaev, S. V. Polyakov, V. O. Rapoport, and V. Y. Trakhtengerts, "The ionospheric Alfven resonator," *Journal of Atmospheric and Terrestrial Physics*, vol. 52, no. 9, pp. 781–788, 1990.

[94] A. I. Sukhorukov and P. Stubbe, "Problems of blue jet theories," *Journal of Atmospheric and Solar-Terrestrial Physics*, vol. 60, no. 7–9, pp. 725–732, 1998.

[95] P. P. Belyaev, S. V. Polyakov, E. N. Ermakova, and S. V. Isaev, "Solar cycle variations in the ionospheric Alfven resonator 1985-1995," *Journal of Atmospheric and Solar-Terrestrial Physics*, vol. 62, no. 4, pp. 239–248, 2000.

[96] G. A. Mikhailova, Y. M. Mikhailov, and O. V. Kapustina, "ULF-VLF electric fields in the external ionosphere over powerful typhoons in Pacific Ocean," *International Journal of Geomagnetism and Aeronomy*, vol. 2, no. 2, 2000.

[97] V. P. Pasko, U. S. Inan, Y. N. Taranenko, and T. F. Bell, "Heating, ionization and upward discharges in the mesosphere due to intense quasi-electrostatic thunderstorm fields," *Geophysical Research Letter*, vol. 22, pp. 365–370, 1995.

[98] C. J. Rodger, M. Cho, M. A. Clilverd, and M. J. Rycroft, "Lower ionospheric modification by lightning-EMP: simulation of the night ionosphere over the United States," *Geophysical Research Letters*, vol. 28, no. 2, pp. 199–202, 2001.

[99] U. S. Inan, "VLF heating of the lower ionosphere," *Geophysical Research Letters*, vol. 17, pp. 729–732, 1990.

[100] P. Stubbe, "Review of ionospheric modification experiments at Tromsø," *Journal of Atmospheric and Terrestrial Physics*, vol. 58, no. 1-4, pp. 349–368, 1996.

[101] V. P. Pasko, U. S. Inan, and T. F. Bell, "Sprites as luminous columns of ionization produced by quasi-electrostatic thundercloud fields," *Geophysical Research Letters*, vol. 23, no. 6, pp. 649–652, 1996.

[102] M. Cho and M. J. Rycroft, "Computer simulation of the electric field structure and optical emission from cloud-top to the ionosphere," *Journal of Atmospheric and Solar-Terrestrial Physics*, vol. 60, no. 7–9, pp. 871–888, 1998.

[103] L. P. Babich, A. Y. Kudryavtsev, M. L. Kudryavtseva, and I. M. Kutsyk, "Atmospheric gamma-ray and neutron flashes," *Journal of Experimental and Theoretical Physics*, vol. 106, no. 1, pp. 65–76, 2008.

[104] M. Füllekrug, R. Roussel-Dupré, E. M. D. Symbalisty et al., "Relativistic runaway breakdown in low-frequency radio," *Journal of Geophysical Research A*, vol. 115, no. 1, Article ID A00E09, 2010.

[105] O. Chanrion and T. Neubert, "Production of runaway electrons by negative streamer discharges," *Journal of Geophysical Research A*, vol. 115, no. 6, Article ID A00E32, 2010.

[106] E. Gerken and U. Inan, "Streamers and diffuse glow observed in upper atmospheric electrical discharges," *IEEE Transactions on Plasma Science*, vol. 33, no. 2 I, pp. 282–283, 2005.

[107] T. Adachi, H. Fukunishi, Y. Takahashi, and M. Sato, "Roles of the EMP and QE field in the generation of columniform sprites," *Geophysical Research Letters*, vol. 31, no. 4, pp. L04107–4, 2004.

[108] O. A. van der Velde, A. Mika, S. Soula, C. Haldoupis, T. Neubert, and U. S. Inan, "Observations of the relationship between sprite morphology and in-cloud lightning processes," *Journal of Geophysical Research D*, vol. 111, no. 15, Article ID D15203, 2006.

[109] N. Liu and V. P. Pasko, "Effects of photoionization on propagation and branching of positive and negative streamers in sprites," *Journal of Geophysical Research A*, vol. 109, Article ID A04301, 2004.

[110] J. Qin, S. Celestin, and V. P. Pasko, "On the inception of streamers from sprite halo events produced by lightning discharges with positive and negative polarity," *Journal of Geophysical Research A*, vol. 116, Article ID A06305, 2011.

[111] V. P. Pasko and J. J. George, "Three-dimensional modeling of blue jets and blue starters," *Journal of Geophysical Research A*, vol. 107, Article ID 1458, 2002.

[112] V. P. Pasko, M. A. Stanley, J. D. Mathews, U. S. Inan, and T. G. Wood, "Electrical discharge from a thundercloud top to the lower ionosphere," *Nature*, vol. 416, no. 6877, pp. 152–154, 2002.

[113] C. L. Kuo, A. B. Chen, Y. J. Lee et al., "Modeling elves observed by FORMOSAT-2 satellite," *Journal of Geophysical Research A*, vol. 112, no. 11, Article ID A11312, 2007.

[114] C. L. Kuo, J. K. Chou, L. Y. Tsai et al., "Discharge processes, electric field, and electron energy in ISUAL recorded gigantic jets," *Journal of Geophysical Research A*, vol. 114, no. 4, Article ID A04314, 2009.

[115] S. A. Cummer, J. Li, F. Han et al., "Quantification of the troposphere-to-ionosphere charge transfer in a gigantic jet," *Nature Geoscience*, vol. 2, no. 9, pp. 617–620, 2009.

[116] V. I. Ermakov and Y. I. Stozhkov, *Thunderstorm Cloud Physics*, Lebedev Physical Institute, Russian Academy of Sciences, 2004.

[117] M. P. McCarthy and G. K. Parks, "On the modulation of X ray fluxes in thunderstorms," *Journal of Geophysical Research*, vol. 97, no. 5, pp. 5857–5864, 1992.

[118] G. J. Fishman, P. N. Bhat, R. Mallozzi et al., "Discovery of intense gamma-ray flashes of atmospheric origin," *Science*, vol. 264, no. 5163, pp. 1313–1316, 1994.

[119] A. C. Aikin and N. C. Maynard, "A Van de Graaf source mechanism for middle atmospheric vertical electric fields," *Journal of Atmospheric and Terrestrial Physics*, vol. 52, no. 9, pp. 695–705, 1990.

[120] S. V. Polyakov, V. O. Rapoport, and V. Y. Trakhtengerts, "the generation of electric fields in the upper atmosphere," *Geomagnetism Aeronomy*, vol. 30, p. 869, 1990.

[121] R. A. Goldberg, "Middle atmospheric electrodynamics during map," *Advances in Space Research*, vol. 10, no. 10, pp. 209–217, 1990.

[122] M. C. Kelley, C. L. Siefring, and R. F. Pfaff Jr., "Large middle atmospheric electric fields, fact or fiction?" *Geophysical Research Letter*, vol. 10, p. 733, 1983.

[123] A. M. Zadorozhny and A. A. Tyutin, "Effects of geomagnetic activity on the mesospheric electric fields," *Annales Geophysicae*, vol. 16, no. 12, pp. 1544–1551, 1998.

[124] A. M. Gokov and S. I. Martynenko, "Changes in the electron collision frequency and electric field in the lower ionosphere," *Geomagnetism Aeronomy* , vol. 37, p. 76, 1997.

[125] S. I. Martynenko, V. T. Rozumenko, A. M. Tsymbal, O. F. Tyrnov, and A. M. Gokov, "Mesospheric electric field measurements with a partial reflection radar," *Journal Atmospheric Electricity*, vol. 19, p. 81, 1999.

[126] S. I. Martynenko, V. T. Rozumenko, and O. F. Tyrnov, "New possibilities for mesospheric electricity diagnostics," *Advances in Space Research*, vol. 27, no. 6-7, pp. 1127–1132, 2001.

[127] C. E. Meek, A. H. Manson, S. I. Martynenko, V. T. Rozumenko, and O. F. Tyrnov, "Remote sensing of mesospheric electric fields using MF radars," *Journal of Atmospheric and Solar-Terrestrial Physics*, vol. 66, no. 10, pp. 881–890, 2004.

[128] I. M. Fuks, R. S. Shubova, and S. I. Martynenko, "Lower ionosphere response to conductivity variations of the near-earth atmosphere," *Journal of Atmospheric and Solar-Terrestrial Physics*, vol. 59, no. 9, pp. 961–965, 1997.

[129] S. I. Martynenko and S. F. Clifford, "On the electrical coupling between the troposphere and the mesosphere," *International Journal of Geomagnetism and Aeronomy*, vol. 6, Article ID GI2007, 2006.

[130] D. Siingh, R. P. Singh, A. K. Singh, M. N. Kulkarni, A. S. Gautam, and A. K. Singh, "Solar activity, lightning and climate," *Surveys in Geophysics*, vol. 32, no. 6, pp. 659–703, 2011.

[131] T. Ogawa, Y. Tanaka, A. Huzita, and M. Yasuhara, "Horizontal electric fields in the middle latitude," *Planetary and Space Science*, vol. 23, no. 5, pp. 825–830, 1975.